Technische Universität München

Fakultät für Chemie

Festkörper-NMR-Spektroskopie

MAS Dependent Sensitivity of Proton Detected Experiments and Off-Magic Angle Measurements to Determine Order Parameters in the Solid-State

Kai Xue

Vollständiger Abdruck der von der Fakultät für Chemie der Technischen Universität München zur Erlangung des akademischen Grades eines

Doktors der Naturwissenschaften (Dr. rer. nat.)

genehmigten Dissertation.

Vorsitzender: Prof. Dr. Franz Hagn
Prüfer:
1. Prof. Dr. Bernd Reif
2. Prof. Dr. Rasmus Linser

Die Dissertation wurde am 18.06.2018 bei der Technischen Universität München eingereicht und durch die Fakultät für Chemie am 19.07.2018 angenommen.

Table of Contents

Abstract

In 1984, the first *de novo* protein structure in solution was solved using NMR in Kurt Wuethrich's group(1). Resolved chemical shift is an essential prerequisite for structure determination. In solid state, observation of the isotropic chemical shift, however, is hindered by large anisotropic interactions such as dipole-dipole interactions and chemical shift anisotropy. High-resolution Solid-State NMR spectra were not possible until the invention of Magic Angle Spinning (MAS) in 1958(2). The first *de novo* structure of a protein in solid state was published in 2008(3). There is still no generally accepted protocol to obtain long-range distance restraints due to dipolar truncation. Solid-state NMR is still going through drastic hardware and method development.

In this thesis I pursued two aims. First, I present a quantitative study of sensitivity and resolution in proton-detected experiments under MAS in the frequency range 10-110 kHz. Using experiments and simulations, we found that for selectively methyl protonated protein samples a MAS rotation frequency beyond 300 kHz is needed for maximal intensity. It is far beyond the previous estimated limits (100-200 kHz) for completely protonated sample. Second, I present a novel scheme to determine order parameters under conditions of off-magic angle spinning. Conventionally, order parameter determination relies on residual dipolar couplings. For dynamic residues, methods become insensitive since dipolar couplings are averaged by motion. Under off-magic angle condition, on the contrary, only mobile residues can be detected with good sensitivity and resolution, thus leading to a more accurate fitting result.

This thesis is constituted with seven chapters. Chapter 1 and 2 present a brief introduction to the principle of NMR and Solid-State NMR (SSNMR). Chapter 3 lists the development of SSNMR in biosolids application. Challenges and future trends in methods are also discussed. Chapter 4 introduces experiments, which will be mainly used for studies in this thesis. Chapter 5 describes the quantitative study of MAS

dependent spectra sensitivity and resolution. Spectra of samples with different proton densities are compared. In chapter 6, an estimation of the MAS frequency that is necessary to achieve maximum sensitivity is given. Chapter 7 discusses Off-Magic-Angle (OMA) methods for order parameter determination.

Abstract (Deutsch)

1984 gelang der Arbeitsgruppe von Kurt Wüthrich die erste *de novo* Proteinstrukturbestimmung mit NMR-Spektroskopie. Eine wesentliche Voraussetzung für solche Strukturbestimmungen sind gut aufgelöste chemische Verschiebungen. In Festkörpern wird dies jedoch erschwert, da zur isotropen chemischen Verschiebung noch große anisotrope Beiträge hinzukommen. Dazu zählen Dipol-Dipol-Wechselwirkungen und chemische Verschiebungsanisotropie. Hochauflösende Festkörper-NMR-Spektroskopie war daher nicht möglich bis zur Erfindung von magic angle spinning (MAS) im Jahr 1958. Die erste *de novo* Strukturbestimmung eines Proteins mit MAS-Festkörper-NMR-Spektroskopie wurde 2008 publiziert. Noch immer fehlen allgemein anwendbare Experimente, um lange Abstände in Proteinen zu messen und den Einfluss dipolarer Trunkierung dabei zu minimieren. Damit einhergehend ist die Festkörper-NMR-Spektroskopie immer noch geprägt von bedeutenden Weiterentwicklungen in Bezug auf Hardware und Methoden.

In dieser Arbeit wurden zwei Ziele verfolgt: Zum einen präsentiere ich eine quantitative Analyse von Empfindlichkeit und Auflösung Proton-detektierter Experimente abhängig von der MAS-Frequenz. Der untersuchte Bereich umfasst die Spanne von 10 bis 110 kHz. Mit einer Kombination aus Experimenten und Simulationen konnten wir zeigen, dass bei selektiv protonierten Methylgruppen die maximale Empfindlichkeit erst oberhalb von 300 kHz erreicht werden kann. Das ist weit jenseits der Grenze von 100 bis 200 kHz, die bislang für vollständig protonierte Proben vermutet wurde. Als zweites Ergebnis dieser Arbeit stelle ich ein neues Verfahren vor, um order Parameter bei einer Rotation abseits des magischen Winkels zu messen. Üblicherweise werden residuale dipolare Kopplungen verwendet, um Order Parameter zu ermitteln. Dies führt zu Problemen bei dynamischen Resten, da dipolare Kopplungen durch Bewegung gemittelt werden. Abseits des magischen Winkels können hingegen dynamische Reste mit besserer Auflösung und Empfindlichkeit beobachtet werden. Somit können die Order Parameter für solche Reste präziser bestimmt werden.

Diese Dissertation besteht aus sieben Kapiteln. In den Kapiteln 1 und 2 wird eine kurze Einführung in die Prinzipien von NMR-Spektroskopie im Allgemeinen und Festkörper-NMR-Spektroskopie im Speziellen gegeben. In Kapitel 3 findet sich eine Darstellung der wichtigsten Entwicklungen der Festkörper-NMR-Spektroskopie für Biomoleküle. Außerdem werden Herausforderungen und zukünftige Trends bei der Methodik diskutiert. In Kapitel vier werden die zentralen Experimente für diese Arbeit vorgestellt. Kapitel 5 ist den quantitativen Untersuchungen zu Empfindlichkeit und Auflösung als Funktion der Rotationsfrequenz gewidmet. Es werden auch Proben mit unterschiedlich hohen Protonierungsgraden analysiert. In Kapitel 6 wird behandelt, wie hoch die Rotationsfrequenz um den magischen Winkel sein müsste, um maximale Empfindlichkeit zu erreichen. Das Thema von Kapitel 7 ist die Messung von Order Parametern abseits des magischen Winkels.

Chapter 1

Basic Concepts of NMR

1.1 Nuclear spin and magnetic moment

NMR spectroscopy analyse samples to the atomic level. All matters in the natural world are constituted by nuclei and electrons. Nuclei consists of two particles: the positively charged proton and neutron which is neutral in electrical charge. In the periodic table, element which has the same number of proton but different in the number of neutron takes the same position in the table and are called isotopes for one element. For example, Hydrogen, Deuterium and Tritium, all of them take the first place in periodic table and could be noted as ${}_1^1H, {}_1^2H, {}_1^3H,$(or H, D, T). The number 1 in the bottom notes down atomic number and the 1, 2, 3 are atomic mass number.

In quantum mechanics and particle physics, spin is an intrinsic form of angular momentum carried by elementary particles, composite particles (hadrons), and atomic nuclei. Total spin angular momentum may only take certain values. According to quantum mechanics, spin angular momentum takes the form of $\hbar\sqrt{S(S+1)}$. $\hbar$ is Planck's constant divided by 2π and S is spin quantum number. As is listed in **Table 1.1**, Values of spin quantum number can only be an integer (0,1, 2, …) or a half-integer (1/2, 3/2, …).

Table 1.1 *A selection of nuclear isotopes and their properties.* www.webelements.com

Isotope	Ground-State spin	Natural Abundance (%)	Gyromagnetic Ratio $\gamma\ (10^6 rad\ s^{-1}T^{-1})$	NMR Frequency at 11.74T $\gamma^0/2\pi(MHz)$
$^{1}_{1}H$	½	~100	267.522	-500.000
$^{2}_{1}H$	1	0.015	41.066	-76.753
$^{3}_{1}H$	½	0	285.349	-533.320
$^{10}_{5}B$	3	19.9	28.747	-53.718
$^{11}_{5}B$	3/2	80.1	85.847	-160.420
$^{13}_{6}C$	½	1.1	67.283	-125.725
$^{14}_{7}N$	1	99.6	19.338	-36.132
$^{15}_{7}N$	½	0.37	-27.126	+50.684
$^{17}_{8}O$	5/2	0.04	-36.281	+67.782
$^{19}_{9}F$	½	~100	251.815	-470.470
$^{23}_{11}Na$	3/2	~100	70.808	-132.259
$^{27}_{13}Al$	5/2	~100	69.763	-130.285
$^{29}_{14}Si$	½	4.7	-53.190	+99/336
$^{31}_{15}P$	½	~100	108.394	-202.606
$^{35}_{17}Cl$	3/2	75.77	10.610	-48.990
$^{37}_{17}Cl$	3/2	24.23	8.832	-40.779
$^{63}_{29}Cu$	3/2	69.17	71.118	-132.577
$^{65}_{29}Cu$	3/2	30.83	76.044	-142.018
$^{107}_{47}Ag$	½	51.84	-10.889	+20.239
$^{109}_{47}Ag$	½	48.16	-12.518	+23.268
$^{129}_{54}Xe$	½	24.4	-74.521	+139.045
$^{207}_{82}Pb$	½	22.1	55.805	-104.603
$^{12}_{6}C$	0	98.9		
$^{16}_{8}O$	0	~100		

The spin angular momentum is a vector $\boldsymbol{S}$. Direction of this vector is called spin polarization axis. Atomic nuclei with a nonzero spin possess a magnetic moment $\boldsymbol{\mu}$ in magnetic field.

$$\boldsymbol{\mu} = \gamma \boldsymbol{S} \tag{1.1}$$

Magnetic moment vector is parallel to the nuclear spin operator. The ratio constant is called gyromagnetic ratio. As in **Table 1.1**, gyromagnetic ratio can either be positive or negative. Sign of the gyromagnetic ratio contains information if magnetic moment vector is parallel or antiparallel to the spin angular momentum.

1.2 Spin in magnetic field

With the presence of an external magnetic field (B_0), nucleus magnetic moment will start precessing around the axis of external magnetic field. The precessing frequency is Larmor Frequency.

$$\omega_0 = -\gamma B_0 \tag{1.2}$$

B_0 is the external magnitude of the external magnetic field. Sign of the Larmor Frequency γ determines whether the precession is clockwise or anticlockwise. In Table 1.1, Larmor Frequency of some nucleis in an external field of 9.4 T are given.

Energy of a nuclear magnetic moment with the present of an external field is given as:

$$E = -\boldsymbol{\mu} \cdot \boldsymbol{B}_0 \tag{1.3}$$

Sign of energy for magnetic moment is related to the sign of gyromagnetic ratio and magnetic moment orientation (parallel or anti-parallel to the external field).

In NMR experiment, radio frequency (rf) pulses are oscillated magnetic field generated from signal coil. Direction of spin magnetization can be manipulated with rf pulses. Macroscopic magnetic moment can be rotated to the xy-plane of the rotating frame. This macroscopic magnetic moment in the xy-plane is called transverse magnetization. The transverse magnetization precesses with Larmor Frequency $\boldsymbol{\omega}_0$ around external magnetic field B_0. The precession of macroscopic transverse magnetization could be detected in a wire coil. The electric signal that is picked up in this coil is called NMR signal or free-induction decay (FID). Decay of the transverse magnetization occur via transverse relaxation process.

1.3 Nuclear spin interactions

Nuclear spin interacts with the surrounding magnetic field and rf pulses, these interactions are called external interactions. The interactions that are induced by the magnetic and electric field originated from the nuclear environment are called internal interactions.

Internal interactions in a diamagnetic substance contains the following terms: 1. Chemical shift: it represents the indirect interactions of the external magnetic field and the nuclear spins, through the involvement of the electrons. 2 Quadrupole interactions: it represents the electric interactions of spin >1/2 nuclei with the surrounding electric field. 3. Direct dipole-dipole couplings: it represents the direct magnetic interactions of nuclear spins with each other through space. 4. J-couplings: it represents the indirect interactions of the nuclear spins with the involvement of the electrons. 5. Spin-rotation interactions. These represents the interactions between nuclear spins and the external magnetic fields generated by the rotation of the molecules.

Based on whether these interactions are related with the relative orientation of the molecules and the external magnetic fields, they are also referred as anisotropies (dependent on the relative orientation) or isotropic interactions (independent of relative orientation)

1.4 Solid and solution state NMR

Solid and liquid samples are commonly used in NMR measurements. Molecules in liquid undergoes translational and rotational motion, over time motion averages all isotropic and anisotropic interactions for all possible orientations. In isotopic liquids, molecule orientation takes the same probability over all directions. Since the molecule motion of liquids happen in a time range faster than the inverse of most anisotropy interactions. Average of anisotropies over time disappears and leads to well resolved NMR spectra. This is the basis for the successful application of Solution State NMR in chemistry and biology.

However anisotropic spin interactions contain important molecular structural information. In solution state NMR, this information is obtained by studying the nuclear relaxation parameters. Relaxation parameters are influenced by anisotropies. In solid state NMR, with the absence of overall molecular motion, anisotropic spin

interactions are not averaged out and direct determinations of structural information of molecules are possible to measure.

Chapter 2

An Introduction to Solid State NMR

2.1 Magic angle spinning

Molecule in solids does not undergo overall tumbling motion as in solution, therefore, anisotropic interactions are not averaged out. The presence of anisotropic interactions leads to broad lines and poor resolution in solid state NMR spectra. High resolution in solid state NMR spectra is not possible without magic-angle-sample spinning (MAS).

In early times, people started to spin samples not for the aim of averaging out dipolar coupling, but to achieve an averaging of the inhomogeneous magnetic field (B_0). People used to spin the sample 90° from the main field (B_0). Later in Gordon Conference(4), John S Waugh reported about his discovery about the correlation between strength of dipolar coupling and dipolar coupling orientation to the main field (Θ_{kl}). Then E.R Andrew and I. Lowe independently reported about the complete averaging of dipolar coupling using a rotor that is placed with an angle of $\arctan(\sqrt{2})$ from the main magnetic field. Soon this angle started to be called the Magic Angle. This discovery has enabled the possibility of achieving high resolution spectra in solid state NMR. This is a new chapter of solid state NMR, people are now able to spin the sample at magic angle with the newest commercial probe head for a MAS frequency of 111kHz (2017).

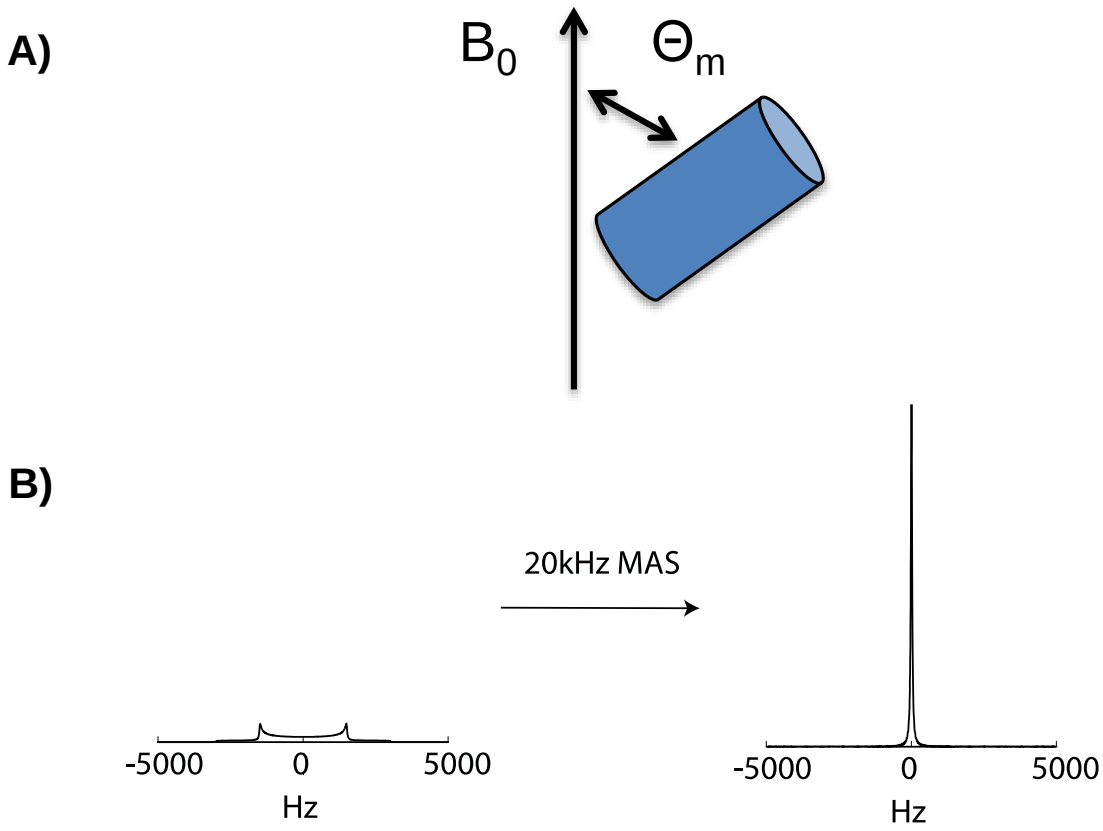

Figure 2.1 A) *Samples are placed in a rotor with* $arctan(\sqrt{2})$ *from the main magnetic field.* ***B)*** *Static and 20kHz MAS spectra are simulated using SIMPSON(5) for a 2 proton system. A dipolar coupling value of 2 kHz is assumed.*

In **Figure 2.1** an example of how rotor is placed is given and a comparison of NMR spectra with and without Magic Angle Spinning is shown.

To describe magic angle spinning, it is necessary to describe rotation in the first place. All NMR Hamiltonians can be written as a summation of products of spin and spatial tensors:

$$\boldsymbol{H_\lambda} = W_\lambda \sum_{l=0}^{2} \sum_{m=-1}^{l} (-1)^m \boldsymbol{A^\lambda_{l,-m} T^\lambda_{l,m}} \qquad (2.1)$$

W_λ is a constant. $\boldsymbol{A^\lambda_{l,-m}}$ and $\boldsymbol{T^\lambda_{l,m}}$ are the spatial and spin tensor of λ interaction. With such separation of the spatial and spin tensor of interactions, rotation in each tensor could be handled separately.

These tensors can be rotated from different coordinate system using operator $\boldsymbol{R}$. For example, spatial tensor $\boldsymbol{A^{\lambda}}$ could be transformed (X, Y, Z) to (x, y, z) coordinate system:

$$\boldsymbol{A}^{\lambda}(x,y,z) = \boldsymbol{R}\boldsymbol{A}^{\lambda}(X,Y,Z)\boldsymbol{R}^{-1} \tag{2.2}$$

If here (X, Y, Z) coordinate system is defined as Principal Axis System (PAS), and the (x,y,z) coordinate system is defined as Laboratory System (LAB), spatial coordinate rotation can be written as:

$$\boldsymbol{A}^{\lambda}_{l,m}(x,y,z) = \boldsymbol{R}(\alpha,\beta,\gamma)\boldsymbol{A}^{\lambda}_{l,m}(X,Y,Z)\boldsymbol{R}^{-1}(\alpha,\beta,\gamma) = \sum_{m'=-l}^{l} \boldsymbol{A}^{\lambda}_{l,m'}(X,Y,Z)\boldsymbol{D}^{l}_{m',m}(\alpha,\beta,\gamma) \tag{2.3}$$

$\boldsymbol{D}^{l}_{m',m}(\alpha,\beta,\gamma)$ are Wigner rotation matrices. It can also be simplified in the exponential form:

$$\boldsymbol{D}^{l}_{m',m}(\alpha,\beta,\gamma) = \boldsymbol{e}^{-im'\alpha}\boldsymbol{d}^{l}_{m',m}(\beta)\boldsymbol{e}^{im\gamma} \tag{2.4}$$

In solid state NMR experiments, sample is rotated with an $\boldsymbol{\theta_m} = \arctan(\sqrt{2})$ to the external magnetic field. Spatial tensors $\boldsymbol{A}^{\lambda}_{l,m}$ could be represented as follow:

$$\boldsymbol{A}^{\lambda}_{l,m} = \sum_{n=-l}^{l} \boldsymbol{\alpha}^{\lambda}_{l,n}\boldsymbol{D}^{l}_{n.m}(\omega_r t,\theta,0) \tag{2.5}$$

$$\boldsymbol{\alpha}^{\lambda}_{l,n} = \sum_{m'=-l}^{l} \boldsymbol{\rho}^{\lambda}_{l,m}\boldsymbol{D}^{l}_{n.m'}(\alpha,\beta,\gamma) \tag{2.6}$$

In **Table 2.1**, second order reduced Wigner rotation matrix elements are given**.**

Table 2.1 *A Reduced Wigner rotation matrix element (second-order),* $d^2_{m',m}(\beta)$ *in terms of Euler angle.*

	2	1	0	-1	-2
2	$\frac{(1+cos\beta)^2}{4}$	$-sin\beta\frac{(1+cos\beta)}{2}$	$\sqrt{\frac{3}{8}}\sin^2\beta$	$-sin\beta\frac{(1-cos\beta)}{2}$	$\frac{(1-cos\beta)^2}{4}$
1	$sin\beta\frac{(1+cos\beta)}{2}$	$\cos^2\beta-\frac{(1-cos\beta)}{2}$	$-\sqrt{\frac{3}{8}}sin\,2\beta$	$\frac{(1+cos\beta)}{2}-\cos^2\beta$	$-sin\beta\frac{(1-cos\beta)}{2}$
0	$\sqrt{\frac{3}{8}}\sin^2\beta$	$\sqrt{\frac{3}{8}}sin\,2\beta$	$(3\cos^2\beta-1)/2$	$-\sqrt{\frac{3}{8}}sin\,2\beta$	$\sqrt{\frac{3}{8}}\sin^2\beta$
-1	$sin\beta\frac{(1-cos\beta)}{2}$	$\frac{(1+cos\beta)}{2}-\cos^2\beta$	$\sqrt{\frac{3}{8}}sin\,2\beta$	$\cos^2\beta-\frac{(1-cos\beta)}{2}$	$-sin\beta\frac{(1+cos\beta)}{2}$
-2	$\frac{(1-cos\beta)^2}{4}$	$sin\beta\frac{(1-cos\beta)}{2}$	$\sqrt{\frac{3}{8}}sin\,2\beta$	$sin\beta\frac{(1+cos\beta)}{2}$	$\frac{(1+cos\beta)^2}{4}$

Rotation properties and tensor ranks of NMR interactions are given in **Table 2.2**:

Table 2.2 *NMR interaction tensor ranks*

Interaction	Spatial Rank	Component	Spin Rank	Component
Isotropic CS	0	0	1	-1, 0, 1
CSA	2	-2, -1, 1, 2	1	-1, 0, 1
Homonuclear Dipolar Coupling	2	-2, -1, 1, 2	2	-2, -1,0,1, 2
Heteronuclear Dipolar Coupling	0	0	1	-1,0,1
Homonuclear J coupling	0	0	0	0
Heteronuclear J coupling	0	0	1	-1, 0, 1

2.2 Average Hamiltonian Theory (AHT) under MAS

In this discussion, we ignore quadrupole interactions and limit the Hamiltonian to spin -1/2 nuclei. We note that interactions with a spatial rank-0 are invariant from under any rotations. These interactions are Isotropic chemical shift (CS) and J-coupling. The rest rank-2 tensors like CSA and Dipolar couplings would be averaged to zero in the limit of secular approximation.

For a system of coupled spin -1/2 nuclei in a strong external field and subject to MAS and time dependent RF, the dependent Hamiltonian:

$$\boldsymbol{H}(t) = \boldsymbol{H_D}(t) + \boldsymbol{H_{CSA}}(t) + \boldsymbol{H_{RF}}(t) + \boldsymbol{H_j} + \boldsymbol{H_{CS}} \tag{2.7}$$

Here the discussion is only about Magic Angle Spinning and how it influences internal and external interactions. So, it is assumed that radio frequency power is 0. Time independent term like J coupling and isotropic chemical shift as discussed will not vanish due to magic angle spinning. The rest time-dependent anisotropic part CSA and Dipolar couplings are the factors to influence sensitivity and linewidth in solid state NMR. Time-dependent parts follow the following formula(6):

$$\boldsymbol{H_{CSA,D}}(t) = \left(e^{-2i\omega_r t}\sqrt{\frac{3}{8}}\sin^2\theta_m \boldsymbol{A_{2,-2}} - e^{-i\omega_r t}\sqrt{\frac{3}{8}} sin(2\theta_m)\boldsymbol{A_{2,-1}} + \frac{3\cos^2\theta_m - 1}{2} A_{2,0} + e^{i\omega_r t}\sqrt{\frac{3}{8}} sin(2\theta_m)\boldsymbol{A_{2,1}} + e^{2i\omega_r t}\sqrt{\frac{3}{8}}\sin^2\theta_m \boldsymbol{A_{2,2}} \right)\boldsymbol{T} \tag{2.8}$$

Here spin operator is different for dipolar and CSA interactions. For dipolar interactions

$T = \frac{1}{\sqrt{6}}(3I_{1z}I_{2z} - \boldsymbol{I_1 I_2})$, and for chemical shift anisotropies $T = \frac{2}{\sqrt{6}} I_z B_0$. Under magic angle spinning, $\frac{3\cos^2\theta_m - 1}{2} A_{2,0}$ becomes to zero but other terms need to be explained with Average-Hamiltonian theory. Average-Hamiltonian theory made it possible to express time dependent Hamiltonian as a series of time independent Hamiltonians:

$$\boldsymbol{H} = \boldsymbol{H}^1 + \boldsymbol{H}^2 + \cdots$$

$$\boldsymbol{H}^1 = \int_0^1 d\tau_1 \, \boldsymbol{H}(\tau),$$

$$\boldsymbol{H}^2 = \frac{-i}{2V_r}\int_0^1 d\tau_2 \int_0^{\tau_2} d\tau_1[\boldsymbol{H}(\tau_2), \boldsymbol{H}(\tau_1)] \ldots \ldots \quad (2.9)$$

It is worth noting that in the higher order term of the expansion contains commutators of Hamiltonian with itself at a different time and a denominator V_r. In order to get rid of the higher order term of the expansion, a faster MAS is always in need.

Chapter 3

Solid State NMR Application in Structural Biology

3.1 Evolution of solid state NMR in protein structure determination

In Solution State NMR, first de novo protein structure was already determined in 1984 in the group of Kurt Wuetrich(1). In solids, assignable spectra of proteins were not obtained until around 2000(7, 8). High resolution structure of a peptide (9) and a protein in solids was shown in 2002(10). Research work related with amyloid fibril was first published in 2004 (11), Amyloid form of the HET-s prion domain were observed in 2005 (12). After three years, Atomic-resolution structure of fibril was reported in 2008 (3). α -synuclein structure was recently reported from Rienstra group (13). Solid State NMR has become a powerful technique for biological solids investigation and has received tremendous success over the past two decades (14).

Structural determination using NMR is based on unambiguous determination of distance restraints. In solids, distance restraints are mainly introduced through dipolar coupling reintroduction through rotor synchronized radio frequency pulses. Then these restraints will be used in simulated annealing programs and calculating for structure. Initial works including accurate structure determination of (U)-^{13}C,^{15}N MLF (methionine-leucine-phenylalanine) and α-spectrin SH3 is accomplished with dihedral angle predicted by chemical shift assignments and distance information extracted from proton-driven spin diffusion (PDSD) type of experiments. Due to an effect of dipolar truncation, longer range distance restraints was extracted with a combination of ^{13}C-sparse labelled sample (10, 15). As is listed in previous paragraph, various of structures were determined with heteronuclear detection. Most of protein samples were prepared with Uniform/Sparsely ^{13}C-^{15}N labelling scheme.

^{1}H-^{1}H distances were firstly measured with a 38-residue U-13C, 15N- labelled protein (16). This trial is based on 13C-13C 2D spectra. Direct measurement of proton

distance was difficult because of dense proton pool. Significant progress has been made for direct proton detected experiments via advances in instrumental design of ultrafast MAS triple-resonance probes and proton diluted labelling methods (17-19). In 2011, a 4D 1H-detected experiments were performed to solve the structure of ubiquitin (20). More recently, the horizon of proton detected experiment was even pushed further. Pintacuda and his workers analysed structures and dynamics of various proteins using complete protonation, proton detection with a MAS of >100kHz (21). In ***Table 3.1***, a list of proteins determined by solid state NMR and the corresponding methods information are shown.

Table 3.1 Some examples of SSNMR determination of protein structure (22)

Restraint	Pulse Sequence	Protein type	Size(kDa)
Dihedral angles	Specific CP (23)	GB1	6.0
Distance restraints (homonuclear dipolar recoupling)	PDSD (24) DARR (25) CHHC (26) PAIN(27) PAR (28) RFDR (29) DRAMA (30) HORROR (31) C7 (32) DREAM (33) DRAWS (34) PARIS (35) SHANGHAI(36)	SH3 domain	7.0
		Kaliotoxin	4.0
		Crh domain	9.5(x2) dimer
		Ubiquitin	9.0
		MPP-12	17.6
		HNP	3.0
		$\alpha\beta$-Crystalline	(20.0) x2
		β2m	2.5(x4)
		WW domain of CA 150	4.5(x4)
		HET-s(218-289) prion	8.6(x5,x3)
		hIAPP	0.75(x8)
		M2TMP	2.75(x4)
		HNP	3.0

(continue)

Distance restraints (heteronuclear	REDOR (37) TEDOR(38)	MLF	0.4
		TTR	6.0

dipolar recoupling)	FRESH (39)	Mastoparan	2.0
		Protegin-1	4.0(x2)
Torsion Angles	T-MREV(40) $R18^{1}_{7}$ (41) ROCSA (42)	TTR	1.0
		HNP-1	3.0

3.2 Challenges and future development

So far, various advances have been made in homo/heteronuclear distance restraints, torsion angles determination of protein structure with SSNMR. Still sensitivity and resolution is the most limiting factor for solid state NMR. This is because most SSNMR experiments are still performed with heteronuclear detection. Even if it's proton detection, sample are prepared with deuteration schemes, which means decreased sensitivity due to diluted proton ratio. Two emerging developments in hardware design are the major trend recently. One is the use of dynamic nuclear polarization (DNP). DNP enhanced SSNMR was introduced in 1950s (43, 44), but it was not used until high power gyrotron sources compatible with high magnetic field was made possible recently. Advances including faster spinning under low temperature, search for assignment protocol with DNP, sample preparation and enhancement mechanism development (45-49). However, in this thesis, fast spinning probe in combination with proton detection will be discussed more into details. Numerical exact simulation will provide evidence on how dense the proton pool with 100kHz of MAS will generate spectra with a reasonable proton linewidth and enough sensitivity for analyse. The conclusion will provide information for solid state NMR biological sample preparation.

Chapter 4

Proton Detected Experiments in the Solid-State

Proton is the nucleus with the highest gyromagnetic ratio and possesses the highest sensitivity for NMR detection. In the past, solid state NMR experiments were restricted to observation of heteronuclear spins. Small chemical shift dispersion of protein protons and broad linewidth made it impossible to resolve individual resonances for large molecules. However, after the introduction of a dilute proton network with chemically perdeuteration, well-resolved microcrystalline protein spectra were already resolved for N-H and C-H correlation even at 20kHz of MAS. In this thesis, the main topic is future development of proton detected experiments.

4.1 Challenges for assignment experiments at very fast spinning

With the upper boundary for MAS spinning frequency being set recently to 111kHz (2017, commercial probe), traditional protein assignment protocols in the solid-state NMR are facing challenges. Since at slower spinning frequency, solid state NMR experiments based on heteronuclear detection. Assignment protocols based on proton detection are widely studied recently. Major challenges remain in the field of polarization transfer, recoupling and decoupling methods.

Recoupling methods

In Solid State NMR experiments, MAS is required for averaging anisotropic interactions while preserving isotopic chemical shift information. But in many cases, anisotropic interactions (e.g. dipolar coupling, etc.) also contain useful structural information. In NMR pulse sequences, some special rf sequences are designed to reintroduce dipolar couplings under rotating frame. These series of rf sequences are called Recoupling Sequences. If the reintroduced dipolar coupling is between one kind of nuclei, the sequence is called a homonuclear recoupling sequences. If the

nuclei are of different kind, it is called heteronuclear recoupling sequence. Also depends on which order Hamiltonian in average Hamiltonian theory are recoupled in the recoupling process, recoupling sequences are also classified into different orders.

With the advent of fast Magic Angle Spinning, higher order term in average Hamiltonian will be more effectively decoupled. Recoupling schemes like DREAM(33) which recouples first order Hamiltonian will be effective but for schemes like PAR(28) which recouples the higher order term will remain challenging.

Decoupling methods

Decoupling methods in Solid State NMR are designed to decouple coherent heteronuclear dipolar coupling and in the end lead to a good resolution. Similar to Recoupling methods, depending on if nucleus is the same or not, decoupling methods are also divided into two classes-homonuclear decoupling and heteronuclear decoupling sequences.

In biosolids, homonuclear decoupling sequence did not succeed in reducing proton linewidths to values below 150 Hz. Instead, application of fast MAS represents an alternative method for homonuclear decoupling. Also chemically perdeuteration of sample to reduce the proton density could help to achieve a proton linewidth as low as 30-50 Hz(50). The faster the spinning, the less level of deuteration is required to obtain spectra of a good quality. At 60kHz of MAS, 100% back exchange rate to the perdeuterated system on amide exchange site allows a proton linewidth of 47 Hz(51). However, even at the fastest spinning rate(111kHz) today, Heteronuclear decoupling sequence is still needed. In recent work from Pintacuda's group, they investigated completely protonated systems at 111 kHz MAS, 30kHz of heteronuclear decoupling is given(21).

Polarization transfer will be discussed in next section when heteronuclear single quantum coherence (HSQC) type of experiment is discussed.

4.2 Proton detection based solid-state NMR methods for quantification of order parameters

Characterization of C-H/N-H Dynamics in Solid State NMR

Conformational flexibility provides information about the function and stability of proteins. Solution state NMR has been proven to be an effective tool in characterizing protein dynamics in a wide time range. In solids, with the absent of fast molecule tumbling, dynamic information over even broader time range are unmasked. Relaxation measurement in solids provides information for internal dynamics that are slower than the over tumbling. Although longitudinal relaxation or cross-correlated relaxation provide rich information about structural rearrangement, accurate determination of order parameter with just relaxation data is not sufficient (52). Order parameter is the ratio of effective dipolar coupling between bonded residues. and the dipolar coupling that is supposed to be through a one-bond distance.

In practice, accurate determination of order parameter is a possible through direct measurement of effective dipolar couplings between two bonded nuclei. Of particular interest in the side-chain C-H and backbone N-H. Considering the influence of the intense homogeneous proton-proton interactions, highly deuterated system is normally used for sample preparation. Two types of pulse sequences- Phase-inverted cross polarization (CPPI)(53) and Rotational echo double resonance (REDOR) (52)type of sequences could both applied for order parameter determination.

In a more recent study(54), it is indicated that CPPI and REDOR both generate very close result in order parameter determination. CPPI suffers from rf inhomogeneity and incapable of detecting residues with order parameter less than 0.5. REDOR is very sensitive to the absent of extra protons but the effect has the potential to be suppressed with faster MAS rotation frequency.

4.3 Introduction to heteronuclear single quantum coherence spectroscopy (HSQC)

HSQC is a highly sensitive NMR experiment. It was first described in a ^{1}H-^{15}N system(55), but it is also applicable to other nuclei such as ^{1}H-^{13}C. In this thesis, design of the pulse sequences is mostly based on HSQC. In this section, HSQC will be discussed in terms of polarization transfer scheme, phase cycling, acquisition methods.

Polarization transfer

In solution state NMR, HSQC involves the transfer of magnetization on proton to the second nucleus via INEPT (insensitive nuclei enhanced by polarization transfer) step. After acquisition in the indirect dimension, magnetization is transferred back to proton via a retro-INEPT process.

INEPT transfer step is as in Figure 4.1a. I_z was excited to $-I_y$ after a $\pi/2$ pulse with a phase on x. Then magnetization evolves with a period of τ. Here in the evolving only J coupling between two spins and chemical shift are considered. Magnetization becomes - $I_y cos\pi J_{IS}\tau + 2I_x S_z sin\pi J_{IS}\tau$. Two π pulse here only refocuses the anisotropic chemical shift on two nuclei. If $\tau = 1/2J_{IS}$, Magnetization becomes $2I_x S_z$, with a final two $\pi/2$ pulses, it becomes $-2I_z S_y$.

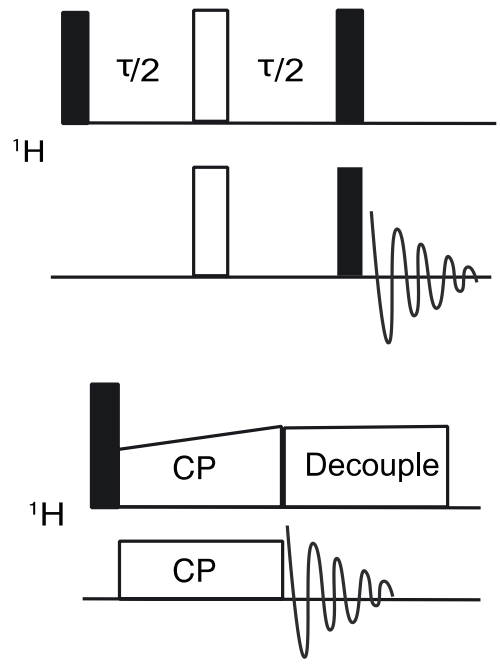

***Figure 4.1**. Up: INEPT pulse sequence; Down: CP pulse sequence*

In INEPT transfer step, an evolving time of $\tau = 1/2J_{IS}$. For H-C one bond J coupling, this is 4 ms, H-N pair, it is 5.6 ms. This demands a long enough spin-spin relaxation time so that INEPT transfer would have a good enough efficiency. However, a long relaxation time is normally not the case in solid state NMR due to the strong dipolar network.

In solid state NMR, a more frequently used heteronuclear transfer step is the cross polarization (CP) transfer. As it is shown in **Figure 4.1**.

Hartmann and Hahn has shown that nuclear spins that consisting of two spins *I* and *S* exchange energy when two strong rf fields B_{1I} and B_{1S} are applied simultaneously at *I* and *S* Larmour frequencies. Energy exchange rate shows a dependence on rf magnitude and reaches maximum when Hartman-Hahn condition is fulfilled $(\gamma_I B_{1I} = \gamma_s B_{1s})$. When Hartman Hahn concept is fulfilled, rate of the energy exchange is proportional to the heteronuclear dipolar interaction between the two spins. Under the rotating frame, Hartman-Hahn condition becomes $(\omega_{1I} = \omega_{1S} \pm n\omega_r)$. Since energy exchange rate is related to dipolar interactions, CP energy build up is also time dependent. It is also shown that CP efficiency is related with dynamics in solids(56).

Experimentally, CP condition is difficult to match completely because of rf inhomogeneity from sample coil, small fluctuations in amplifier output can cause a miss -setting. In practice, normally instead of a continuous wave (CW) pulse, a ramp or adiabatic shape is given to increase transfer efficiency.

CP/INEPT based HSQC

As mentioned in last chapter, HSQC in solid state NMR have two possible schemes. One is the transfer with CP step the other is transfer with INEPT step. As shown in **Figure 4.2.**

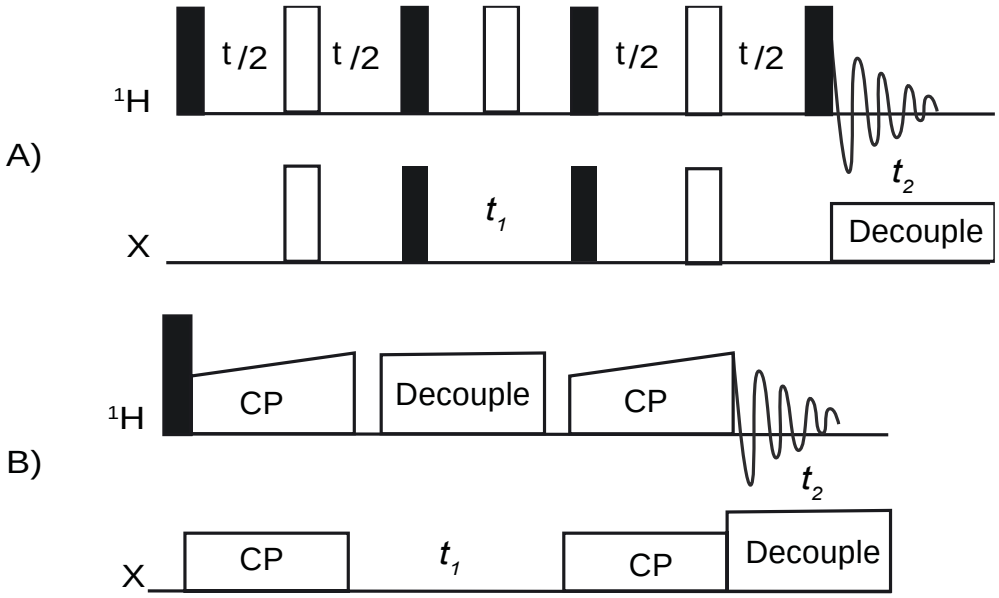

Figure 4.2. *INEPT (A) and CP (B) based HSQC.*

The application of INEPT and CP version in solid state NMR is governed by signal lifetime. INEPT efficiency is based on the T_2' and CP efficiency is based on T_{HC} and $T_1\rho$ (56). For protonated system, CP based transfer method is mostly used. There are special cases for example, in a completely protonated system spinning at 20kHz, but some residues are very dynamic and have a small order parameter (S^2). Transfer step based on J coupling can still be valid. For a proton dilute system, CP and INEPT can both be valid. In faster spinning region (MAS>100kHz), CP or INEPT transfer efficiency remains to be a topic which can be further explored.

Phase cycling

Due to delay time in indirect dimension, apart from in-phase magnetization in HSQC, extra multiple quantum term is also introduced before detection. Phase cycling are needed in filtering out undesirable magnetization. In **Table 4.1**, a four-step phase cycling is using as an example to INEPT based HSQC.

Table 4.1. *4-step phase cycling in INEPT-HSQC*

	ϕ_1	ϕ_2	ϕ_R	Proton(bounded) Signal in detection	Proton(unbounded) Signal in detection
1	x	x	x	$I_y cos\pi J_{is} t_1 - 2I_x S_x sin\pi J_{is} t_1$	I_y
2	-x	x	-x	$I_y cos\pi J_{is} t_1 - 2I_x S_x sin\pi J_{is} t_1$	$-I_y$
3	x	-x	-x	$I_y cos\pi J_{is} t_1 + 2I_x S_x sin\pi J_{is} t_1$	$-I_y$
4	-x	-x	x	$I_y cos\pi J_{is} t_1 + 2I_x S_x sin\pi J_{is} t_1$	I_y

Summation of phase cycled signals not only cancels out the unwanted multiple quantum term, but also cancels out signal of protons that is irrelevant to the single quantum coherent transfer.

An obvious question to **Table 4.1** above would be if only a two-step phase cycling step1+step3 are performed, still only single quantum coherent signal is preserved. This question will be explained in next section about the acquisition methods in indirect dimension.

Acquisition mode in indirect dimension

Quadrature detection in direct dimension enables us to set carrier position in the middle of the spectra. Both positive and negative offsets information could be differentiated through detecting both real and imaginary part of signal. Here in the discussion about HSQC, States-Haberkorn-Ruben (States, SHR), Time proportional

phase incrementation (TPPI) and States-TPPI methods in indirect dimension acquisition will be discussed more into detail.

States (SHR) method is to record a cosine modulated data set and a sine modulated data set. In direct dimension, this is possible by shifting receiver phase. In indirect dimension, this is made possible by shift phase of the appropriate pulses. In HSQC, it is made possible by shift the phase of $\pi/2$ pulse on S spin before T1 evolving.

TPPI is to arrange things that all peaks have positive offsets without rearranging carrier position. Then, there is no frequency ambiguity in a cosine modulated data. TPPI methods add an extra frequency in T1 evolving so that all peak frequencies become positive and spectral width doubles. As in the following:

$$\cos\big(\Omega t_1 + \Phi(t_1)\big) = \cos(\Omega t_1 + \omega_{add} t_1) = \cos(\Omega + \omega_{add})\, t_1 \qquad (4.1)$$

Ω is the peak offset from the carrier frequency, ω_{add} is the extra frequency to all the offsets in the spectrum. Extra frequency is made possible by putting a time (t_1) dependent phase increment.

A universal extra frequency offset is given to all peaks in the spectrum while carrier position is kept fixed. Overall spectral window ($SW_1/2$) will need to be doubled (SW_1). Which means sampling interval (Δ_1) needs to be halved ($\Delta_1/2$).

In indirect dimension t_1 is $n\Delta_1$for the nth increment. Extra frequency offset $\omega_{add} t_1$ for the nth increment in indirect dimension will be express in the following form:

$$\omega_{\mathrm{add}} t_1 = 2\pi \left(\frac{SW_1}{2}\right)(n\Delta_1) = 2\pi \left(\frac{SW_1}{2}\right)\left(\frac{n}{2SW_1}\right) = \frac{n\pi}{2} \qquad (4.2)$$

In another word, TPPI method means with each t1 increment, phase of the signal should also be incremented by $\pi/2$. This can be done by incrementing the phase of pulses.

States-TPPI methods is based on States method but changing axial peaks (arising from magnetization which does not evolve during t_1) appear at F_1=0; In State-TPPI axial peaks are moved to the edge of the spectrum through TPPI method. Although axial peaks can be suppressed with the aid of extra phase cycling, it is an unnecessarily time-costing. States-TPPI will be premium for higher dimensional NMR where phase cycling is at premium.

4.4 Site-Specific CP and INEPT transfer efficiency measurements

The efficiency of dipolar based transfer and J-coupling based transfer are of interest in SSNMR. Recently transfer efficiency comparison is performed on exchangeable amide site with 100kHz of MAS (57). Previous reports measuring overall and site-specific CP and INEPT efficiency used index parameters T_1^{ρ} and T_2' respectively. In this thesis, site specific J-coupling efficiency is also estimated with T_2'. Results have been compared with the scheme that is supposed in the following. Following schemes in ***Figure 4.3*** proposed a faster way of measuring site specific HSQC efficiency with transfer step based on either dipolar or J-coupling.

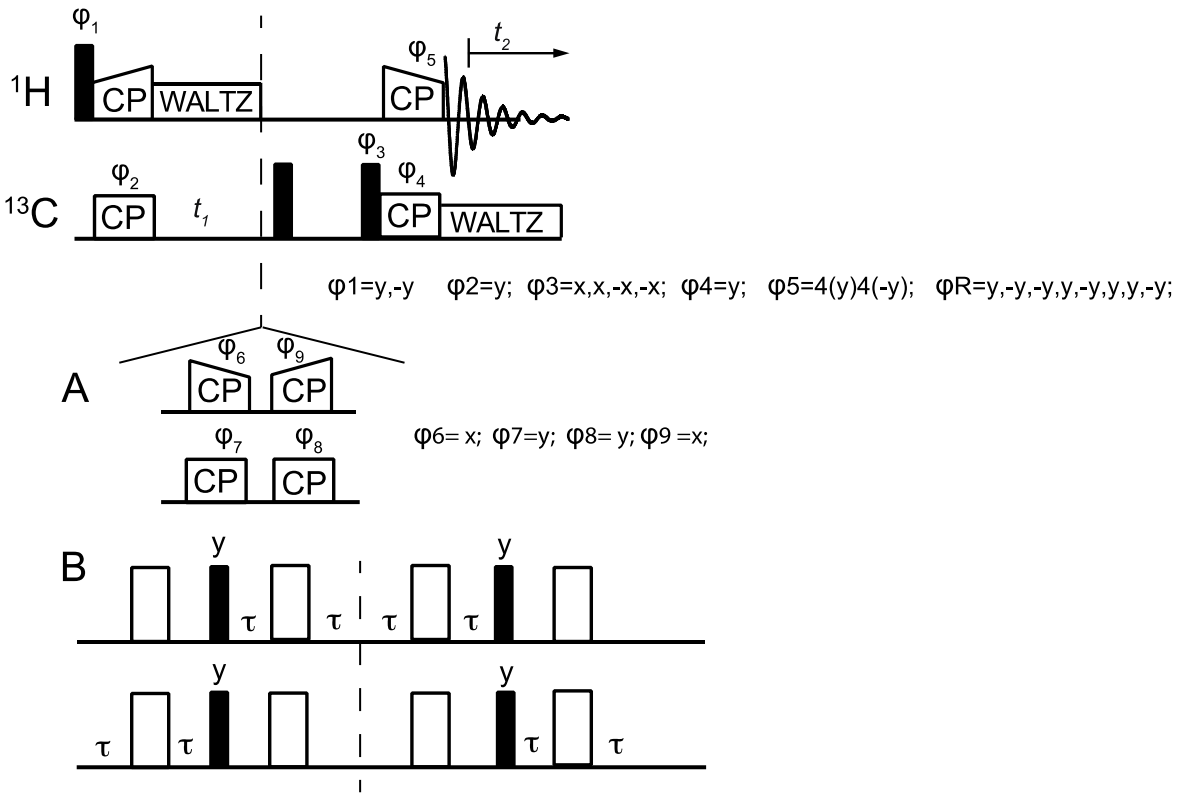

Figure 4.3 *HSQC type of pulse sequences for residue specific J-coupling and Dipolar coupling transfer efficiency.*

As is shown in ***Figure 4.3***, reference experiment is a CP based HSQC pulse sequence. Extra transfer steps are added after indirect *t1* evolution. Here, it is assumed that H-C and C-H two transfer steps have the same efficiency. In this way, only two 2D experiments are needed for residue specific CP/INTEPT efficiency.

Samples under different deuteration scheme and MAS frequency will have different CP/INEPT transfer efficiency. For proton detected experiment under MAS >100kHz, best experiment conditions (sample preparation and pulse sequence schemes) are still in development. Also, a probe beyond the MAS limitation now is intriguing for discussion. Such analysis will provide information for which deuteration levels should be applied under certain MAS frequency. Meanwhile, a future goal for probe design development could be speculated.

Chapter 5

High Resolution Side Chain Proton Spectra

Sensitivity and resolution together determine the quality of NMR spectra in biological solids. For high-resolution structure determination with solid state NMR, proton-detection emerged as an attractive strategy in the recent past. The interplay between the concentration of protons and available MAS frequency governs the spectral quality of proton-detected experiments. Such interdependence has been relatively well characterized where exchangeable amide protons are used as probes. The situation is different for covalently bonded sidechain protons, which are important reporters of structure. Here we describe how the quality of solid-state NMR spectra changes upon varying the amount of protons at moderate MAS frequencies (< 60 kHz). Based on our results, we suggest the appropriate isotope-labelling scheme for a given MAS frequency.

5.1 Introduction to protein sidechain measurement

Solid state NMR for biological samples has taken a large leap forward during the past years (3, 10, 58, 59). Advancements in the NMR technology such as the development of ultrahigh magnetic fields, emergence of ultrafast spinning probes, isotopic labelling strategies and development of new NMR methods are some of the key points behind the success. Solid state NMR samples are spun in rotors at the magic angle (Arctan [√2] = 54.74°) with respect to the main magnetic field. The maximum achievable frequency of sample spinning in the magic angle is inversely proportional to the diameter of the rotors (60) for solid state NMR. Therefore, faster spinning rotors imply smaller volumes with less sample amounts and to start out with less sensitivity in the NMR spectra. Other parameters such as the diameter of the *rf* coil, detection of protons instead of heteronuclei can counteract the decrease of sample volume(51).

For proton detection, isotope-labelling schemes have to be tailored according to the available NMR hardware. For example, only partial deuteration (H: D ≈ 20:80) of the exchangeable amide sites in heavily deuterated environments is necessary to obtain optimal spectral quality for rotors with 3.2 mm diameter (10-20 mg sample), which allows a maximum Magic Angle Spinning (MAS) frequency of 24 kHz (61, 62). With the emergence of 1.3 mm probes (2 mg sample, maximum of ~ 60 kHz MAS), 100% protons in the exchangeable amide sites in an otherwise deuterated sample yield optimal spectral quality for backbone resonances. Using the fastest spinning commercial probes with up to ~ 110 kHz MAS (0.5 mg sample), it has been proposed that deuteration is not anymore required to achieve high resolution. Deuteration is still needed for the highest spectral quality, according to Meier et al, 250kHz MAS is not enough to get rid of all the homo-DD (63).

In comparison to amide backbone, the proton density in the aliphatic sidechain is significantly higher. It was shown in the past that fractional labelling of protons in the amino acid sidechains yields excellent spectral resolution under moderate MAS frequency (64-67). Nonetheless, replacing protons by deuterons reduce the sensitivity of sidechain resonances. Methyl groups in the hydrophobic core of proteins are important reporters for structures. Even with the highest MAS frequency commercially available today, spectral broadening is still a major impediment in fully protonated samples (6). Nevertheless, it has been demonstrated recently (21) that for ~ 110 kHz MAS, it is possible to obtain high-resolution structural data without using any deuteration at all.

In general, the periodic NMR Hamiltonian under MAS may (termed inhomogeneous) or may not (termed homogeneous) commute with itself at all times (68). Coherent averaging of the inhomogeneous interactions by MAS can be achieved when the rotor frequency is larger than the size of the interactions. However, for homogeneous interactions, coherent averaging is insufficient even when the MAS frequency is set significantly larger (10 times) than the strength of the interactions (6).

To reduce the proton spin density, we suggest employing methyl protonated samples that are otherwise perdeuterated. We show here whether intra- or inter- methyl proton - proton interactions dominate the spectral appearance. The absolute

sensitivity for each labelling approach at a given MAS frequency can be quantitatively estimated.

5.2 Sample preparation

The SH3 domain of chicken alpha-spectrin was expressed in 100% D_2O M9 medium supplemented with Ammonium Chloride-^{15}N and D-Glucose-^{13}C, d7. The appropriate precursors (SH3 alpha-ketoisovalerate-$^{13}CH_3$: 2-Keto-3-(methyl-d_3)-butyric acid-4-^{13}C,3-d sodium salt, Sigma Aldrich; SH3 alpha-ketoisovalerate-$^{13}CH_2D$: 2-Keto-3-(methyl-^{13}C,d_1)-butyric-3,4,4,4-d_4 acid sodium salt, Sigma-Aldrich; SH3 DLAM-LV^{proS}-$^{13}CHD_2$: 2-(^{13}C,D_2)methyl-(1,2,3,4-^{13}C), 4-(D_3)-acetolactate, NMR-Bio) were added 1h prior to induction (1mM IPTG at OD_{600} 0.5-0.6). Expression was carried out over night at 22°C. The SH3 domain was purified via anion exchange (HiLoad 16/10 Q-Sepharose High Performance, GE) and size exclusion chromatography (HiLoad 16/600 Superdex75 pg, GE) as described before (50). For crystallization, pure protein was lyophilized and dissolved in 100% D_2O (final concentration: 8-10mg/ml). Ammonium sulphate (dissolved in 100% D_2O) was added to a final concentration of 100mM and the pH was adjusted to 8.0 by adding NaOD. The final microcrystals were packed into three 1.3 mm rotors by centrifugation.

5.3 NMR measurements and results

The proton detected CP based HSQC experiments (**Figure5.1**) were carried out using a static magnetic field where ^1H Larmor frequency is ~ 500 MHz and in a MAS probe of 1.3mm stator diameter. The n=1 Hartmann-Hahn condition were optimised for every MAS frequency with an average proton B1 field of 89 kHz. A linear ramp on protons with 70-100% amplitude was used for ^1H-^{13}C CP and 100-70% amplitude for ^{13}C-^1H CP, respectively with a contact time of 800us. For hard pulses, B1 amplitudes of 100kHz and 103 kHz were used for ^1H and ^{13}C, respectively. Low power scalar decoupling using WALTZ16 was used for ^{13}C and ^1H with $\omega_1/(2\pi)$ = 5kHz, respectively. Deuterium decoupling during the F1 and F2 dimensions was achieved with WALTZ16 and $\omega_1/(2\pi)$ = 2kHz. Water suppression was achieved using MISSISIPPI of $\omega_1/(2\pi)$ = 10 kHz for 100ms. The phase-cycle was same as described by Barbet-massin et al. (69). For all the experiments, the real sample temperature was calibrated to 289 K using DSS. The acquisition times in the F1 and F2

dimensions in all the experiments were set to 40ms (^{13}C) and 76ms (^{1}H), respectively. The relaxation delay (d_1) was set to 1.5s in all cases.

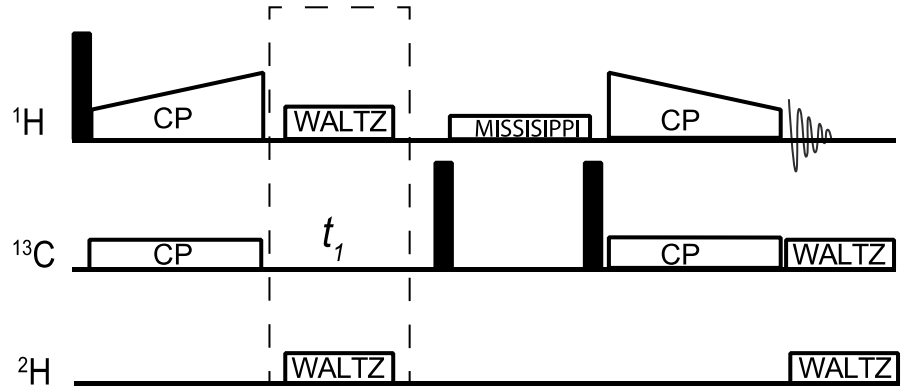

***Figure 5.1**. Pulse sequence used for CP based HSQC experiments.*

Results

In solution-state NMR, -CH_3 methyl yield the highest sensitivity with comparable resolution when comparing -CHD_2, -CH_2D and -CH_3 isotopomers. CH_3 methyls is therefore the preferred labelling strategy in the investigation of large molecular weight systems (70, 71). In solids, the situation is quite different. Although CH_3 has the highest proton density, intra-methyl as well as inter-methyl dipole-dipole couplings are significant and efficient averaging by MAS difficult to achieve.

We recorded ^{1}H detected ^{13}C,^{1}H correlation spectra as a function of MAS frequency in the range of 20-50 kHz, employing Cross Polarization (CP) (72) for magnetization transfer. We used selectively methyl protonated samples of the α-spectrin SH3 domain that are perdeuterated otherwise. In particular, we investigated protein samples containing either the isotopomers $^{13}CH_3$, $^{13}CH_2D$, $^{13}CHD_2$. In principle also INEPT based HSQC experiments could have been recorded (73). In scalar coupling based experiments, however, the cross peak intensity is affected significantly by the loss of magnetization during the magnetization transfer steps, as T'_2 increases with MAS [ref Asami et al., 2012]. (74) (75). We therefore employed CP in all experiments. We find that cross peak intensities vary significantly for the three samples (**Figure 5.2**).

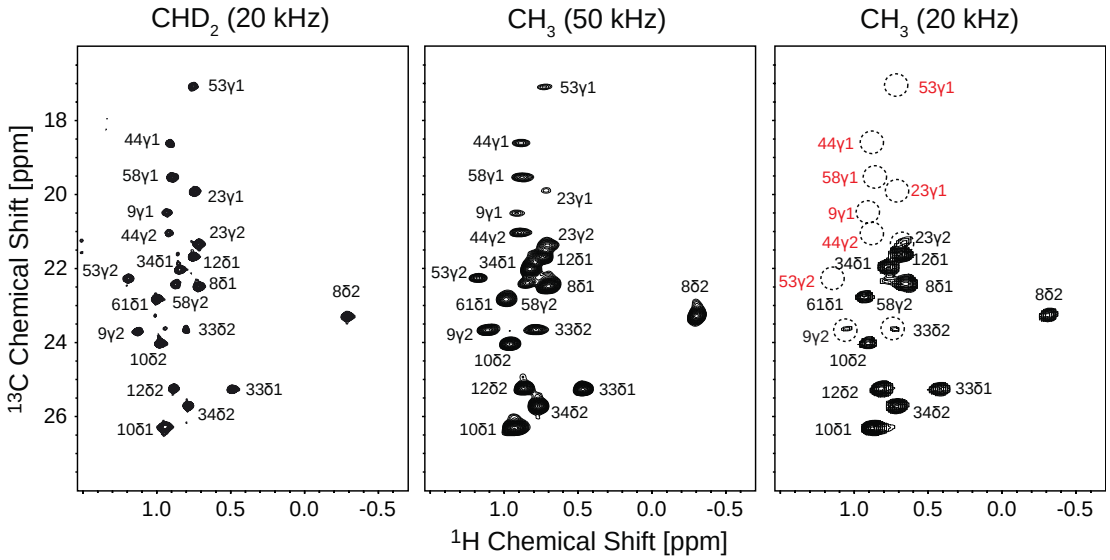

Figure 5.2. *CP based HSQC spectra recorded for CHD_2 and CH_3 selectively methyl protonated α-spectrin SH3 domain samples. Spectra were recorded at MAS frequencies of 20 kHz and 50 kHz, respectively. For the CH_3 sample, several peaks are missing in the spectrum recorded at 20 kHz. These peaks reappear when the MAS frequency is increased to 50 kHz. However, cross peak intensities are still very different for different residues in the sample. By contrast, HSQC cross peak intensities are uniform for the CHD_2 sample even at a MAS frequency of 20 kHz.*

For all samples, cross peak intensities increase with MAS frequency. The intensity profile is most uniform for the CHD_2 sample spinning at 50 kHz. We attribute the distribution of peak intensities to the effective intra- and inter-methyl proton-proton dipolar couplings (d^{RSS}) in the sample. d^{RSS} is defined as square root of the sum of squared dipolar couplings, following the convention of Zorin et al. (76)

$$d_i^{RSS} = \frac{\mu_0}{4\pi}\gamma_H^2\sqrt{\sum\left(\frac{1}{r_{i,j}^3}\right)}$$

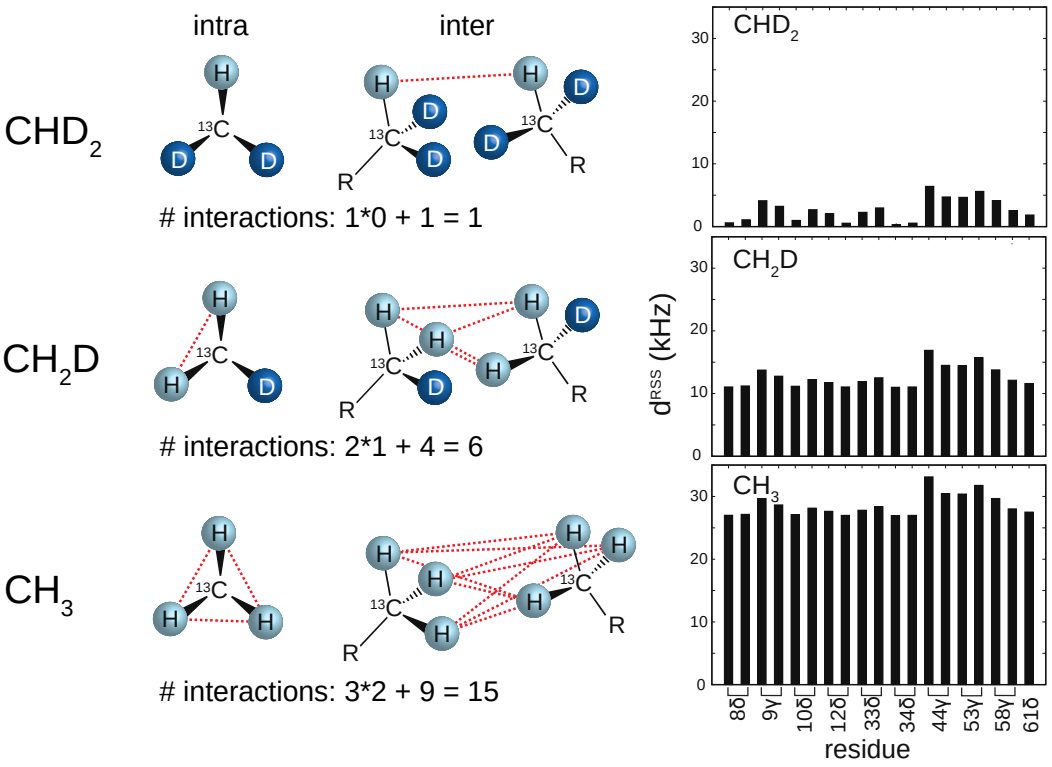

Figure 5.3. *Effective ^1H, ^1H dipolar coupling (d^{RSS}) that a methyl proton experiences in CHD_2, CH_2D or CH_3 selectively protonated protein sample. (Left) Schematic representation. d^{RSS} increases from CHD_2 to CH_3 labelled samples. Whereas there is only one inter-residual interaction for a CHD_2 group (assuming 1 methyl group in close vicinity), a CH_2D methyl group is involved in 1 intra-methyl and 4 inter-methyl interactions. By contrast, the CH_3 methyl group experiences 6 intra-methyl and 9 inter-methyl contacts. (Right) For the α-spectrin SH3 domain, d^{RSS} has been calculated using a distance cut-off of 15 Å. For the CH_3 selectively labelled sample, the intra-methyl ^1H-^1H dipolar couplings are on the order of 45 kHz, whereas the inter-methyl ^1H-^1H couplings vary between 0 and 50 kHz for different residues in the protein. For CHD_2, the inter-methyl dipole-dipole couplings are scaled by a factor 9 in comparison to CH_3 due to the dilution of proton spin system. The dashed, horizontal line in the figure indicate the contribution from intra-methyl interactions.*

The distance between two protons in a methyl group is on the order of 1.78 Å, corresponding to a dipole-dipole coupling of 21 kHz. Assuming a rigid CH_3 group, d^{RSS} is ~90 kHz (=√2*3*21 kHz). Due to fast methyl group rotation, the methyl anisotropic interactions are scaled by a factor of -1/2, yielding an averaged value of ~45 kHz. For CH_3, the inter-methyl contribution to d^{RSS} varies between 0 and 45 kHz.

For CHD_2, 1/9 of these interactions remain, and d^{RSS} is reduced to a value on the order of 0-5 kHz.

Build-up curves for three showcase residues are shown in **Figure 5.4A**. In the plot, intensities were normalized with respect to the amount of protein in each rotor, employing a direct excitation ^{13}C-1D experiment for quantification. Intensity build-up curves for all residues for all labelling schemes are represented in Figure S3.
For the CHD_2 selectively protonated sample, only a small increase in cross peak intensity is found for MAS rotation frequencies above 40 kHz. We therefore assume that under these circumstances all anisotropic interactions are effectively averaged by MAS. Build-up curves are represented for three selected residues that are involved in different proton dipolar coupling networks. L34 is the residue which experiences the least dipolar interactions, and has an effective dipolar coupling of d^{RSS} = 0.5 kHz. L33 and V44 have effective dipolar couplings on the order of 2 kHz and 4 kHz, respectively. Apparently, d^{RSS} has an influence on the build-up rate and the cooperativity of the transition, even in these very extensively deuterated samples. Whereas a MAS rotation frequency of 50 kHz is sufficient to yield coherent averaging of proton dipolar interactions in the CHD_2 sample, this is clearly not the case for the CH_2D and the CH_3 selectively protonated samples. For CH_3, the effective dipolar coupling d^{RSS} adopts values in the range of ~ 45 kHz for V44 and < 5 kHz for L34δ1 (**Figure 5.3 right**). For L33δ1, d^{RSS} is ~ 25 kHz. Again, the build-up rate and the cooperativity of the transition depend on the strength of the proton dipolar coupling network and are reflected in the absolute value of d^{RSS}. We have empirically fit the MAS dependent cross peak intensities using the function $y = a * ArcTan(b * x + c) + d$. In comparison to CHD_2, CH_2D and CH_3 selectively protonated samples contain 2x and 3x, respectively, more protons and thus yield - in the limit of very fast spinning - a 2x or 3x, respectively, higher sensitivity. Given the fact that all anisotropic interactions are effectively averaged by MAS for the CHD_2 selectively protonated sample at a MAS frequency of 50 kHz, we employ this value to calculate in the empirical fit the maximum intensity expected for CH_2D and CH_3 selectively protonated samples in the limit of very fast MAS.

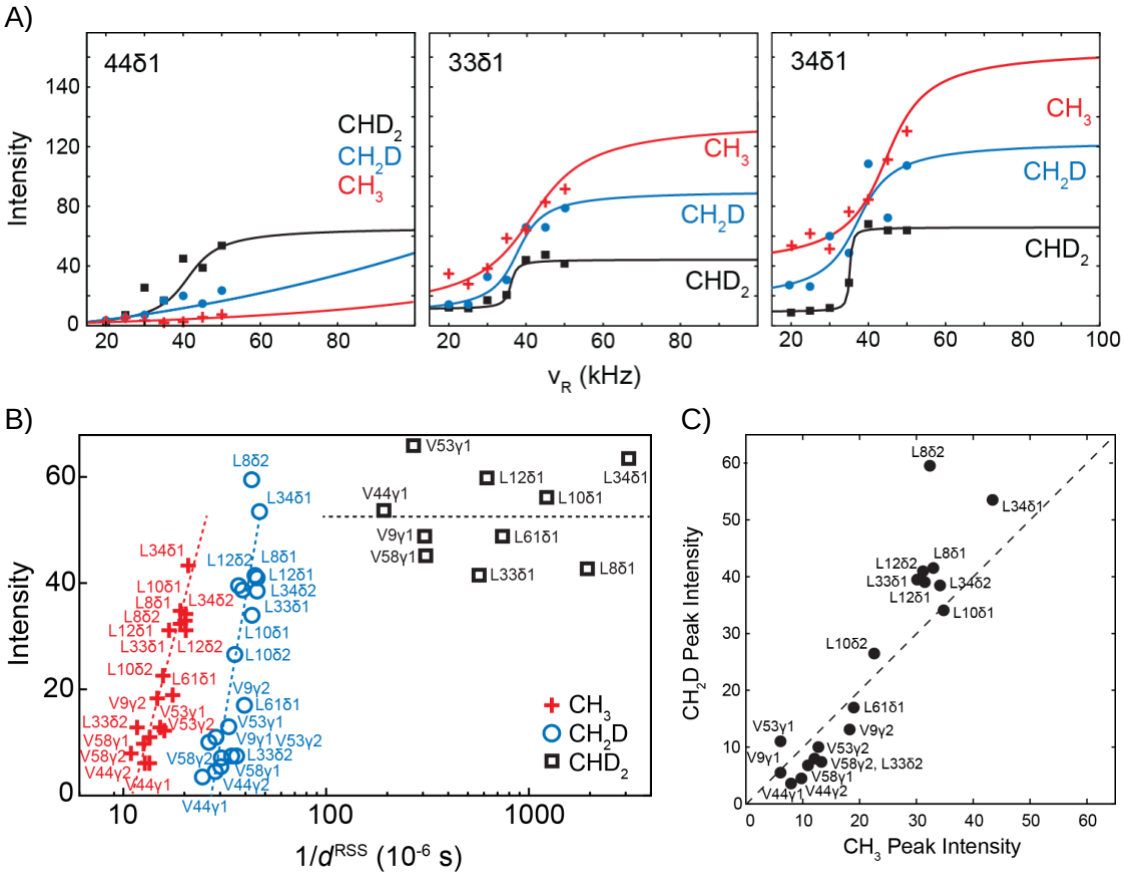

Figure 5.4. *A) Cross peak intensity build-up curves for three methyl groups in the α-spectrin SH3 domain as a function of MAS frequency for CHD_2, CH_2D and CH_3 selectively protonated samples. Residues V44, L33 and L34 are embedded in different proton coupling networks and experience differential effective proton dipolar couplings d^{RSS}. Intensities were normalized with respect to the amount of protein in each rotor, employing a direct excitation ^{13}C-1D experiment for quantification. B) Correlation plot of the $^{1}H,^{13}C$ cross-peak intensities at a MAS rotation frequency of 50 kHz and the inverse of the effective proton dipolar coupling d^{RSS} for CH_3 (red), CH_2D (blue) and CHD_2 (black) selectively protonated samples, respectively. In the plot, intensities are scaled by 1/3 and 1/2 for CH_3 and CH_2D, respectively, to enable a direct comparison of the three data sets. C) Correlation plot of the intensities of the CH_3 and CH_2D selectively protonated samples at a MAS rotation frequency of 50 kHz.*

In the following, we set out to simulate the MAS dependent $^{1}H,^{13}C$ cross peak intensities using the software package SIMPSON (77). In the simulation, the ^{1}H, the ^{13}C dimension as well as the two magnetization transfer steps are calculated separately and ultimately multiplied to yield the global transfer efficiency. The overall

sensitivity (I_{final}) is thus calculated as $I_{final} = \varepsilon_{CP}^2 * \varepsilon_C * I_H$. At slow MAS frequencies, the total intensity is distributed over the spinning side-band manifold yielding a reduced center-band intensity.

Schanda and co-worker have reported recently a study on the effect of the MAS frequency on the spectral resolution of methyl resonances of the 468 kDa protein complex TET2 and the 1.6 MDa 50S ribosome subunit of *Thermus thermophilus* (78). The authors find comparable linewidths for CH_3 and CHD_2 selectively protonated samples, and suggest to employ CH_3 isotopomer containing samples in case MAS frequencies on the order of 60 kHz are used. We also observe no differences in spectral resolution when selectively CH_3, CH_2D and CHD_2 protonated α-spectrin SH3 domain samples are compared (**Figure 5.5**). However, we point out here that the proton dipolar environment has an impact on the sensitivity of the experiment, as inhomogeneous and homogeneous proton interactions impact the center-band intensities.

The sensitivity of the cross-peaks modulates as a function of d_{rss}, as described in the main text. However, the line-widths remain similar under various MAS frequencies (**Figure 5.5**).

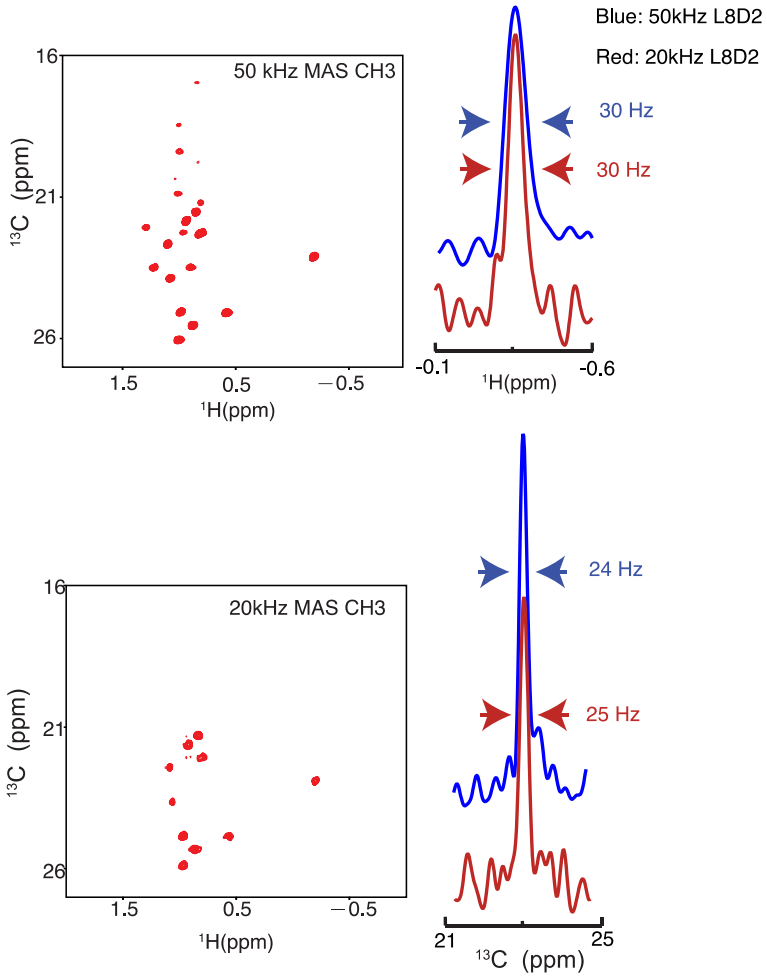

Figure 5.5. *^{13}C and ^{1}H line-widths at MAS frequencies of 20kHz and 50kHz respectively. A slice for L8 has been shown, however, all the residues show the same behaviour. A α-spectrin SH3 domain methyl group in valine and leucine CH_3 selectively protonated samples were used.*

Chapter 6

MAS Frequency Dependent of Cross Peak Intensities

6.1 Limits of resolution and sensitivity of proton detected MAS Solid State NMR at 111kHz in deuterated and protonated proteins.

MAS solid-state NMR is capable of determining structures of protonated solid proteins using proton-detected experiments. These experiments are performed at MAS rotation frequency of around 110 kHz, employing 0.5 mg of material.
Here, we compare 1H, 13C correlation spectra obtained from protonated and deuterated microcrystalline proteins at MAS rotation frequency of 111 kHz, and show that the spectral quality obtained from deuterated samples is superior to those acquired using protonated samples in terms of resolution and sensitivity. In comparison to protonated samples, spectra obtained from deuterated samples yield a gain in resolution on the order of 2 and 3 in the proton and carbon dimensions, respectively. Additionally, the spectrum from the deuterated sample yields approximately 3 times more sensitivity compared to the spectrum of a protonated sample. This gain could be further increased by a factor of 2 by making use of stereospecific precursors for biosynthesis.
Although the overall resolution and sensitivity of 1H, 13C correlation spectra obtained using protonated solid samples with rotation frequencies on the order of 110 kHz is high, the spectral quality is not optimal. We believe that experiments involving large protein complexes in which sensitivity is limiting will benefit from the application of deuteration schemes.

In this work, we compare ^{1}H, ^{13}C correlation spectra obtained from protonated and deuterated samples of a microcrystalline protein at a MAS rotation frequency of 111

kHz, and show that the spectral quality obtained from deuterated samples is superior to those acquired using protonated samples in terms of resolution and sensitivity.

Figure 6.1 shows the $^{1}H,^{13}C$ correlation spectra obtained for a protonated and two types of deuterated samples of a microcrystalline SH3 sample. The 25% and 5% deuterated RAP samples are prepared using u-[$^{2}H,^{13}C$]-glucose, and a D_2O based M9 growth medium that has been diluted with 25% and 5% H_2O to yield selective incorporation of protons at the aliphatic sites, respectively.(79) The SH3 sample in which pro-R or pro-S methyl groups of valine and leucine residues are randomly protonated was produced using α-ketoisovalerate as a precursor for amino acid biosynthesis.(80, 81)

6.1 Limits of resolution and sensitivity of proton detected MAS Solid State NMR at 111kHz in deuterated and protonated proteins.

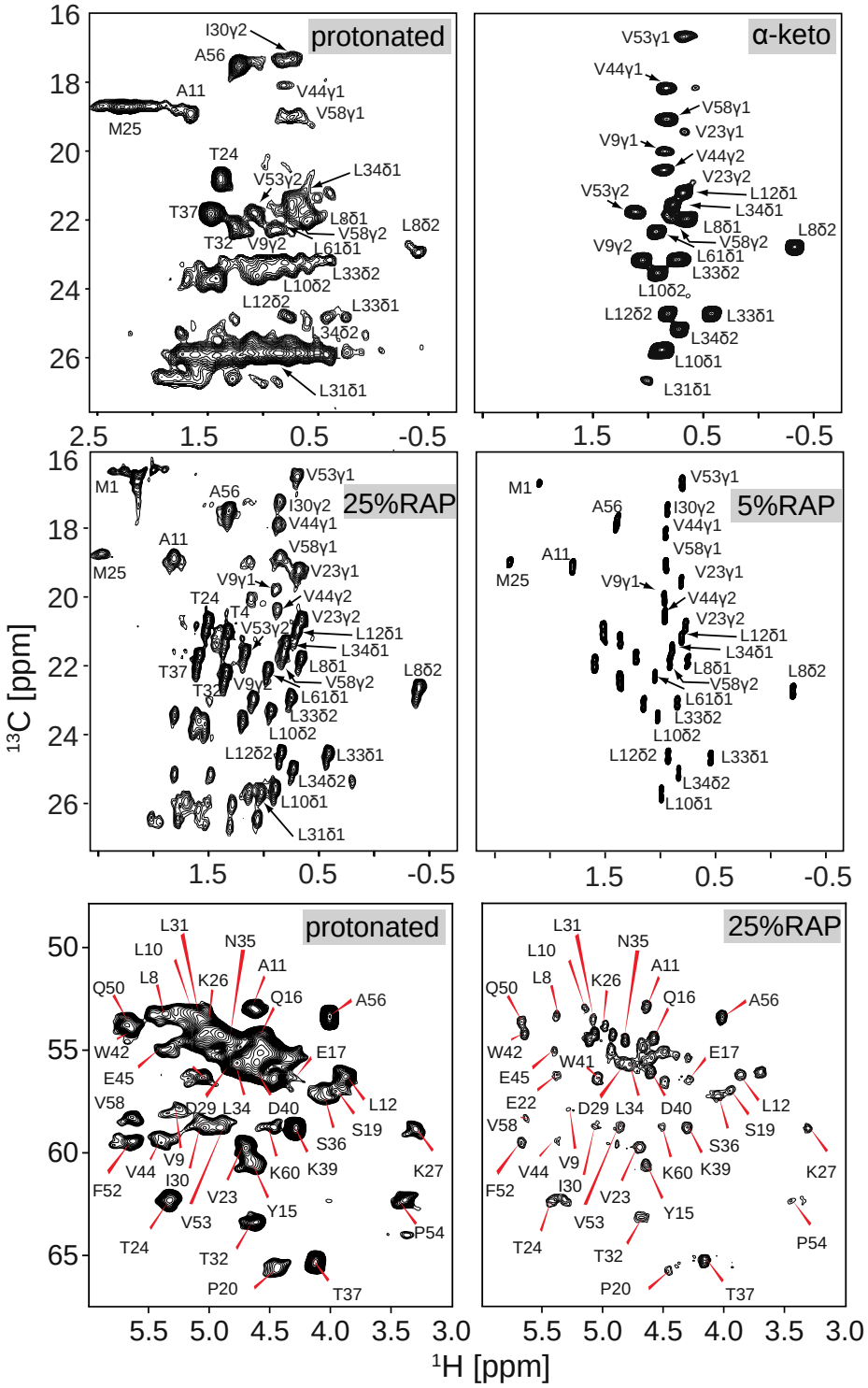

Figure 6.1. *Comparison of MAS solid-state NMR ^{1}H,^{13}C correlation spectra obtained for protonated and deuterated samples of microcrystalline SH3.* ***Top****: Methyl region of the spectra from protonated (left) and α-ketoisovalerate (right) samples (81) are shown.* ***Middle****: Methyl region of ^{1}H,^{13}C correlation spectra from 25% (left) and 5% (right) RAP (79) labelled samples are shown.* ***Bottom****: Backbone H$^{\alpha}$, C$^{\alpha}$ chemical shift correlations for protonated (left) and 25% RAP (right) labelled samples. The fully*

protonated and the valine, leucine selectively methyl protonated sample (α-ketoisovalerate labelled) were recorded at 11.8 T (500 MHz), using a 0.7 mm MAS probe with a MAS rotation frequency of 111 kHz. The spectra from the 25 % and 5% RAP labelled samples are represented for comparison.

We found that the cross peak intensities in the $^{1}H,^{13}C$ correlation spectra obtained using the protonated sample vary significantly in comparison to the spectra obtained using the two deuterated samples. In particular, several methyl peaks are broadened or missing in the spectrum from the protonated sample. Of note, the resolution of the spectrum from the 25% RAP labelled sample is compromised due to the presence of three methyl isotopomers CH_3, CH_2D, CHD_2 which yield isotope induced chemical shift changes.(17) However, this problem can be alleviated by using 5% RAP labelled sample. By contrast, the spectral region containing the α-carbon chemical shifts seems rather well dispersed at first sight, for both the protonated and the RAP labelled samples. However, in this case, the spectrum from the protonated sample yields significant overlap of cross peaks clustering around proton/carbon chemical shifts in the 4.7/55 ppm region.

6.1 Limits of resolution and sensitivity of proton detected MAS Solid State NMR at 111kHz in deuterated and protonated proteins.

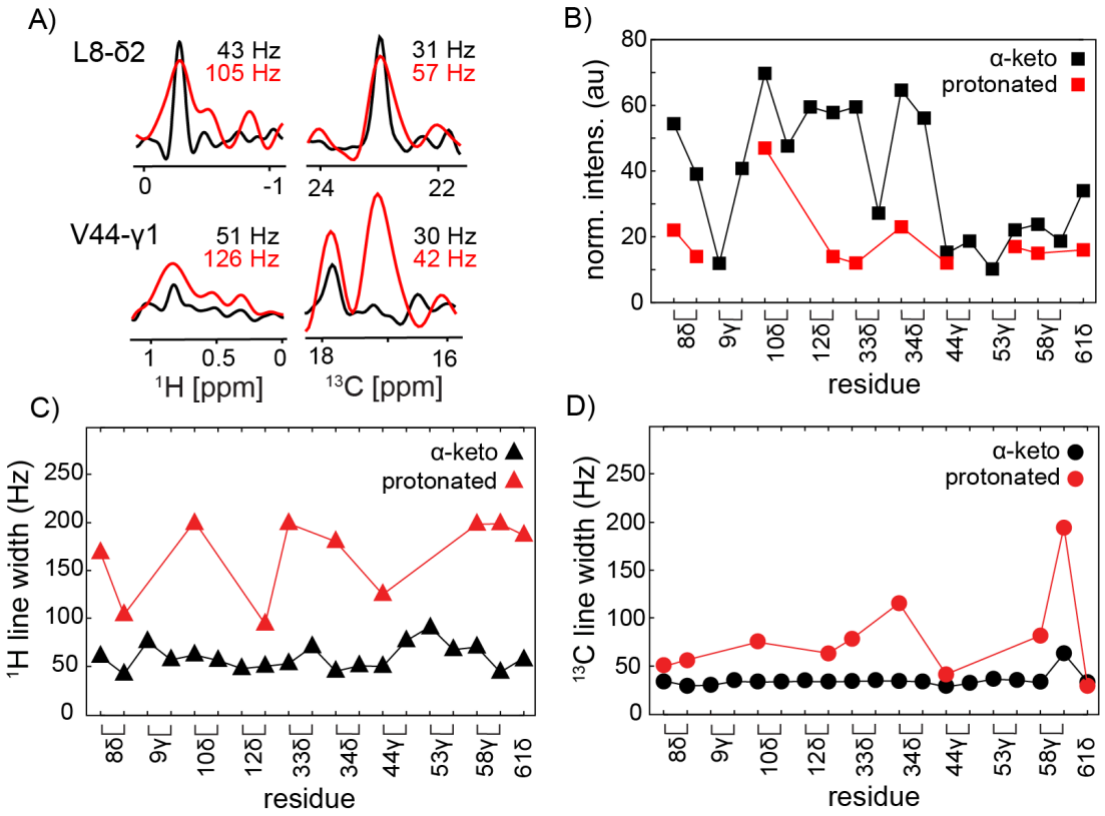

Figure 6.2. *A) 1D traces from the $^{1}H,^{13}C$ correlation spectra represented in Figure 1 along the ^{1}H and ^{13}C dimension for the residues L8 and V44. Spectra from the protonated and the α-ketoisovalerate labelled sample are depicted in red and black, respectively. B) Cross peak intensities for all methyl residues in the α-spectrin SH3 domain. The protonated sample is drawn in red, whereas spectra of the deuterated protein are shown in black. C, D) ^{1}H and ^{13}C line width for all methyl bearing residues in the α-spectrin SH3 domain for the protonated (red) and deuterated (black) SH3 sample.*

To quantify the differences between the spectra, we analysed the experimental ^{1}H and ^{13}C line widths and the sensitivity in detail. The results are summarized in **Figure 6.2**. Representative traces for two residues along the proton and carbon dimension of the correlation experiment are shown in **Figure 6.2A**. Comparing the spectra using α-ketoisovalerate labelled sample with the fully protonated sample, we observe an average gain in resolution on the order of 2 and 3 in the proton and carbon dimensions, respectively (**Figure 6.2 C, D**). We quantified the sample amount by performing ^{13}C 1D experiments using direct ^{13}C excitation, in order to account for the

difference in the amounts of material (~ 1.76 times) in the two rotors (**Figure 6.3**). This difference is used to normalize the cross peak intensities represented in **Figure 6.2B**. In total, we find approximately a 3x higher sensitivity for the α-ketoisovalerate labelled sample. This enhancement could potentially be further increased by an additional factor of 2 by making use of stereospecific precursors for amino acid biosynthesis(82).

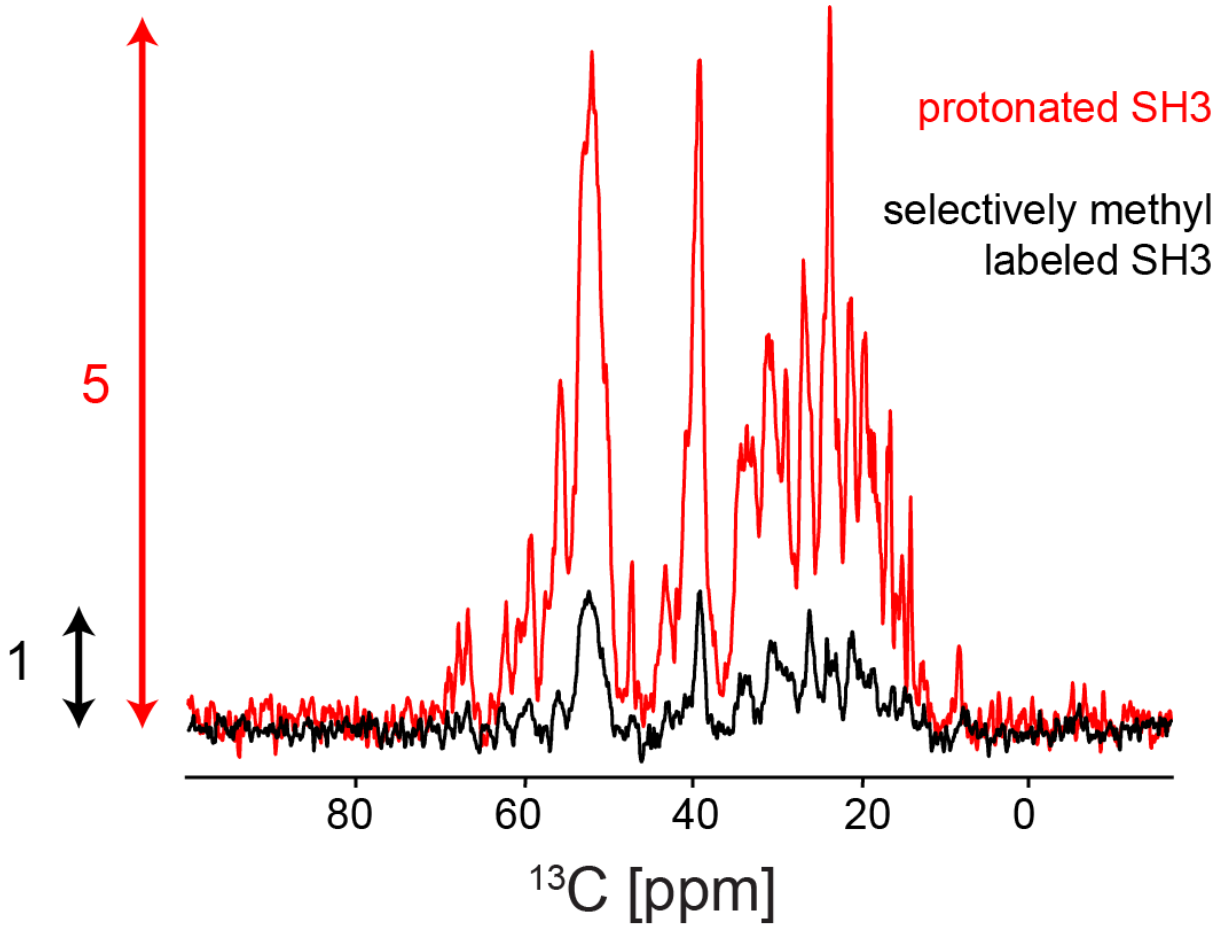

Figure 6.3. *Normalization procedure to determine the relative amount of material in the two 0.7 mm MAS rotors. One rotor contained protonated, microcrystalline SH3 protein, the second rotor was filled with deuterated, methyl protonated (α-ketoisovalerate) microcrystalline SH3. For both samples, ^{13}C-1D experiments have been recorded using ^{13}C direct excitation (relaxation delay = 30s). The protonated sample was recorded using 512 scans, whereas the deuterated protein was recorded with only 64 scans. The signal to noise ratio of the protonated sample is approximately 5 times larger in comparison to the signal to noise ratio achieved in the deuterated sample. To yield a similar noise level, the spectrum of the deuterated*

sample was scaled with √8 to account for the different number of scans. In total, the protonated sample should thus contain 5 / √8 = 1.76 more material in comparison to the deuterated sample.

As in last chapter we attribute the differences in peak intensities to the effective intra- and inter-methyl proton-proton dipolar couplings in the sample.

In the deuterated protein sample (back-substituted with 100 % protons at exchangeable sites), the average proton, proton dipolar couplings for amides are on the order of 7 kHz, and thus approximately 3x smaller in comparison to the effective dipolar couplings in the protonated sample. In the deuterated protein sample, high d^{RSS} values are obtained primarily in the turn regions (RT-loop around residue 20, the N-src-loop at residue 40, the distal loop with residues 47-49), for which short amide-amide distances are found. Apparently, a MAS rotation frequency of around 50 kHz is sufficient to yield efficient averaging of d^{RSS} for the amide protons in perdeuterated samples. Under these conditions, average $^{1}H^{N}$ line widths are on the order of 50 Hz.(83)

For the selectively methyl protonated sample, the effective proton, proton dipolar coupling is on the order of 27 kHz for methyl protons (**Figure 6.4**). This value is similar in magnitude to the Hα d^{RSS} values for a protonated sample. The $^{1}H,^{13}C^{\alpha}$ correlation spectrum for a protonated sample at a MAS rotation frequency of 111 kHz is of very high quality with an average proton line width on the order of 100 Hz. Suggesting that this spinning frequency is sufficient to yield efficient averaging of d^{RSS} in selectively methyl protonated samples. In contrast, the d^{RSS} values for methyl protons in a fully protonated sample are approximately 1.5x larger, indicating that MAS frequencies on the order of 160 kHz and above are necessary to yield methyl $^{1}H,^{13}C$ correlation spectra with acceptable resolution.

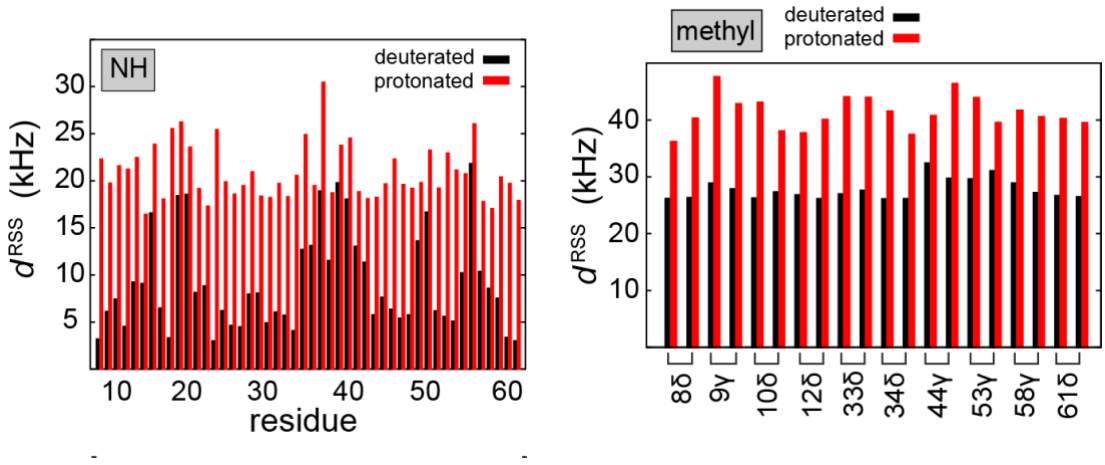

Figure 6.4. *Effective $^1H, ^1H$ dipolar interactions d^{RSS} for amide and methyl protons in the α-spectrin SH3 domain. The protonated and deuterated protein are represented in red and black, respectively. d^{RSS} has been calculated using a distance cut-off of 10 Å and (Eq. 1). For the calculation, the coordinate file 2nuz of the PDB database has been employed.*

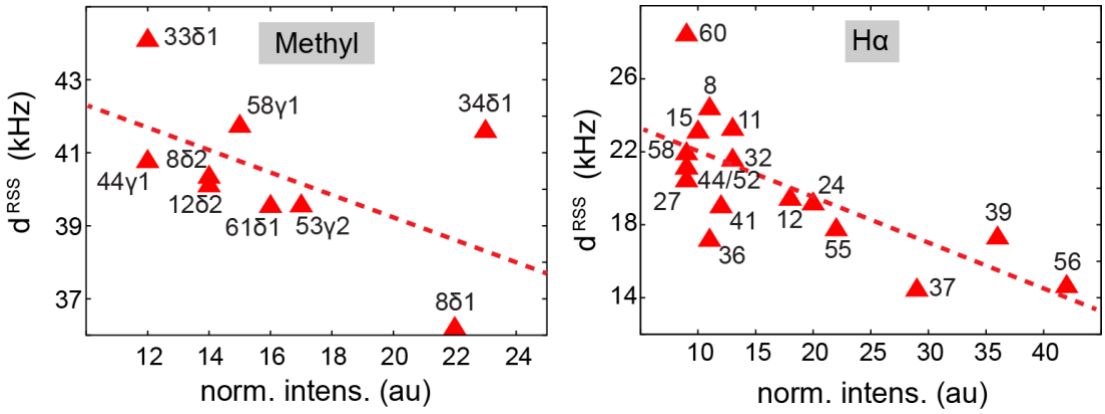

Figure 6.5. *Correlation plot between the effective proton, proton dipolar coupling d^{RSS} and the normalized peak intensities for methyl and Hα protons in a protonated SH3 sample.*

In order to test whether d^{RSS} is a good descriptor for the proton spin network in MAS solid-state NMR, the calculated effective proton, proton dipolar couplings is represented as a function of the normalized cross peak intensities in **Figure 6.5**. In general, higher peak intensities are found for smaller d^{RSS} values. Proton isotropic

chemical shifts are not included in the analysis. *n=0* rotational resonance effects may potentially yield line broadening, which can be alleviated at higher magnetic fields. For Hα, intensity values around 12 yield large variations in d^{RSS}.

The d^{RSS} from the methyl protons is not efficiently averaged at a MAS frequency of 110 kHz. This in agreement with a previous study, where it has been suggested that homogeneous interactions require MAS frequencies that are significantly larger (10 times) than the strength of the interaction.(84) In a typical protein sample, the effective proton, proton dipolar interactions are on the order of 15-45 kHz. In that sense, rotation frequencies greater than 300 kHz are required in order to efficiently average all homonuclear proton dipolar couplings.

Even though fully protonated samples would be ideal for spectroscopy, a brute-force approach bears risks for structure determination protocols: Resonances of protons, which are involved in strong dipolar interactions, are potentially weak or not observable. These residues do not yield long-range distance restraints. If especially long-range distance restraints are missing, structure calculation protocols might end up with a wrong fold.

We demonstrated that at MAS rotation frequencies of 110 kHz, the spectral quality obtained from selectively methyl protonated samples is superior in comparison to the spectrum obtained from a fully protonated sample. The deuterated sample yields a gain in resolution on the order of 2 and 3 in the proton and carbon dimension, respectively. Sensitivity is enhanced by approximately a factor of 3, which could be further increased by a factor of 2 by making use of stereospecific precursors for amino acid biosynthesis. We believe that in particular experiments involving large non-symmetric protein complexes in which sensitivity is limiting will benefit from such deuteration schemes.(18, 85)

Methods

The perdeuterated, selectively methyl group protonated microcrystalline SH3 sample was prepared as described previously.(81) In brief, expression was carried out in 100% D_2O M9 medium supplemented with ^{15}N-Ammonium Chloride and D-Glucose-^{13}C, d7. α-ketoisovalerate (2-Keto-3-(methyl-d3)-butyric acid-4-13C, 3-d sodium salt,

Sigma Aldrich) was added to the M9 minimal medium 1h prior to induction with 1mM IPTG (at OD_{600} 0.5-0.6). Subsequent to overnight expression, SH3 domain was purified via anion exchange and size exclusion chromatography as described before. For crystallization, pure protein was lyophilized and dissolved in 100% D_2O (final concentration: 8-10 mg/ml). Ammonium sulfate (dissolved in 100% D_2O) was added to a final concentration of 100mM and the pH was adjusted to 8.0 by adding NaOD. In order to produce the RAP labelled samples, the deuterated M9 minimal medium was supplemented with H_2O (25% H2O and 5 % H_2O for 25% and 5% RAP samples, respectively).(79) The protonated sample was prepared employing only protonated chemicals.

The proton detected CP based HSQC experiments for the protonated and α-ketoisovalerate labelled samples were carried out using 11.8 T static magnetic field (^{1}H Larmor frequency 500 MHz) at a H/C/N MAS probe of 0.7mm stator diameter. The best Hartmann-Hahn condition was found at nominal RF amplitudes of 70 kHz and 40 kHz on ^{1}H and ^{13}C, respectively. A linear ramp on ^{1}H with 70-100% amplitude was used for ^{1}H-^{13}C CP (contact time 800 us) and 100-70% amplitude for ^{13}C-^{1}H CP (contact time 500us), respectively. For hard pulses, B_1 amplitudes of 156 kHz and 100 kHz were used for ^{1}H and ^{13}C, respectively. Low power decoupling using swept TPPM ($\omega_{1H}/2\pi$ = 30 kHz)(86) during t_1 and WALTZ16 ($\omega_{13C}/2\pi$ = 5 kHz) during acquisition was used. Water suppression was achieved using MISSISIPPI with $\omega_{1H}/2\pi$ = 30 kHz for 300ms. For all the experiments, the real sample temperature was calibrated to 288 K using DSS (set temperature 263 K with 480 l/h VT gas flow). The acquisition times in the F1 and F2 dimensions in all the experiments were set to 70ms (^{13}C, ^{1}H) and the relaxation delays (d_1) were set to 0.5s and 1.5s in the protonated and α-ketoisovalerate samples, respectively.

The spectrum of the 25% RAP labelled sample was recorded at 20 T (850 MHz) with a MAS frequency of 40 kHz. Whereas the spectrum of the 5% RAP sample was recorded at 14.1 T (600 MHz) with a MAS frequency of 20 kHz. Scalar coupling based HMQC type experiments were used. 2-3 kHz of WALTZ16 decoupling was used during proton detection.

6.2 MAS rotations frequencies beyond 300kHz are necessary to yield maximum sensitivity

Despite the success of proton detected experiments at very high MAS rotation frequencies, it is not clear which gains in sensitivity are to be expected if it would be possible to increase the MAS rotation frequency even further. The general benefits for proton detection have been discussed extensively in the literature (87, 88). Resolution of proton spectra in solids has always been an Achilles heel. In the recent years, two strategies have been applied to overcome this issue. On one hand, partial site-specific deuteration (17, 19, 66, 89-93), on the other hand design of probes that yield increased rotation frequencies up to 111 kHz as of today.

It is not clear which gains in sensitivity can be achieved when faster spinning is employed. The relative gain in sensitivity while detecting protons instead of other heteronuclear has been discussed in the literature (94), (95). Following the reciprocity principle(96), the detection sensitivity is proportional to the transfer efficiency and the full width at half height ($\Delta\nu_{1/2}$), which change with MAS frequency employed in the experiments. However, the maximum achievable sensitivity for a given sample is hard to predict. The standards for resolution are set by comparison to spectra obtained from deuterated samples. The expected gains in terms of sensitivity are not well understood as also perdeuterated samples yield a strong increase in sensitivity at faster MAS. In a recent study (97), we have shown that deuterated samples yield higher sensitivity and better resolution in comparison to a completely protonated protein when ^{1}H-^{13}C correlations are recorded under the fastest MAS frequency commercially available (111 kHz). This observation is attributed to the reduced effective dipolar-coupling (d^{RSS}) present among the residual protons in the deuterated sample(98). It is observed that for a α-ketoisovalerate CH_3 labelled SH3 sample (80), 111 kHz MAS is inadequate in averaging out the effect of d^{RSS}. However, the apparent transverse relaxation rate constant of protons (T_2') increases as the MAS frequency increases due to better averaging of d^{RSS}.

6.2 MAS rotations frequencies beyond 300kHz are necessary to yield maximum sensitivity

On the contrary to solution NMR, both dipole-dipole and scalar couplings can be used for coherence transfer in the solid state. Dipolar coupling between two nuclei in solids are often found stronger than the corresponding scalar coupling constants. Therefore, the time required for coherence transfer is usually longer in the case of scalar coupling based methods. During coherence transfer, second order relaxation processes take toll in reducing the overall efficiency of NMR experiments. For a 100% ^{15}N-^{1}H back exchanged solid protein sample, dipolar based transfers (^{15}N to ^{1}H or back) are preferred when operating at 60 kHz MAS or lower(83), whereas the efficiency of scalar based transfers perform equally well at MAS frequency of 111 kHz (21, 99, 100). In protein resonance assignment experiments, a variety of coherence transfer steps between different nuclei are involved such as ^{15}N -> Cα, ^{15}N-> CO, CO-> Cα, Cα-> Cβ. Such coherence transfers can be carried out using both scalar and dipolar based transfer methods. Penzel et al has(100) thoroughly compared the efficiency of all such transfer steps using scalar and dipolar based methods for a model Ubiquitin sample at 111 kHz. It turns out that the relative efficiency of such transfers depends on the apparent transverse relaxation time constants of the involved nuclei where magnetization is stored for most of the time. As a result, dipolar coupling based methods are more attractive at slower MAS frequencies as coherence transfer strategies in solids, since scalar coupling based methods suffer more severely from relaxation effects. However, when the T_2's get longer as a result of faster MAS and/or due to less proton density in a sample, INEPT based coherence transfer methods perform better.

In the fast MAS regime, the optimum Hartmann-Hahn (HH) matching required for cross polarization (CP) is very narrow and difficult to maintain in the case of probe detuning. Homogeneity of *rf* fields becomes extremely crucial when experiments are carried out at fast MAS frequency and high B_0 fields, since the *rf* fields become a significant fraction of the MAS frequency(91). It is often found that the *rf* profiles in solid state NMR probes are inhomogeneous across the sample. In such situations, the HH matching conditions cannot be fulfilled simultaneously everywhere in the rotor. It is possible to restrict the sample volume to the centre of the detection coil(101), using coil with variable pitch and width of winding wire(102) or using a coil that is resonant in a wide range of frequencies(91). In addition, the HH condition gets

broadened and results in significant drop in sensitivity of the CP experiments when the *rf* fields in different channels are not coincident. On the other hand, INEPT based methods are easier to implement since the transfer period only depends on the scalar coupling constant between the involved spins and the transverse relaxation rates. The deleterious effects of *rf* inhomogeneity are smaller as INEPT based experiments rely upon infinitesimal hard pulses.

Experimentally we find indeed the INEPT based methods perform significantly better than the CP based experiments; all experiments shown in this work are recorded using INEPT based magnetization transfer steps. A comparison of CP and INEPT based ^{1}H-^{13}C correlation spectra recorded at 111 kHz MAS is provided in the supporting information (**Figure 6.7**).

The cross peak intensities of ^{1}H-^{13}C correlation spectra increase as a function of MAS frequencies (**Figure 6.6**). Only a few cross peaks can be observed at 40 kHz MAS, whereas the number of cross peaks increase significantly at 70 kHz MAS and it is possible to observe all the expected valine, leucine cross peaks at 111 kHz MAS.

6.2 MAS rotations frequencies beyond 300kHz are necessary to yield maximum sensitivity

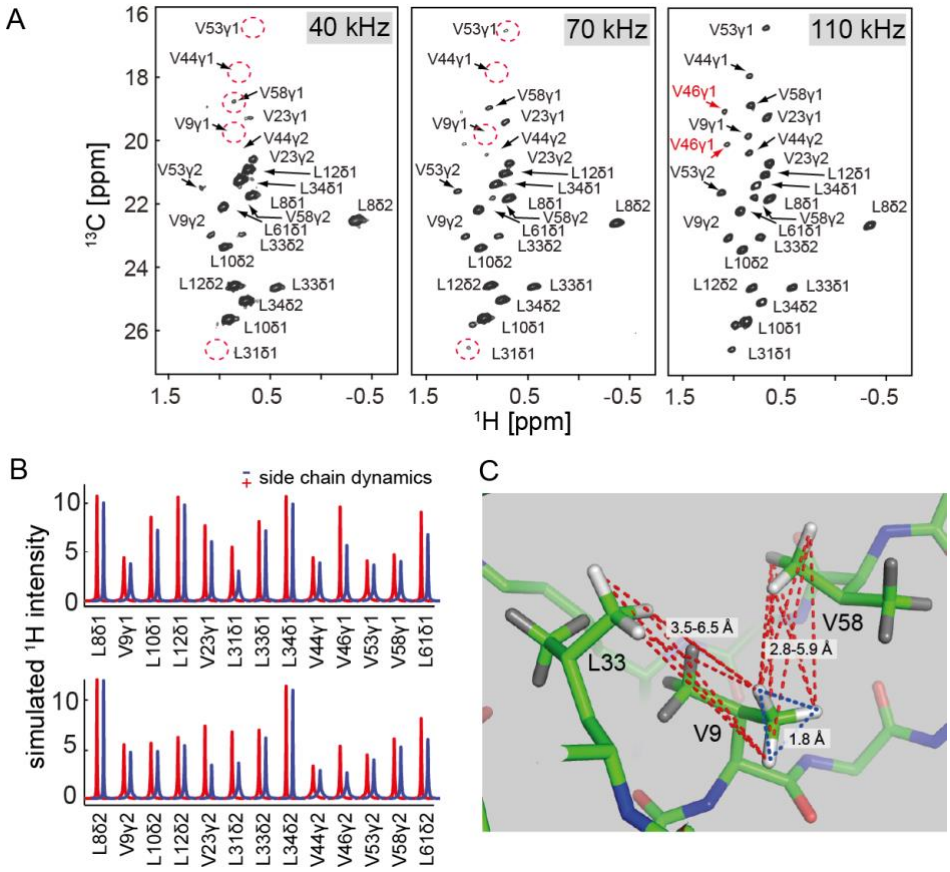

Figure 6.6. *(A) ^{1}H,^{13}C correlation spectra for a selectively methyl protonated micro-crystalline sample of the chicken α-spectrin SH3 domain. The protein was produced by adding α-ketoisovalerate to the perdeuterated M9 minimal medium yielding CH_3 isotopomers (80). Experiments were recorded at MAS frequencies of 40, 70 and 111 kHz using INEPT for magnetization transfer. The measurements were performed at 11.8 T (500 MHz) using a 0.7 mm MAS probe. All spectra were recorded and processed using the same parameters and plotted with the same contour levels (setting the maximum contour level to the cross peak of L8δ2). (B) Simulated ^{1}H spectra for every methyl group in the protein assuming a MAS rotation frequency of 110 kHz (black: without side chain dynamics; red: with side chain dynamics using experimental order parameter values (90)). Calculations are performed using the program SIMPSON (103, 104). (C) In the simulations, a 9-proton spin system is considered using the atomic coordinates from the PDB file of the α-spectrin SH3 domain (2NUZ). Inter-methyl interactions were treated using methyl pseudo-atoms.*

We have chosen selectively methyl protonated protein samples, as this kind of labelling allows to reduce the complexity of the numerical simulations and restrict the

number of involved proton spins to < 10. We first numerically simulated the proton line shapes (**Figure 6.6B**), considering the explicit geometry of the atoms from the α-SH3 structure, PDB ID: 2NUZ (105). The numerical simulations were carried out using 9 proton spins employing the program SIMPSION (103, 104). Thus, two neighbouring valine or leucine residues are accounted for (**Figure 6.6C**). Typical dipolar couplings are on the order of -10.5 kHz and < 5.7 kHz for intra- and inter-methyl dipolar interactions, respectively. As the protein was re-crystallized from D_2O, no additional exchangeable protons had to be taken into account. Additional simulations for isolated methyl groups, as well as for two methyl groups that are dipolar coupled are presented as part of the Supporting Information (**Figure 6.10-6.16**).

In the simulations, $^1H,^1H$ dipolar interactions are scaled due to the three-fold rotation around the C-C axis. We have found recently, that there is significant motion in the protein hydrophobic core (81, 90, 106). We have employed REDOR derived order parameters (107), and repeated the simulations to find out how dynamics affects the sensitivity of the MAS dependent proton spectra. In the simulations, the order parameters have been employed to yield a re-scaling of the intra-methyl $^1H,^1H$ dipolar interactions. Dynamics of inter-methyl dipolar interactions are not taken into account.

Comparison of CP and INEPT efficiency at 111 kHz MAS:

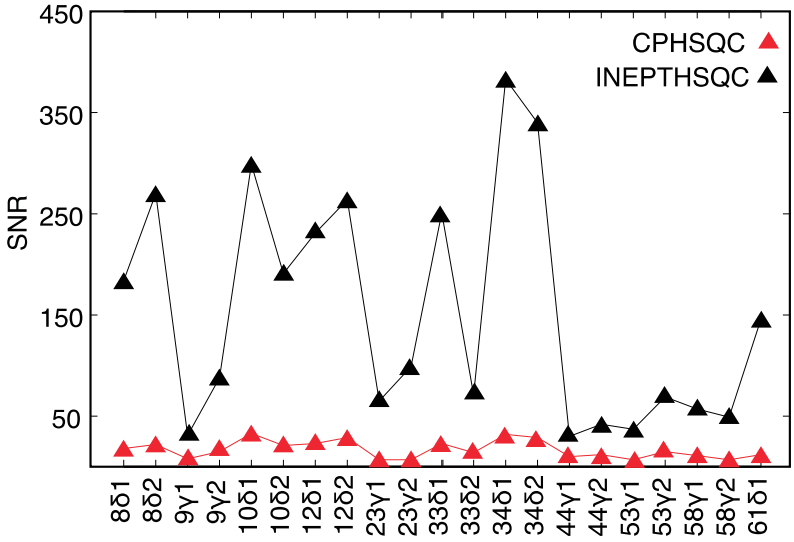

Figure 6.7a *INEPT and CP based ^{13}C-^{1}H correlation spectra recorded at 111 kHz MAS frequency are shown in* ***Figure 5.6*** *(A and B). Signal-to-noise ratio (SNR) for the INEPT based correlation for most of the residues is higher compared to CP based experiments.*

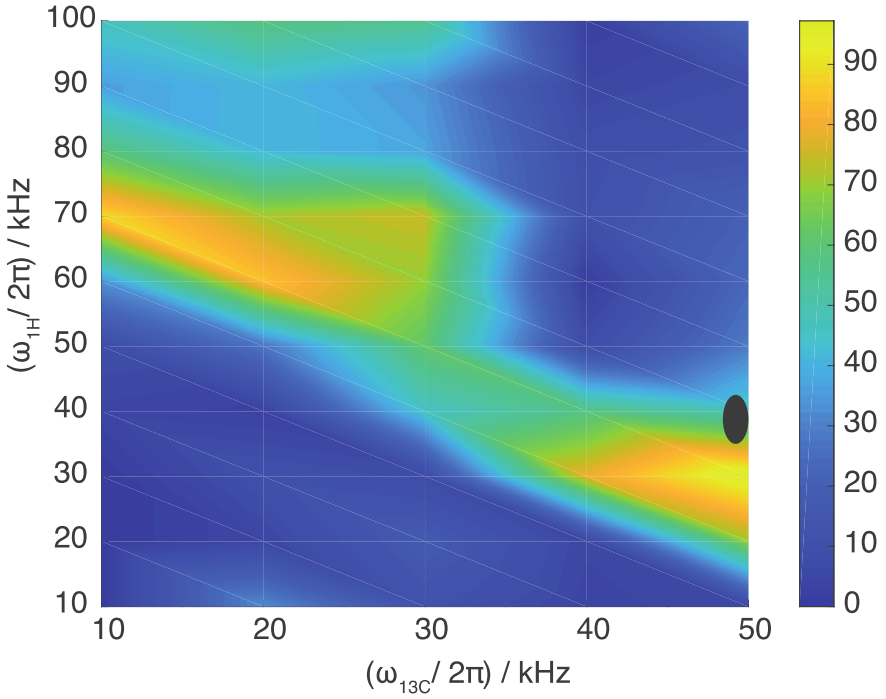

Figure 6.7b *^{1}H -> ^{13}C CP efficiency as a function of rf amplitudes at 90 kHz MAS frequency. The black symbol represents the actual value that was used for experiments. The CP experiment (^{1}H-> ^{13}C-> ^{1}H) using the optimised rf amplitudes (black dot) yields about 6% intensity when compared to a proton Bloch decay spectrum.*

To validate whether the simulation can accurately describe the experiments, we correlated the simulated and the experimental peak intensities. The site-specific variations in SNR in the INEPT based correlation can be attributed to differences in the ^{1}H and ^{13}C line widths, and to differences in the proton T_2' relaxation times resulting in different transfer efficiencies. The site-specific proton T_2' relaxation times are shown in **Figure 5.8.** We find that proton T_2' relaxation times vary significantly presumably as a function of the proton density around a particular methyl group. As expected, ^{1}H T_2' increases with faster MAS.

6.2 MAS rotations frequencies beyond 300kHz are necessary to yield maximum sensitivity

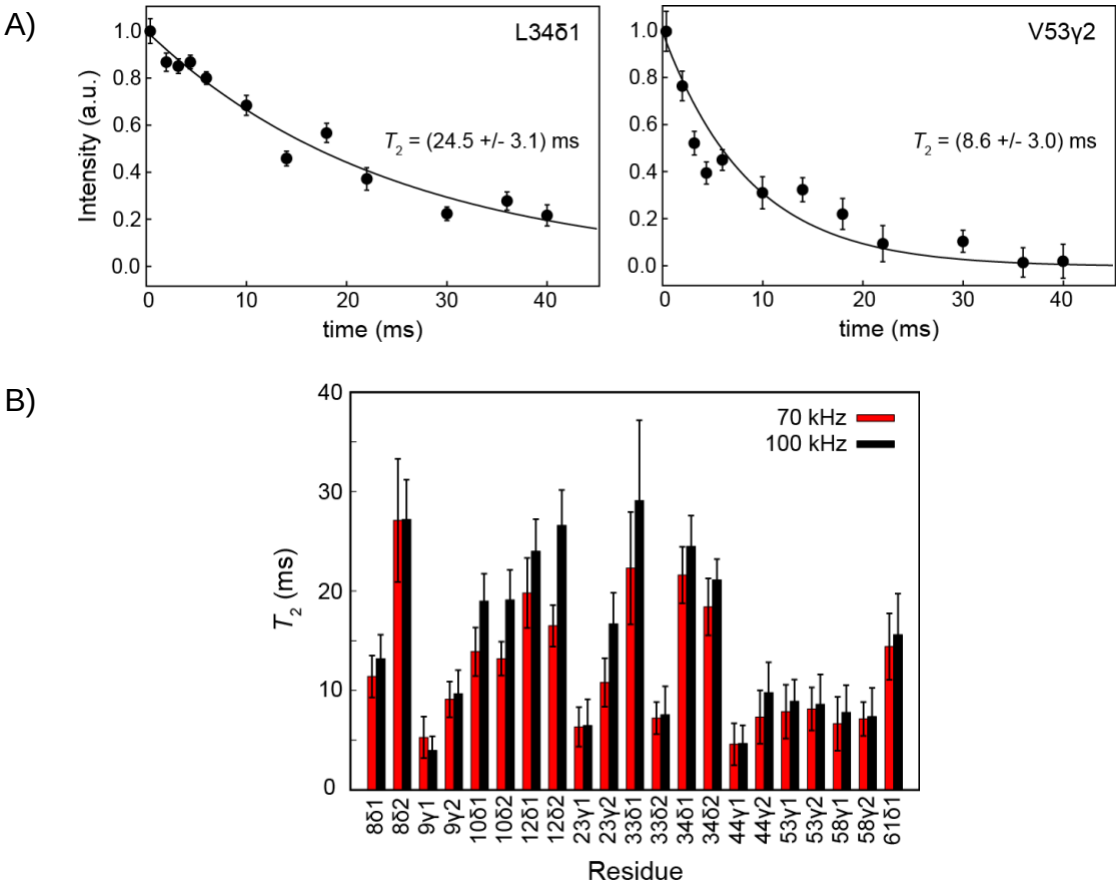

Figure 6.8. *(A) Representative site-specific ^{1}H T2' decay curves for V44γ1 and L34δ1 in α-ketoisovalerate CH_3 labelled SH3. (B) ^{1}H T2' as a function of the amino acid sequence. Experiments were recorded at a MAS frequency of 100 kHz at a magnetic field strength of 11.8 T (500 MHz).*

To account for the T_2' signal decay in the INEPT based experiments, we corrected the simulated intensities according to

$$\mathrm{INT}_j^{\mathrm{exp}}(i) = k_j \mathrm{INT}_j^{sim}(i)\ \mathrm{e}^{-\mathrm{D}/T_2'} \qquad \text{(Eq. 1)}$$

where κ_j is an empirical fitting factor that has been determined for each experiment (recorded at the MAS rotation frequency *j*). Δ refers to the total INEPT magnetization transfer delay, and was set to 7.9 ms in all experiments. κ_j is obtained by analysis of the correlation diagrams in **Figure 6.9 A-C**. To normalize the simulations, we followed the following protocol: We find that at a MAS frequency of 10 MHz and above the intensities of the simulated spectra do not improve any further. The simulated FID was then folded with an exponential line broadening of 20 Hz. The

maximum intensity of the respective Fourier transformed spectrum was set arbitrarily to 100. To compare the intensities of the simulated spectra at different MAS rotation frequencies, we assumed that the integral over the total spectral range for all spectra is equal, and used this to re-normalize the peak intensities at the slower MAS rotation frequencies. For each MAS frequency (70, 90 and 111 kHz), we obtain a linear fit yielding an excellent correlation ($R^2 > 0.7$) between experiments and numerical simulations.

Since the numerical simulations describe the proton spectra and their relative intensities for each MAS frequency rather well, we set out next to predict the MAS frequency that is necessary to completely average out the proton-proton dipolar interactions for these kinds of samples. **Figure 6.9D, E** show simulated (black) and experimental (red) proton peak intensities for a few representative residues in the SH3 domain sample. Simulated MAS dependent proton spectra for all methyl groups of the valine and leucine residues of the α-spectrin SH3 domain are represented in the supporting information (**Figure 6.16**) in the MAS frequency range from 10 kHz to 10 MHz. Matched simulated and experimental intensities for all experimentally accessible valine and leucine methyl groups are shown in **Figure 6.17**.

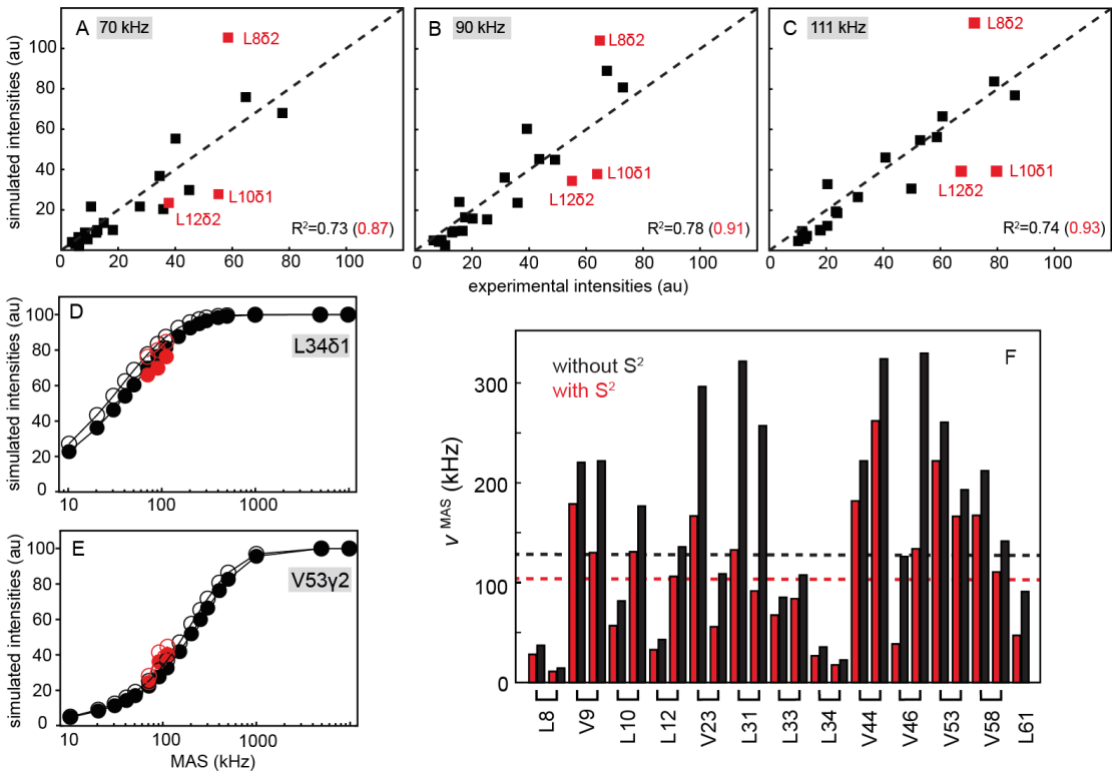

Figure 6.9. *Comparison of simulated and experimental cross-peak intensities at 70 (A), 90 (B) and 111 kHz (C) MAS and at an external magnetic field of 11.8 T (500 MHz), respectively. The dashed line represents a linear fit. The correlation coefficient improves significantly if the outliers (L8δ2, L10δ1 and L12δ2) are excluded from the fit (in red). (D), (E) Simulated intensities (black), as well as experimental intensities (red) for the methyl groups L34δ1 and V53γ2 as a function of the MAS frequency. Inclusion of side chain dynamics (open symbols) yields higher proton intensities at a given MAS frequency, as the strength of the proton dipolar coupling network is reduced due to local structural fluctuations. (F) Characteristic MAS frequencies ν^{MAS} (frequency that yields 50% of the maximum possible intensity) for each methyl group in α-spectrin SH3. The average characteristic MAS frequency in the absence (black) and in the presence of dynamics (red) amounts to (135.0 ± 88.0) kHz and (104.0 ± 68) kHz, respectively, and is indicated with a dashed line.*

The simulated MAS dependent intensity curves show all a sigmoidal like shape in the semi-log plots. To simplify the quantitative description of the MAS dependent peak intensities, we introduce the characteristic MAS frequency ν^{MAS} which is defined as

the MAS frequency that is required to yield 50 % of the maximum possible intensity in the numerical simulations for a given residue (**Figure 6.9F**). We find that the characteristic MAS frequency ν^{MAS} covers a relatively broad range of frequencies. For V44γ2, a MAS frequency of 20 kHz is sufficient, whereas for V53γ1 a rotation frequency of 324 kHz is necessary to yield 50 % of the maximum possible signal intensity or amplitude.

In order to account for side chain dynamics and its consequences on scaling of the $^{1}H,^{1}H$ dipolar couplings, we repeated the simulations, assuming the experimental values for methyl side chain order parameters (90). As only very few residues (V23, L31 and V46) undergo significant side chain dynamics, inclusion of side chain dynamics has a negligible effect on the matching of experimental and simulated intensities. Surprisingly, we find that these dynamic residues have proton intensities that are lower than expected or are even only barely visible. We speculate that these side chains undergo ns-μs dynamics (108). The intensity of their proton methyl peaks is presumably affected by transverse relaxation effects.

d^{RSS} is a simple descriptor of the dipole-dipole coupling environment and does not include explicit chemical shifts, the spin topology and the dependence on the MAS frequency. In order to find out if d^{RSS} can be employed to characterize the proton spin density, we have represented the characteristic MAS frequency ν^{MAS} as a function of d^{RSS}. Even though d^{RSS} drastically simplifies the proton spin system, we find that it describes the experimental results rather well (**Figure 6.18**). We note that the proton spectrum resulting from a methyl group ($^{13}CH_3$) under MAS is found sensitive to chemical shift differences, relative orientation of the methyl groups and MAS frequency (**Figure 6.13-15**).

We have simulated proton spectral line shapes and intensities of the methyl groups in a selectively methyl protonated (CH3) microcrystalline sample of the chicken α-spectrin SH3 domain. The simulated spectra were validated by solid-state NMR experiments recorded at MAS rotation frequency of 70, 90 and 110 kHz. We find that the characteristic MAS frequency ranges from as low as 20 kHz up to 324 kHz with the average value of (135.0 ± 88.0) kHz at an external magnetic field strength of 11.7 T (500 MHz), and to yield 50 % of the maximum peak intensity. Faster rotation

frequencies are presumably required to achieve dipolar decoupling for fully protonated protein samples.

MATERIALS AND METHODS

The perdeuterated, selectively methyl protonated sample of the micro-crystalline SH3 domain was prepared as described previously (81). In brief, expression was carried out in 100 % D_2O M9 medium, supplemented with ^{15}N-ammonium chloride and u-[^{2}H, ^{13}C]-D-glucose. α-ketoisovalerate (2-keto-3-(methyl-d_3)-butyric acid-4-^{13}C sodium salt, Sigma-Aldrich) was added to the M9 medium 1 h prior to induction with 1 mM IPTG (at OD_{600} 0.5-0.6). Subsequent to overnight expression, the SH3 domain was purified via anion exchange and size exclusion chromatography as described before. For crystallization, pure protein was lyophilized and dissolved in 100 % D_2O (final concentration: 8-10 mg/ml). Ammonium sulfate (dissolved in 100 % D_2O) was added to a final concentration of 100 mM and the pH was adjusted to 8.0 by adding NaOD.
All NMR experiments were carried out using a 0.7 mm H/C/N triple resonance MAS probe operating at a static magnetic field of 11.8 T (500 MHz ^{1}H Larmor frequency). RF field strengths of 156 kHz and 100 kHz on the ^{1}H and ^{13}C channel was applied for hard pulses, respectively. For decoupling, a ^{1}H π pulse was applied in the middle of t_1, and WALTZ-16 ($\omega_{13C}/2\pi$ = 5 kHz) during acquisition. As the sample was re-crystallized from 100 % D_2O, no solvent suppression was employed. For all experiments, the effective sample temperature was adjusted to 15 °C, using DSS and the residual water signal for calibration (109). The acquisition times in the F1 and F2 dimensions (^{13}C, ^{1}H) were set to 70 ms. A recycle delay of 1.5 s was employed. ^{1}H T_2' relaxation times were measured employing a CP based experiment, inserting a (τ-π-τ) refocussing element on the ^{1}H channel prior to the ^{13}C t_1 evolution period. The pulse sequence that have been employed are represented in the supporting information (**Figure 6.19**). The ^{1}H T_2' data was acquired as an interleaved pseudo 3D experiment to minimize systematic errors in the measurement. The site specific intensities were extracted using NMRGLUE (110) based python scripts and fitted with a mono exponential function to obtain the ^{1}H T_2' values.
In order to estimate the MAS frequency that is necessary to average residual methyl proton dipolar interactions for a specific methyl group in the α-SH3 domain, we

simulated first numerically the proton line shapes considering the explicit geometry of the atoms in the structure, PDB-ID: 2NUZ (105). For the calculation, we assumed that the protein is perdeuterated except for the methyl groups of valine and leucine residues. The amide groups were assumed to be fully deuterated, as the sample was recrystallized from 100 % D_2O. Protein biosynthesis yielded labelling of $^{13}CH_3$ in only one of the two valine / leucine methyl groups, while the other methyl group is NMR silent $^{12}CD_3$. (80).

The numerical simulations were carried out using a 9-proton spin system, thus accounting for two neighbouring methyl containing side chains. Since the incorporation of $^{13}CH_3$ and $^{12}CD_3$ into the pro-R and pro-S position occurs at random, selecting the two closest neighbouring methyl groups for a given site overestimates the involved dipole-dipole couplings. Using the program SIMPSON (103, 104), we have therefore calculated the methyl proton spectra for all permutations to reflect the actual isotope labelling of the sample. Subsequently, the average spectrum has been calculated.

In the following parts, Figures are provided to give more information about proton peak shape simulation.

6.2 MAS rotations frequencies beyond 300kHz are necessary to yield maximum sensitivity

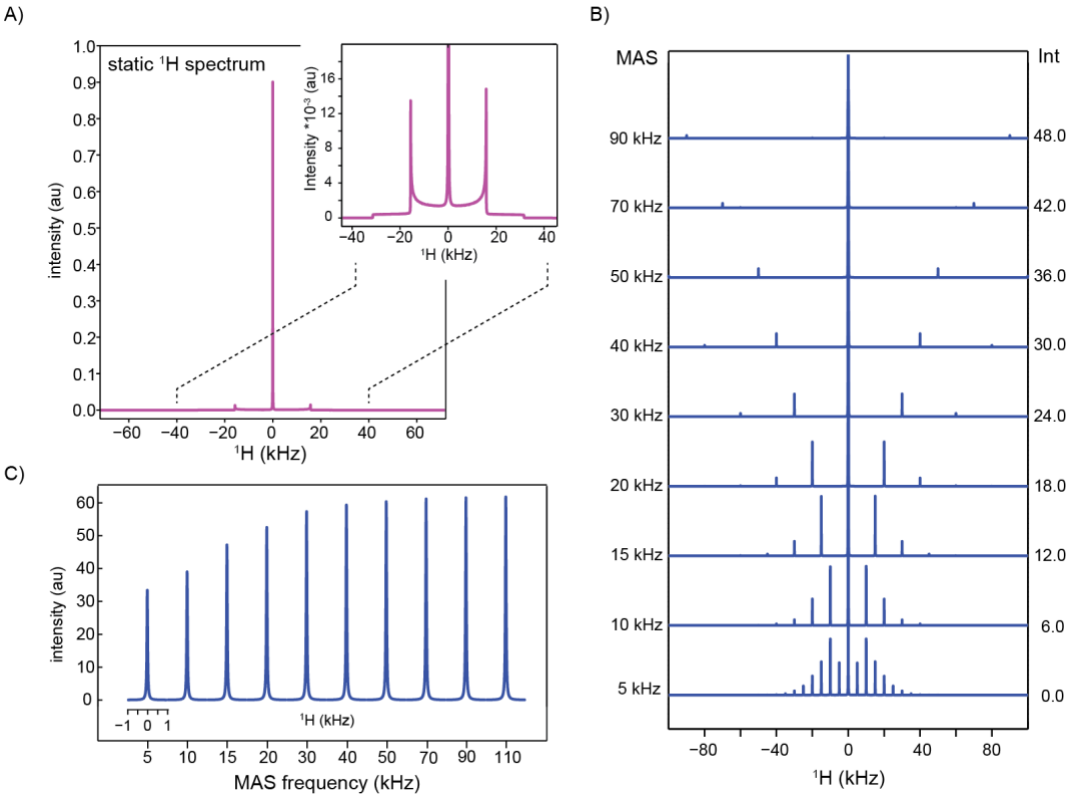

MAS freq [kHz]		*central*	*first SSB*	*second SSB*
5	*amplitude*	*32.13*	*2.90*	*4.96*
	integral	*410.8*	*37.8*	*63.8*
10	*amplitude*	*37.52*	*7.04*	
	integral	*481.2*	*90.8*	

***Figure 6.10**. **Simulated ^{1}H spectra of an isolated methyl group**. A) Static methyl proton spectrum. The ^{1}H,^{1}H dipolar interaction within the methyl group is scaled to -1/2 due to the 3-fold rotation around the C-C axis (i.e. 10.500 kHz). The center peak is most prominent. In order to recognize the dipolar Page pattern in the baseline, the spectrum is shown magnified in the inset. B) MAS dependent ^{1}H spectra of an isolated methyl group. The focus is put into the baseline. MAS yields a spinning sideband pattern. The simulations are separated vertically by 6 kHz (intensity scale). The intensities of the center band and the 1st and 2nd spinning side bands are tabulated below the figure. The total integral over full spectral range is 767.8. The maximum intensity (in case of a non-decaying signal that is folded with 20 Hz line*

broadening) amounts to 59.5. C) MAS dependent ^{1}H intensities. a spectral window of 2 kHz is shown.

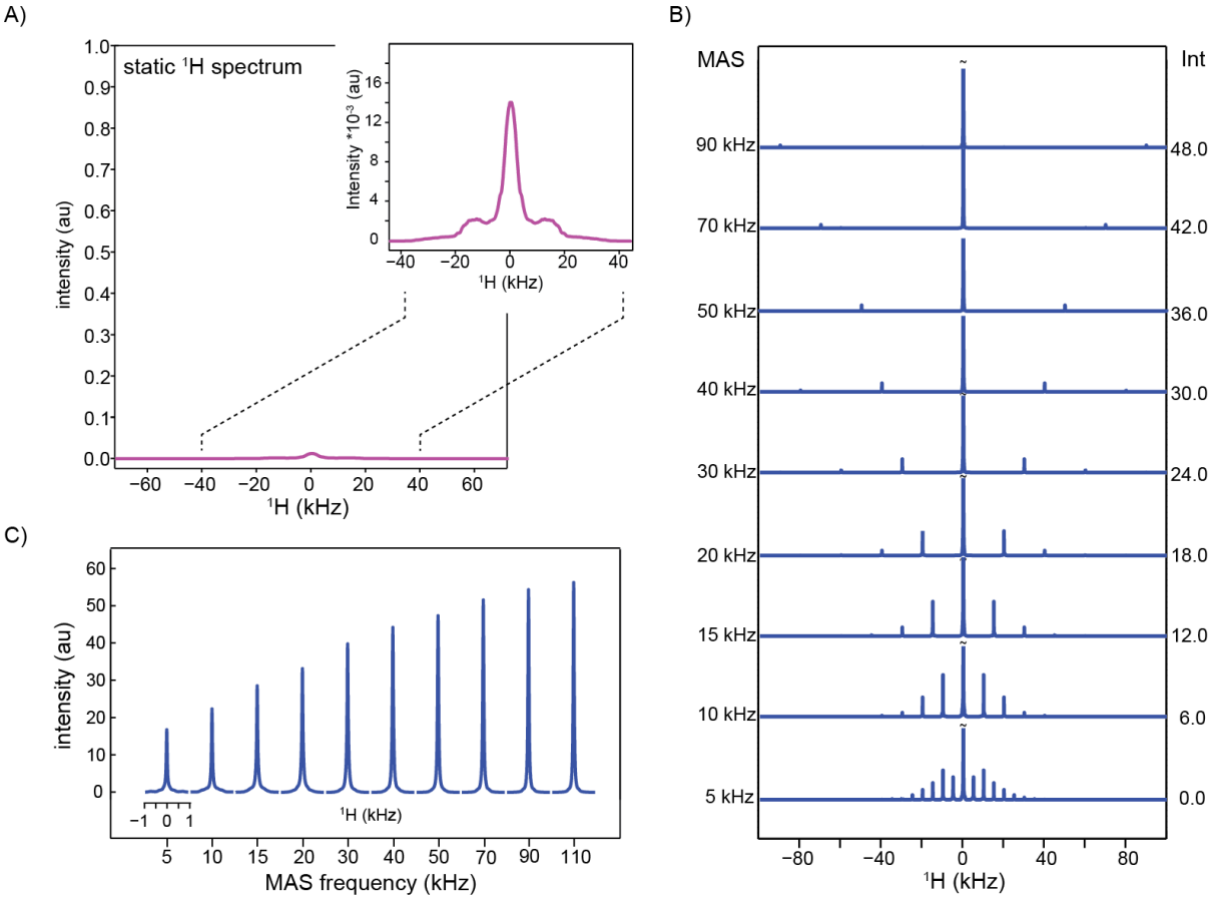

MAS freq [kHz]		*central*	*first SSB*	*second SSB*
5	*amplitude*	*16.23*	*1.97*	*2.55*
	integral	*353.3*	*65.1*	*65.2*
10	*amplitude*	*21.59*	*3.63*	
	integral	*470.8*	*93.9*	

Figure 6.11. MAS frequency dependence of the ¹H lineshape for a methyl group interacting with a second methyl. *A) Static ¹H spectrum. In contrast to the scenario in which only a single methyl group is considered, the static proton spectrum is very broad with significant intensity over a range of 40 kHz. Methyl-methyl interactions introduce a homogeneous Hamiltonian in the sense of Maricq and Waugh (111). In the simulation, a chemical shift difference of 200 Hz, a inter-methyl proton-proton dipolar constant of 2000 Hz and the relative methyl-methyl orientation (C) as described in* ***Figure 6.13*** *below has been employed. Qualitatively, a similar behaviour is obtained for other orientations. B) Under MAS, the intensity of the powder pattern distributes into a spinning sideband manifold, with more and more*

intensity cumulating in the center band at faster spinning. The simulations are separated vertically by 6 kHz (intensity scale). The intensities of the center band and the 1st and 2nd spinning side bands are tabulated below the figure. The total integral over full spectral range is 767.8. The maximum intensity (in case of an non-decaying signal that is folded with 20 Hz line broadening) amounts to 59.5. The simulations are thus directly comparable to the simulations shown in ***Figure 6.10****. C)* ^{1}*H methyl spectrum focussing on the center band. The same scale and normalization as in* ***Figure 6.10*** *has been employed. The full width at half maximum is very similar in case of a single methyl and two dipolar coupled methyl groups. However, the intensity at the base of the peak is distributed over a large spectral range if a methyl group interacts with a neighbouring methyl group (see* ***Figure 6.12****).*

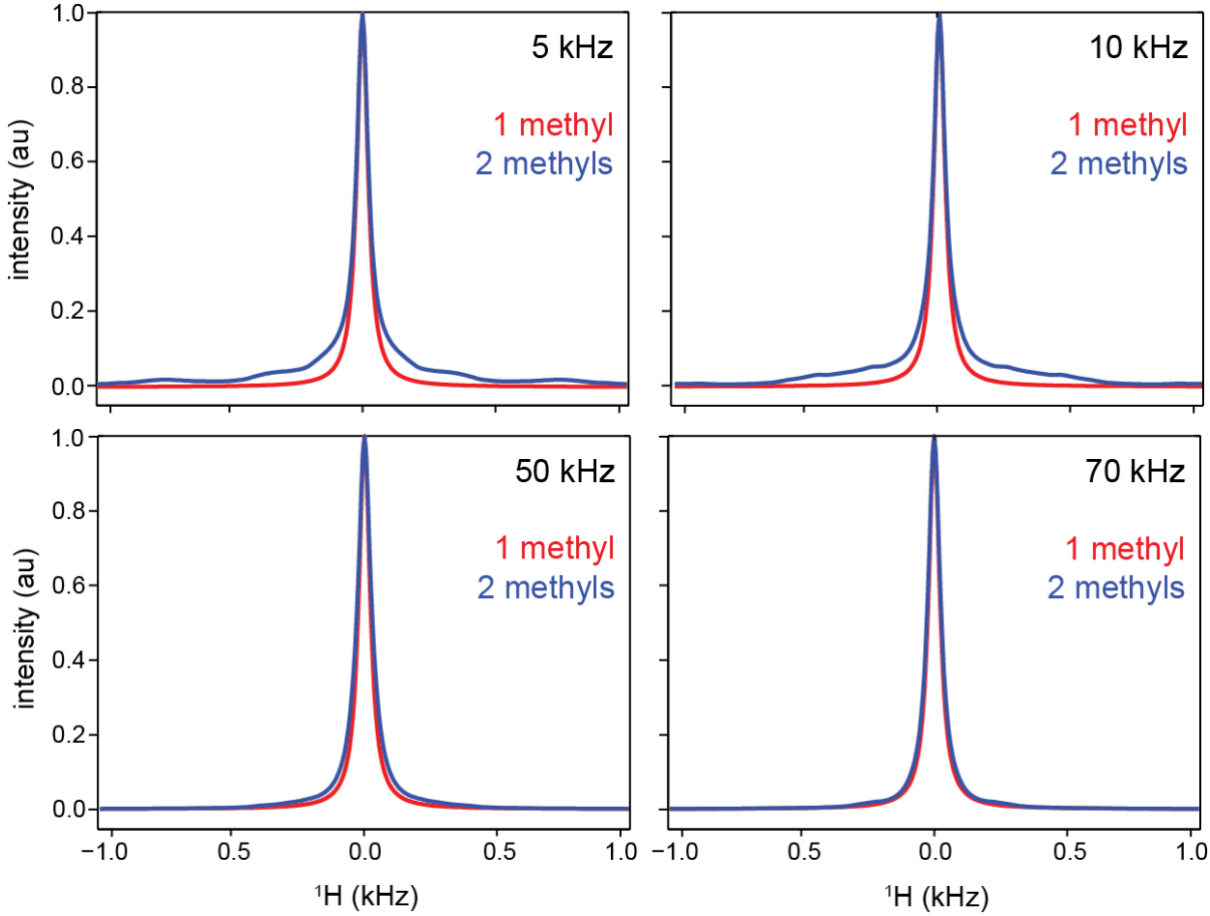

Figure 6.12. *Comparison of the ^{1}H methyl spectrum of a single methyl group, and two interacting methyl groups. focussing on the baseline of the center band at a MAS frequency of 5, 10, 50 and 70 kHz. In the simulation, a chemical shift difference of 200 Hz, an inter-methyl proton-proton dipolar constant of 2000 Hz and the relative methyl-methyl orientation (C) as described in* ***Figure 6.13*** *below has been employed. The plot focusses on a spectral range of ±1 kHz. Both spectra (single methyl, red; two coupled methyl groups, blue) are normalized to yield the same maximum intensity. In case of two dipolar coupled methyl groups, some of the intensity is distributed over a large frequency range in the base of the peak. As a consequence, the intensity of an isolated methyl group yields an approximately 2x higher intensity at a rotation frequency of 5 kHz. At 110 kHz, the ratio amounts to 1.1.*

6.2 MAS rotations frequencies beyond 300kHz are necessary to yield maximum sensitivity

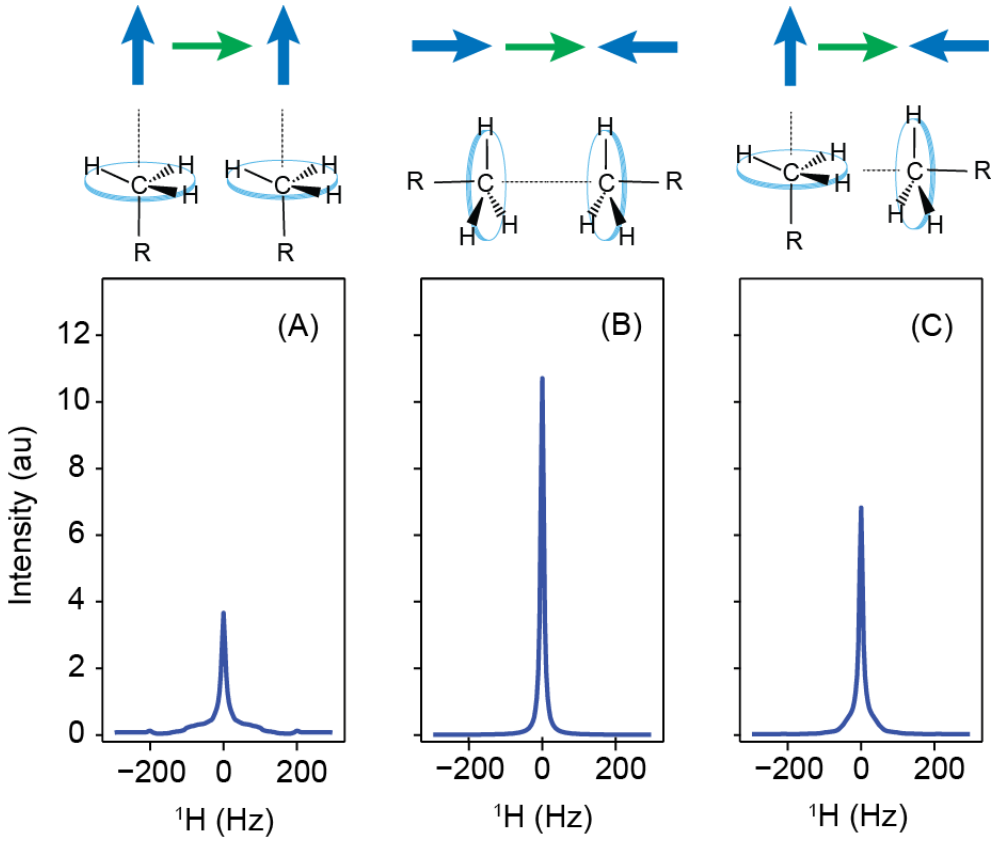

Figure 6.13. Dependence of the ^{1}H lineshape on methyl-methyl orientation. *Spectra are simulated for different geometrical configurations. In the simulation, 3 explicit protons for each methyl group (6 spins in total) are assumed. Due to fast motion the dipole-dipole interaction of the protons within the group is averaged to -10.500 Hz, with the anisotropy point along the R-C rotation axis. Furthermore, a MAS frequency of 50 kHz, a chemical shift difference of 200 Hz and an inter-methyl proton-proton dipolar coupling constant of 2 kHz is assumed. Spectral changes arise due to different arrangements of the intra- and inter-methyl dipolar coupling tensors, depicted with blue and green vectors for intra-and inter-methyl interactions, respectively.*

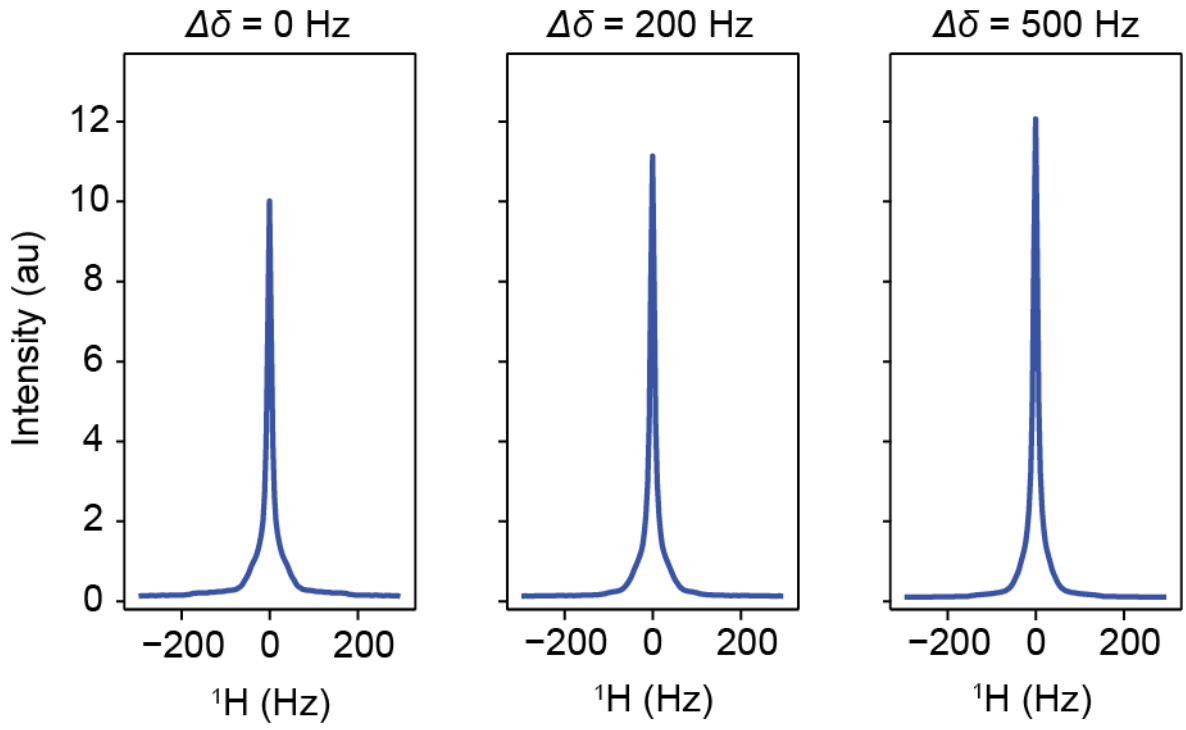

Figure 6.14. ^{1}H lineshapes for two interacting methyl groups as a function of the proton chemical shift difference. *Proton chemical shift differences assist to suppress homogeneous proton-proton dipolar interactions by avoiding n=0 rotational resonance. In the simulation, a MAS frequency of 50 kHz, an inter-methyl proton-proton dipolar coupling of 2000 Hz and the relative orientation C (see figure above) is assumed.*

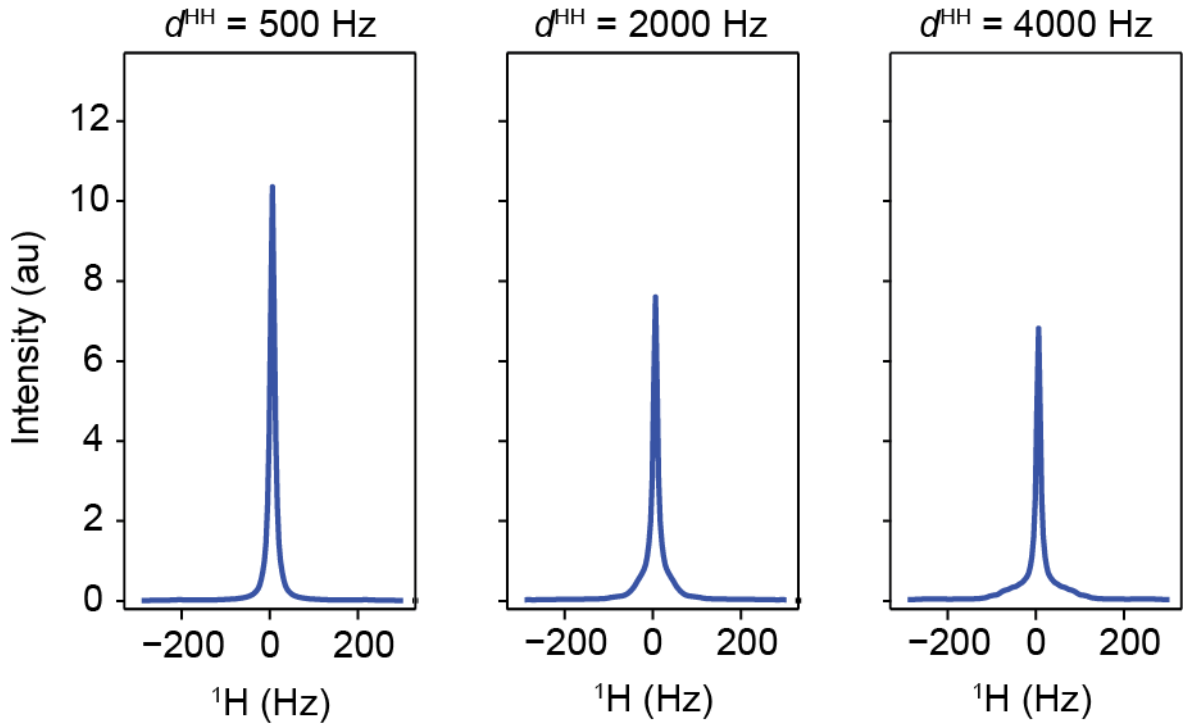

Figure 6.15. ^{1}H lineshape as a function of the proton-proton dipolar interaction. *As the inter-methyl proton-proton dipolar coupling constant increases, the proton line shape broadens. In the simulation, a MAS frequency of 50 kHz, a chemical shift difference of 200 Hz and the configuration C in the figure above has been assumed. Values of dipolar coupling values 500, 2000 and 4000 Hz correspond to ^{1}H,^{1}H distances of 6.2, 3.9 and 3.1 Å, respectively.*

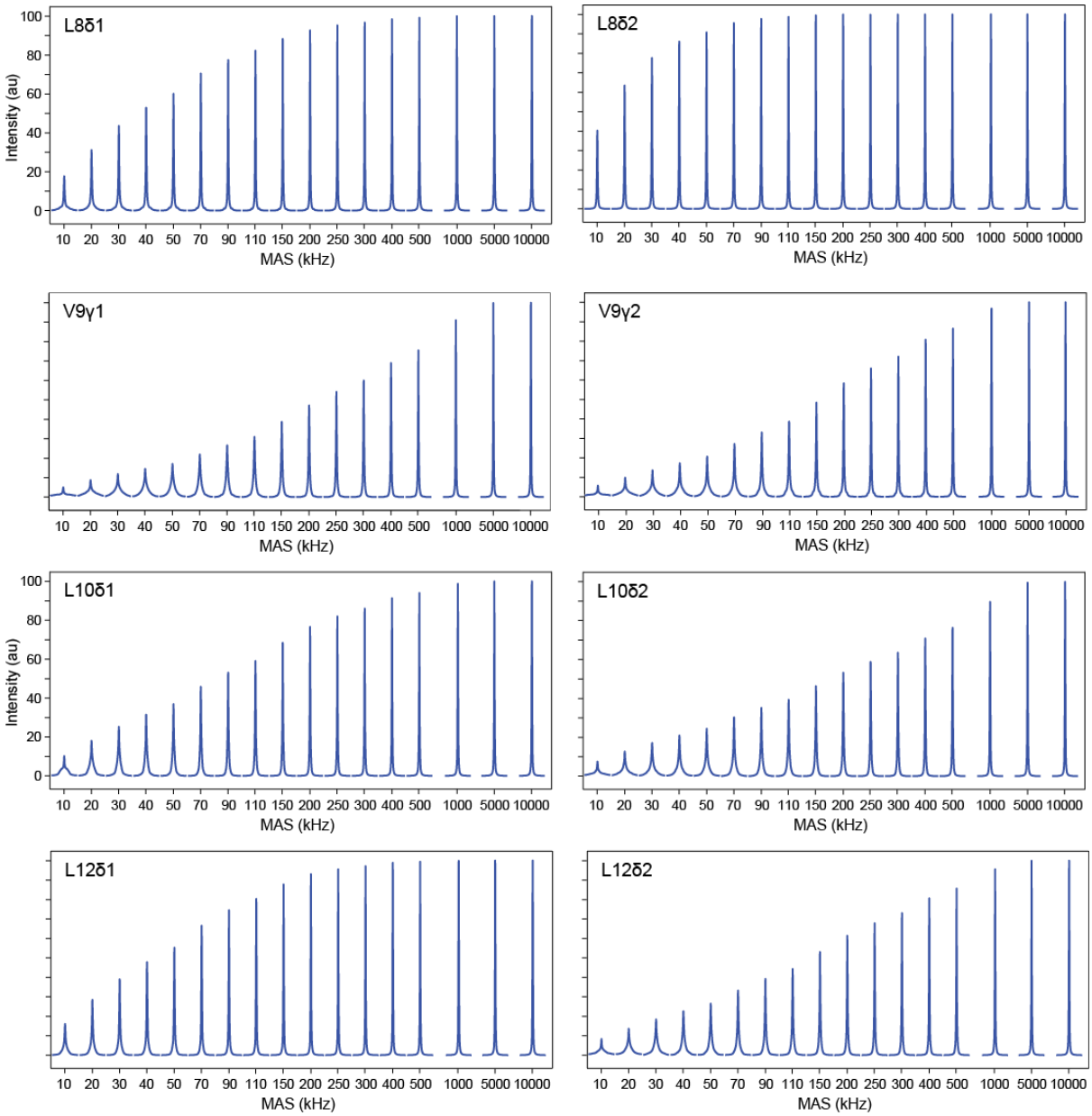

***Figure 6.16**. Simulated ^{1}H spectral intensities for all valine and leucine methyl groups α-spectrin SH3 as a function of MAS frequency. In the simulations, a 9-proton spin system is considered using the atomic coordinates from the PDB file of the α-spectrin SH3 domain (2NUZ) (105). The simulations were performed using the program SIMPSON (103, 104). Except for methyl group rotations, no additional side chain dynamics is assumed.*

6.2 MAS rotations frequencies beyond 300kHz are necessary to yield maximum sensitivity

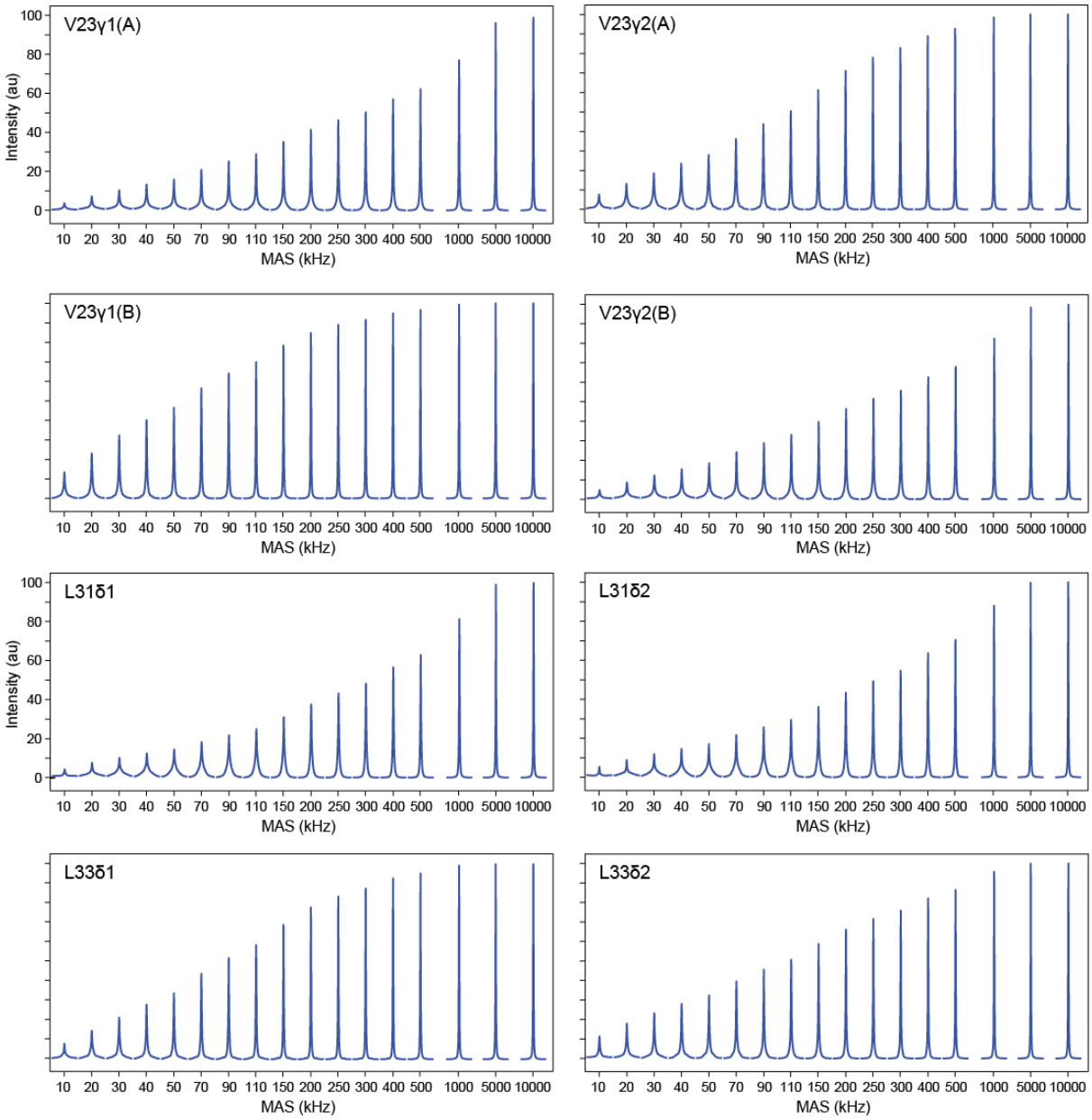

***Figure 6.16**. Continued (1).*

6.2 MAS rotations frequencies beyond 300kHz are necessary to yield maximum sensitivity

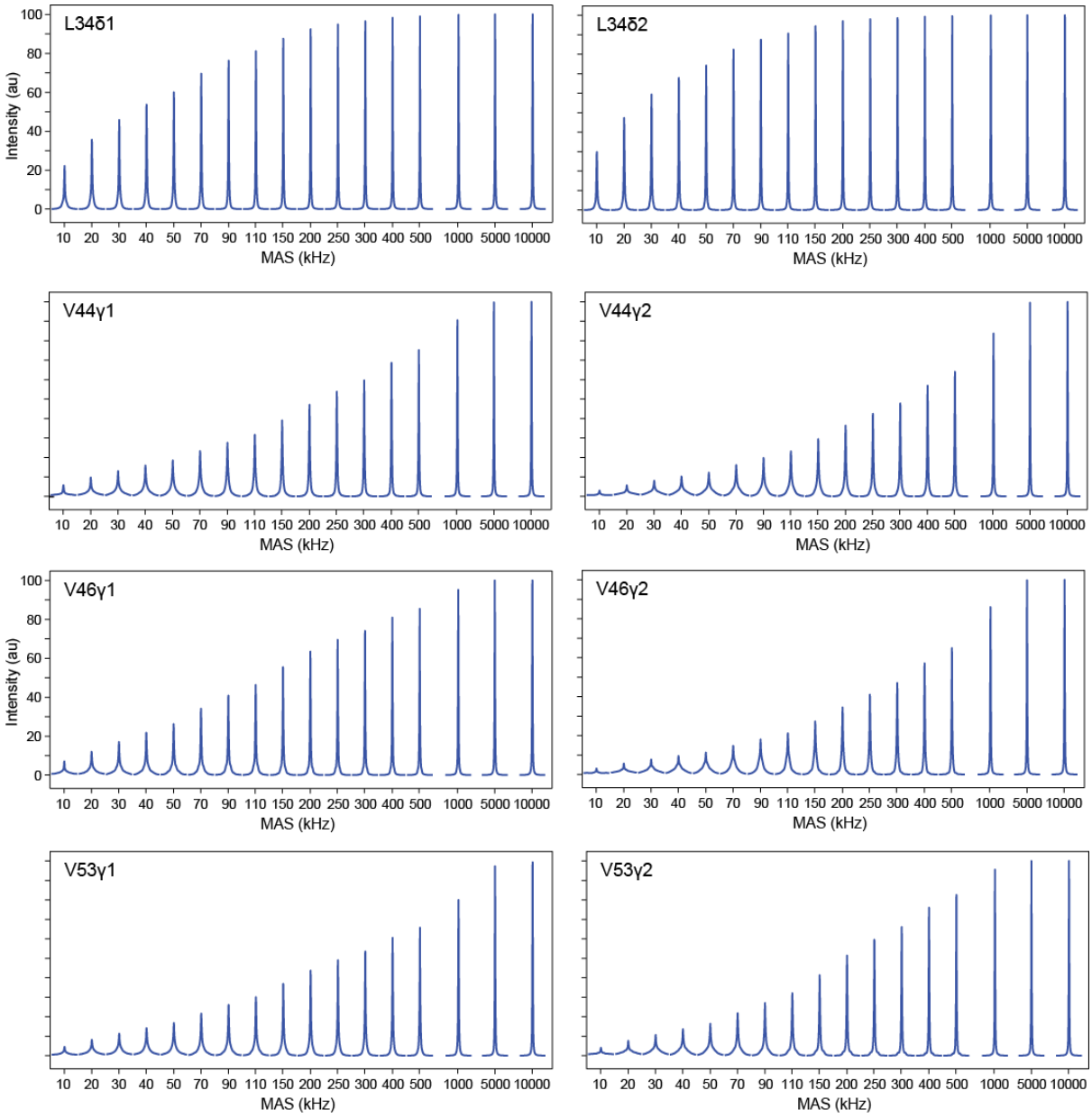

***Figure 6.16**. Continued (2).*

6.2 MAS rotations frequencies beyond 300kHz are necessary to yield maximum sensitivity

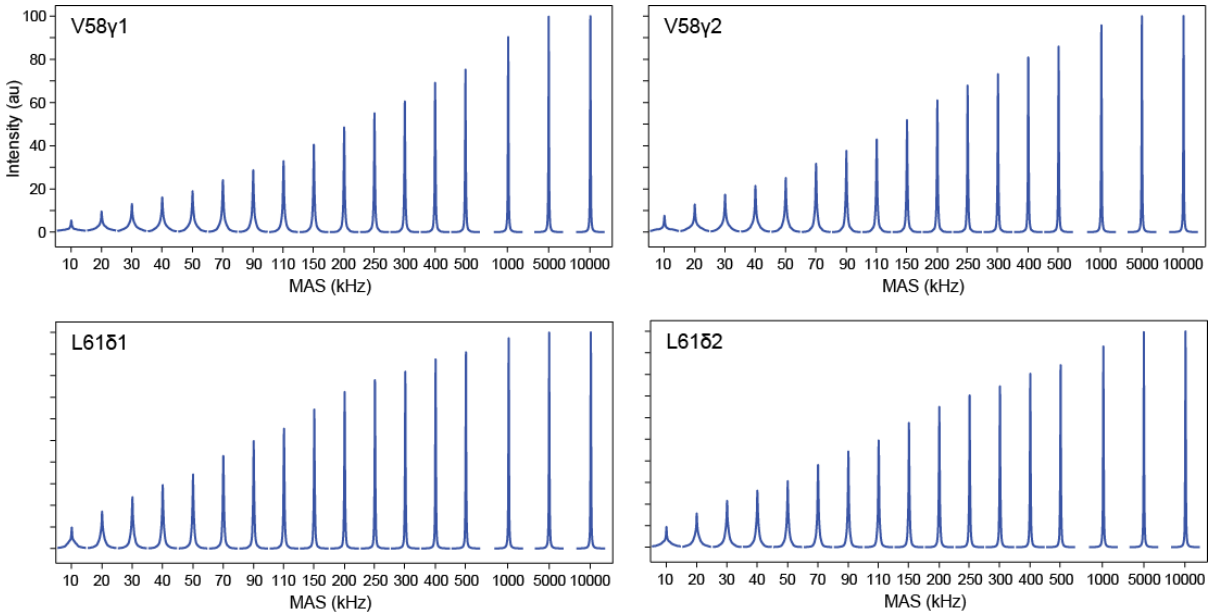

***Figure 6.16**. Continued (3).*

6.2 MAS rotations frequencies beyond 300kHz are necessary to yield maximum sensitivity

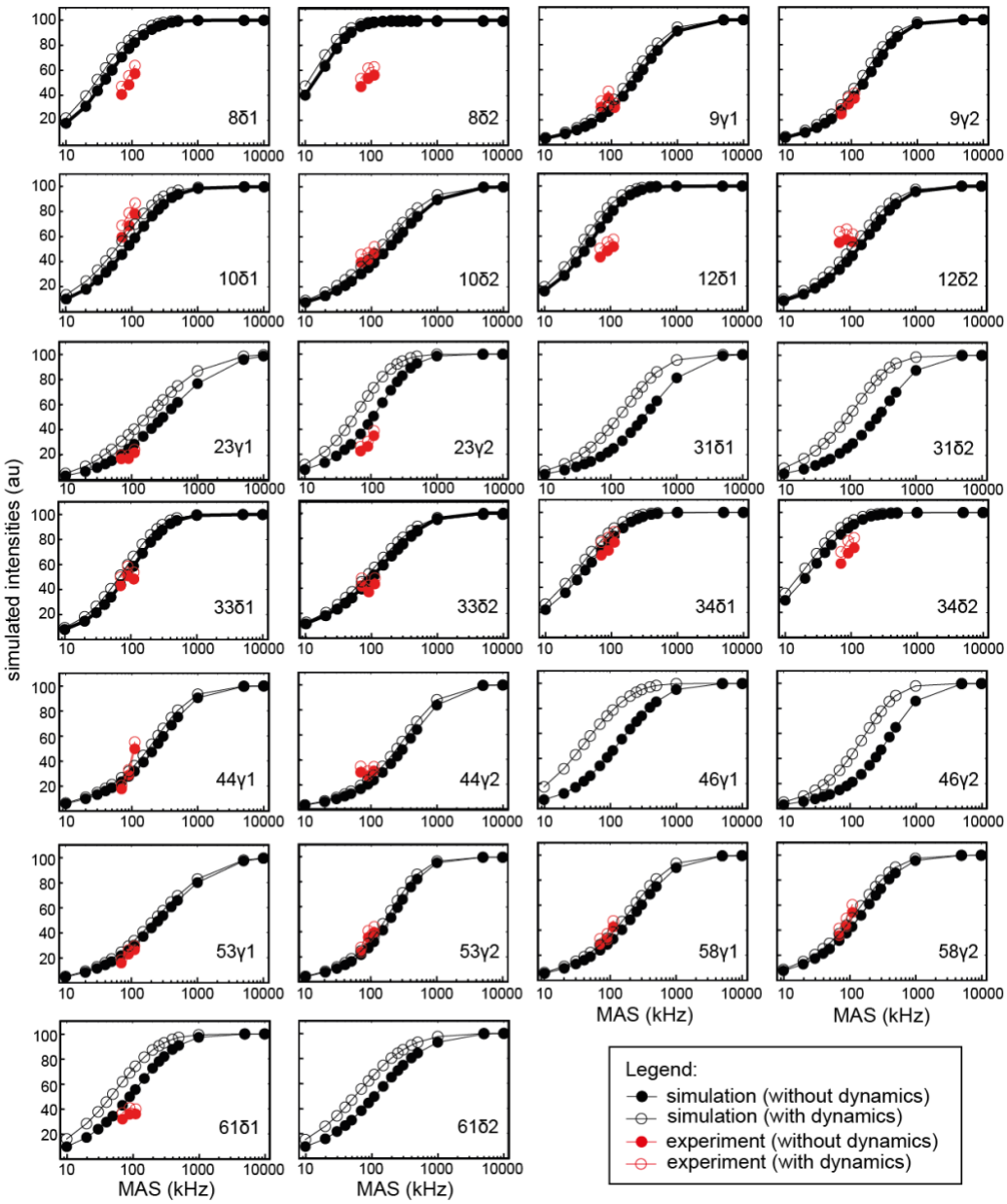

Figure 6.17. *Simulated and experimental INEPT HSQC ^{1}H spectral intensities for all valine and leucine methyl groups α-spectrin SH3 as a function of MAS frequency. The experimental intensities were corrected for the experimental ^{1}H T_2 relaxation times as described in equation 2 of the main manuscript. Simulations have been carried out assuming no dynamics (closed symbols) and using the experimental order parameters obtained from REDOR type experiments (90) (open symbols). The inclusion of side chain dynamics has a negligible effect on the matching of experimental and simulated dat, i.e. the obtained κ_i values are rather similar (without*

dynamics: κ_i = 38, 38 and 49 for 70, 90 and 110 kHz; with dynamics: κ_i = 35, 35 and 45 for 70, 90 and 110 kHz).

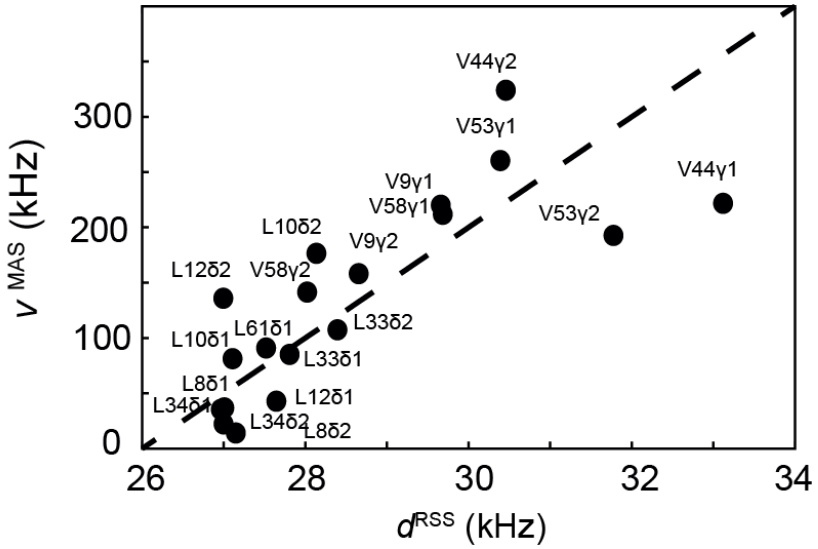

Figure 6.18. *Site specific ν^{MAS} (MAS frequencies required to yield 50% of the maximum possible intensity) as a function of the effective $^1H,^1H$ dipolar coupling d^{RSS}.*

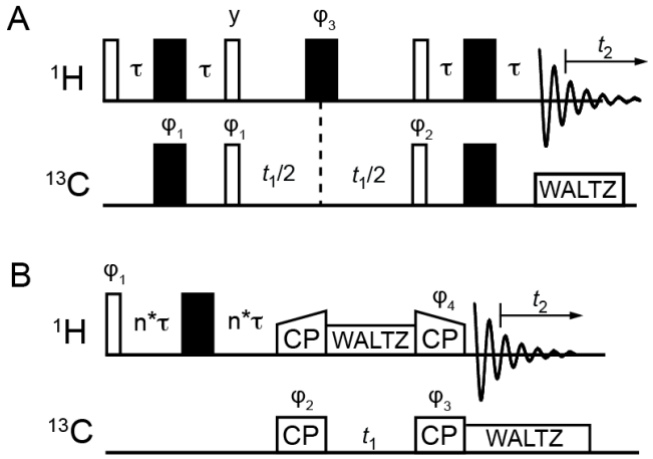

Figure 6.19. *NMR pulse schemes. (A) INEPT based $^{1}H,^{13}C$ correlation experiment. (B) Experiment to record residue specific ^{1}H-T_2' relaxation times. Thin open rectangles denote $\pi/2$ pulses, thick filled bars indicate π pulses, respectively. φ_1= x,-x; φ_2= 2 (x), 2(-x); φ_3= 4(y), 4(-y); φ_R= x,-x,-x, x (A) and φ_1= y, -y; φ_2= 2(y)2(-y); φ_3= 4(y)4(-y); φ_R= y,-y, -y, y, -y, y, y, -y (B). If not otherwise indicated, phases were set to x.*

Chapter 7

Off-Magic Angle Measurements, a Novel Method for the Determination of Order Parameters

7.1 Introduction

Magic angle spinning is a prerequisite to obtain high resolution solid state NMR spectra. Setting sample position to magic angle is an important task. Experimentally, stators are adjusted mechanically by a screw under the probe. One of the ways for calibrating the adjustment of the magic angle is by maximizing the spinning side band intensity in ^{79}Br spectrum of a KBr powder sample(112). The ^{79}Br resonance frequency is very close to ^{13}C. This is possible with most triple channel probes.

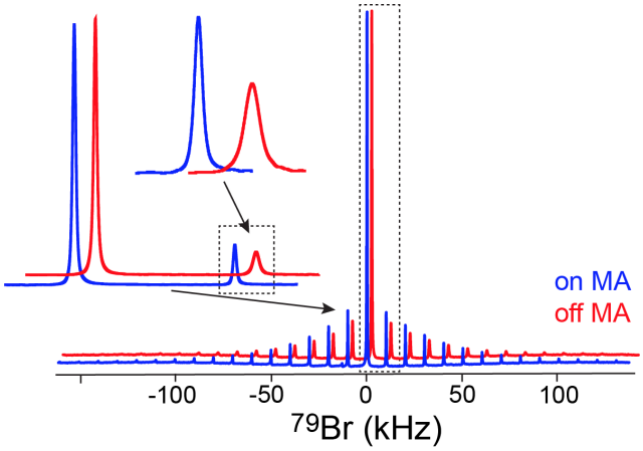

***Figure 7.1**. ^{79}Br spectra at 5kHz spinning.*

As it is shown in **Figure 7.1**, the sideband intensities decrease with miscalibration of magic angle. For biosolids application, the intensities ratio 11% for central band and first spinning side band close to optimum. Alternative ways of setting the rotor angle include satellite transition MAS using ^{1}H detection in glycine or $BaClO_3H_2O$, quadrupole detection in $^{23}NaNO_3$ or Hall effect magnetic flux sensors. Although quadrupole detection and Hall effect sensor have better accuracy to determine the rotor angle. Quadrupole detection, in biosolids application, is normally tuneable. As

most commercial probes are not employed to this frequency. Hall effect device are also not commercially available. There is no report about comparison on the accuracy between ^{1}H detection and ^{79}Br, but KBr provide very sensitive signals and has short T_1.

In a report by Sarkar and Reif(113), the accuracy and robustness of magic angle adjustment using KBr is analysed. It is found that even the intensity ratio of central and first sideband is set to 11%. An error of maximal 0.2° in magic angle is still found. The spinning angle is accurately determined by a procedure suggested by Pileio et al(114). In brief, ^{13}C signal intensities for [1,2]-13C-glyine are measured as a function of the echo delay (pulse sequence as in **Figure 7.2**). When the magic angle is accurately set ($\Delta\theta_{RL} = 0°$), the echo delay curve oscillates with $J(C\alpha, C')$ coupling. An extra dipolar coupling and damping factors are introduced when $\Delta\theta_{RL} \neq 0°$. The dipolar coupling modulation is related with magnitude of $\Delta\theta_{RL}$ and can be analytically fitted with a formula provided by Pileio et al (*Eq 7.1-7.5* in Section 7.2). In another word, $\Delta\theta_{RL}$ is difficult to be accurately diminished using conventional magic angle calibration methods. Most experiments are still performed under off magic angle condition. The residue dipolar coupling from off-magic angle effect broadens linewidth in spectra. It will influence peak assignment and structure determination. In another thought, fitting the spin echo curve to extract the dipolar coupling information might provide a new approach to quantify order parameters for assessment of dynamics.

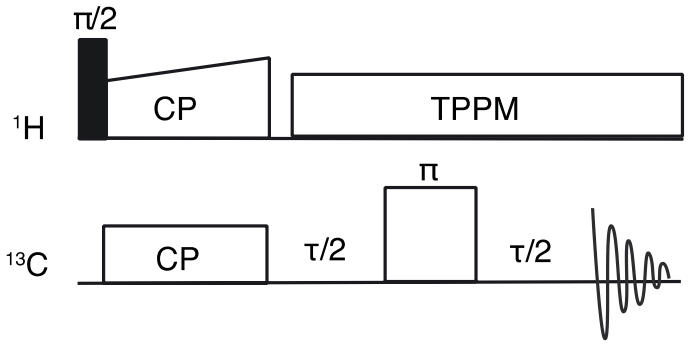

Figure 7.2 *Spin Echo pulse sequence for Glycine*

7.1 Introduction

Studying protein dynamic processes has always been of great interest in solid state NMR. A comprehensive description of protein dynamics would include time scales of correlation times and amplitudes of the conformational fluctuations. Among them, the amplitudes can also be represented by the scaling of anisotropic interactions such as dipolar couplings. Measuring one-bond dipolar couplings leads to a direct determination of order parameters. The order parameter is calculated by taking the ratio between the experimental dipolar couplings values and dipolar coupling in the rigid limit. It describes the amplitude of motion on time scales up to the inverse of the coupling strength(52). Of all back bone and side chain coupling, determination of dipolar coupling between directly bonded ^{1}H-^{13}C and ^{1}H-^{15}N are of particular interest and difficulty. This is because of the presence of the dense proton network which makes direct proton detection difficult in solid state NMR. As described in previous chapters, proton detection becomes possible in recent years. Schemes for the measurement of ^{1}H-^{15}N dipolar couplings are also proposed accordingly. Chevelkov and Reif (53)applied Phase Inverted CP on a perdeuterated microcrystalline SH3 sample which only 10% of all exchangeable amide sites contain proton at 20kHz MAS. Although a phase inversion is applied, CP based method suffers from RF inhomogeneity of the solenoidal coil. Also, in the faster spinning (MAS>100kHz) regime, when the CP condition becomes narrow, the feasibility of this method remains questionable. The REDOR based method proposed by Schanda, Ernst and Meier is less influenced by RF inhomogeneity when proper phase cycling is applied. Also, 20% back exchanged ubiquitin with 60kHz MAS was reported. A cross check of order parameter determined by these two methods was reported by Asami and Reif(54). Recent years, a combination of faster spinning and completely protonated samples for determination of order parameter was reported by Polenova and Lewandovsky. However, the dense proton network and the interplay between proton CSA and dipolar coupling are always an issue in accurate determination of dipolar coupling. Further report on accuracy of this R symmetry based sequences will still be interesting.

In this chapter, we propose a new method for determination of order parameter. The spin-echo curve was fitted for a 20% back-exchanged SH3 sample at 20kHz MAS. Fitting results are cross checked with order parameters that are previously reported.

7.2 Experimental results for amide groups

Samples

Cu doped 20% back exchanged SH3:

SH3 protein was expressed in triply labelled M9 minimal media as previously reported. A 350 mM $(NH_4)_2[Cu_9edta]/(NH_4)_2SO_4$ stock solution was prepared by dissolving $CuSO_4$(1.0 eq.) and H_4edta in H_2O (1.05 eq.). PH was adjusted to 5-6 using NH_4OH. The stock solution was added to $(NH_4)_2SO_4$. In Crystallization, defined volume of a 12mg/mL protein solution (PH 3.5) was lyophilized. Similarly a specific $(NH_4)_2SO_4$ stock was lyophilized for preparation of the copper-free samples. Protein and $(NH_4)SO_4$ powder were dissolved in 20% H_2O and 90%D_2O, yielding a final concentration of 5g/mL of protein and 150mM $(NH_4)SO_4$. After a complete precipitation at 4 °C overnight. The microcrystalline SH3 were spun into a 3.2 mm rotor.

Methyl labelled CH_3 SH3 sample were expressed in the same way as in previous chapters

Results

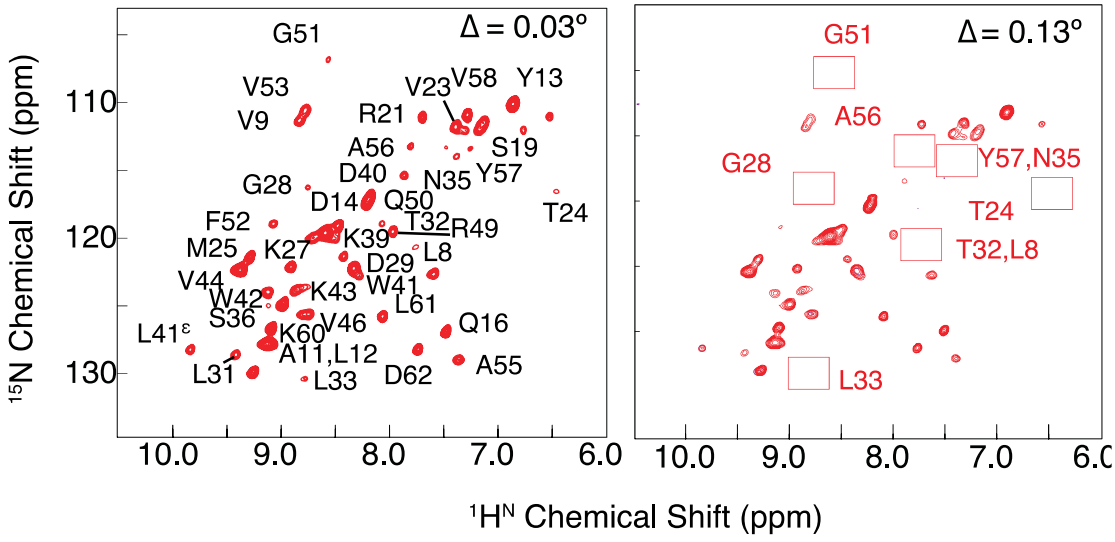

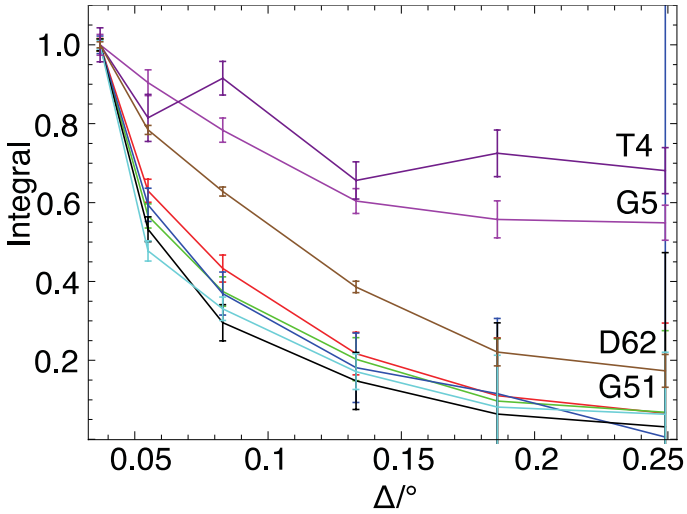

Figure 7.3 *a) HSQC for a 20% back-exchanged SH3 sample are measured at different $\Delta\theta_{RL}$. The MAS frequency was adjusted to 20kHz MAS. 400MHz external field. b) Peak intensities were measured for dynamic and rigid residues as a function of $\Delta\theta_{RL}$. T4 and G5 are residues with order parameters less than 0.2. D62 is a residue with order parameter less than 0.5. G51 is a residue with order parameter more than 0.8.*

As it is shown in **Figure 7.3a**, The HN correlation spectrum was measured at a $\Delta\theta_{RL}$ of 0.13°. The spectrum still has a good resolution. In $\Delta\theta_{RL} = 0.03°$ spectra proton linewidth goes down to 23Hz on average, in the $\Delta\theta_{RL} = 0.13°$ spectrum, the proton linewidth is still around 40 Hz. However, sensitivity of the HSQC deteriorates severely with the increase of the off-magic angle. The decrease in intensity is different for rigid and dynamic residues. For a dynamic residue, the effective dipolar coupling scales down with internal motion. When dipolar averaging due to magic angle spinning becomes ineffective. The residual dipolar coupling is thus smaller in comparison to a rigid residue. From on-magic-angle to 0.25°-off, residue T4 shows a decrease of the HSQC peak sensitivity by 20%, whereas G51, is decreased more than 90 percent.

Accuracy of magic angle calibration are also different in different probe design. It is found from our study that in a standard-bore Bruker probe with stator flip settings,

even after magic angle was carefully calibrated with KBr, when sample is replaced with real sample $\Delta\theta_{RL}$ can go up to 0.3° again.

Figure 7.3 qualitatively shows that the HSQC sensitivity behaves different for residues with different magnitude of internal motions. For an accurate determination of residual dipolar coupling. The following pulse sequence is applied.

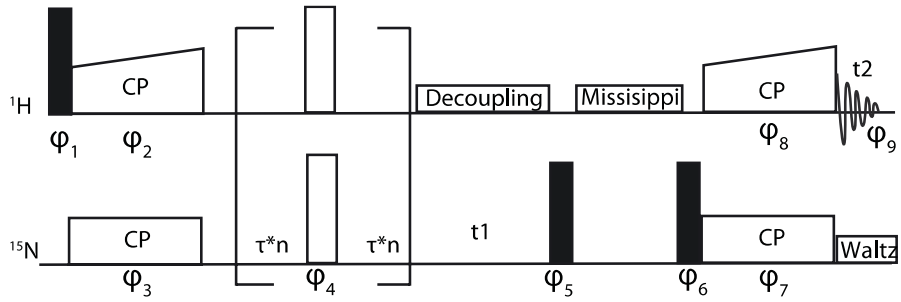

Figure 7.4 *Spin-echo pulse sequence for ^{1}H-^{15}N dipolar coupling determination. Phase cycling goes φ_1=y, -y, φ_2 = x, φ_3= y, φ_4= (x)x4, (y)x4, (-x)x4, (-y)x4, φ_5= x, φ_6= x, x, -x, -x, φ_7= y, φ_8= y,y,y,y,-y,-y,-y,-y, φ_9= y,-y,-y,y,-y,y,y,-y,-y,-y.y,y,-y,y,-y,-y,y. 0.1s of wáter supression is given. Waltz scheme was used both for direct and indirect dimension decoupling.*

In the spin echo part two π pulses are given on both channels to refocus the chemical shift anisotropy. Heteronuclear *J* coupling and dipolar coupling are allowed. Considering a heteronuclear scaler coupling of approximately 93 Hz, an increment of 6 ms has been chosen. The spin-echo is evolved up to 96 ms is given to allow accurate fitting.

The decay curve can be described by the following form:

$$S(\tau) = pexp\left\{-\frac{\tau}{T_2^0}\right\} + (1-p)S_{mod}(\tau,\delta)\exp\{-\frac{\tau}{T_2^J}\} \qquad (7.1)$$

T_2^0 and T_2^J are phenomenological dephasing time constants. T_2^J takes into account the homogeneous decay of the J-modulated component, while T_2^0 corresponds to an inhomogeneous spread of different frequencies modulation.

The modulated component is given by:

$$S_{mod}(\tau, \Delta) \cong \frac{1}{2}\int_0^{\pi} \cos\left(\pi J\tau + b\Delta 2^{\frac{1}{2}} d_{00}^2(\beta_{PR})\tau\right) sin\beta_{PR} d\beta_{PR} \quad (7.2)$$

The analytical solution is derived as follow:

$$S_{mod}(\tau, \Delta) = x^{-1}(F_c(x)cos\theta + Fs(x)sin\theta)$$
$$F_c(x) = \int_0^x \cos\left(\frac{\pi y^2}{2}\right) dy$$
$$F_s(x) = \int_0^x \sin\left(\frac{\pi y^2}{2}\right) dy \quad (7.3)$$

Where

$$x = \left(\frac{6b\Delta\tau}{\pi\sqrt{(2)}}\right)^{1/2}$$
$$\theta = \left(\pi J + 2^{-\frac{1}{2}} b\Delta\right)\tau \quad (7.4)$$

S_{mod} reduces to to a modulation due to J coupling in the case of on-magic-angle spinning.

For ^{1}H-^{15}N polarization transfer, in a highly deuterated system, T_2 can be long enough to yield an efficient scaler transfer. In this chapter, we applied CP for almost all order parameter measurements, with the exception of dynamic residues which cannot be viewing with CP experiments.

CP based HSQC is applied for SH3 sample with 20% protons at exchangeable amide sites. In **Figure 7.5**, The analytic formula given above is preserved assuming empirical values and an off-magic angle of 0.1° .

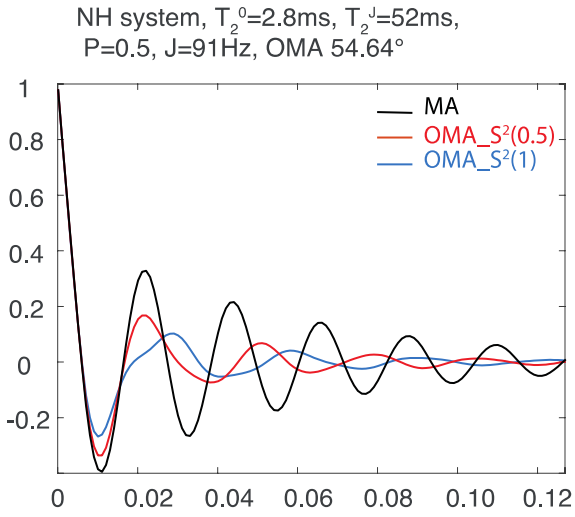

Figure 7.5 *Simulated dipolar and scaler coupling oscillation curve according to Eq 7.2. X axis are spin-echo delay time, Y axis are normalized peak intensities. J coupling and dipolar coupling values for a rigid N-H spin pair have been used. The black curve describes an J coupling oscillation with no dipolar coupling modulation. In the red curve, an order parameter of 0.5 (DD 7kHz) is used while in the blue curve, an order parameter of 1 (DD 11kHz) is applied. In this simulation, all three oscillation curves converge to zero after 15 ms. This is due to the assumption of 2.8 ms and 52 ms for decaying factors of* T_2^0 *and* T_2^j*. The effect of the dipolar modulation is observed after the first period.*

In a directly bonded N-H system, the dipolar coupling amount to 11kHz. The J coupling value is 91Hz. Since dipolar coupling is scaled with the spinning angle ($b\Delta$). J coupling oscillation is affected by $b\Delta$ term. If a modulation of 11Hz is to be induced, an off-magic angle of at least 0,06° is required. For a dynamic peak with only 5.5kHz of effective dipolar coupling ($S^2 = 0.25$), an angle of 0.12° is needed. Vice versa, if the off-angle is set to 0.06°, for a minimum change of 1Hz In J coupling oscillation, approximately 1kHz in dipolar coupling is required. Larger the off-magic angle enable a more sensitive determination of the order parameter.

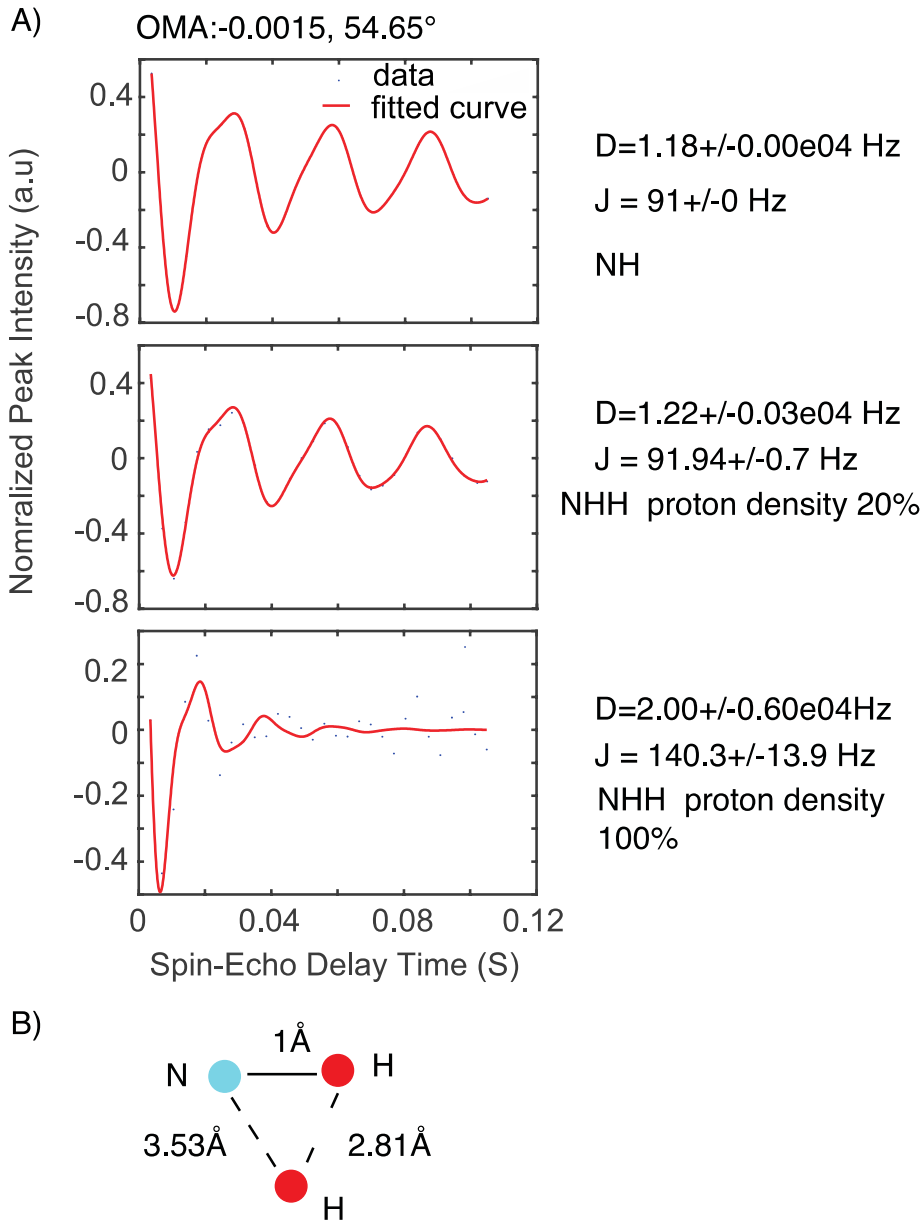

Figure 7.6 ***A)*** *SIMPSON simulation of the spin echo curve at 54.65° directly bonded N-H. For the curve at the* ***bottom,*** *a remote proton is taken into account. Crystal structural information and atomic coordinates are obtained for residue V44 from the pdb file 2NUZ using SIMMOL.* ***Middle*** *simulation considering 20% back exchangeable protons, 80%* ***top (0% remote proton)*** *and 20%* ***bottom (100% remote proton)*** *signal are added in order to product* ***middle (20% remote proton)*** *datasets. On the right side, simulated data are fitted with analytic formula. Dipolar coupling and J coupling values determined with the fitting shows that, the present of a second proton to the N-H 2 spin system will influence the theoretical spin-echo curve description.* ***B)*** *Distance information for the assumed N-H-H system is shown.*

Figure 7.6, shows that H-H dipolar coupling have a large effect on spin echo curve. Experimentally a protein sample that is highly deuterated is needed to carry out the off-magic angle experiments.

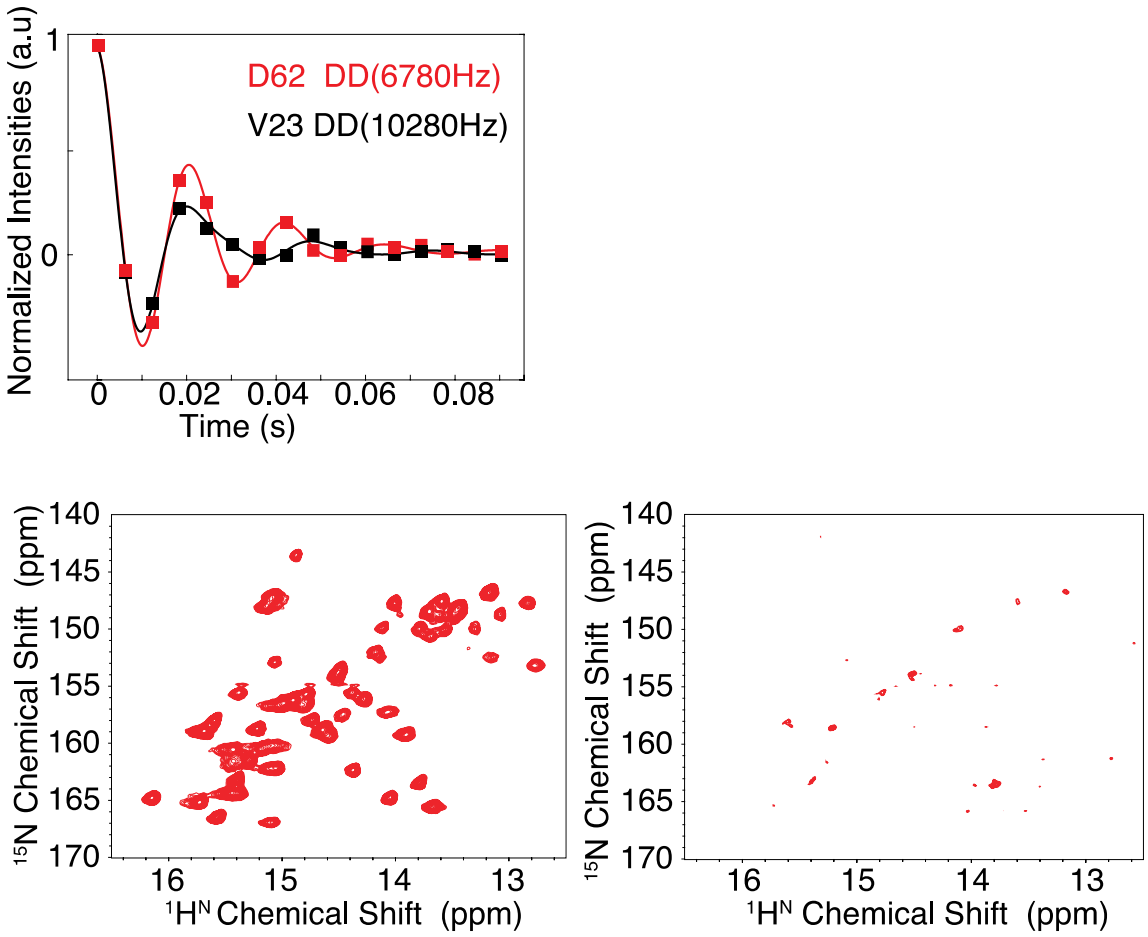

Figure 7.7 Top: *A spin-echo curve for residues 62 and 23 which represent a dynamic and a rigid residue respectively. In this experiment, an off-magic angle of 0.088° was selected.* ***Bottom:*** *HSQC spectra quality is show for the first and last spectrum of the echo curve. Off-Magic angle was set at 0.09° off and only dynamic residues are observed after 96 ms of delay.*

The off-magic angle is determined by fitting the analytical formula simultaneously for all residues. In the fit six parameters (P, T_2^0, T_2^J, J, DD, $\Delta\theta_{RL}$) are kept as variables. $\Delta\theta_{RL}$ is then selected for residues with the best fit (minimum error bar). In the second

round of fitting $\Delta\theta_{RL}$ keeps the same for all residues. D62 has a signal to noise ratio of 36 in the first point and 1.1 in the last data point after a defocusing delay of 96 ms.

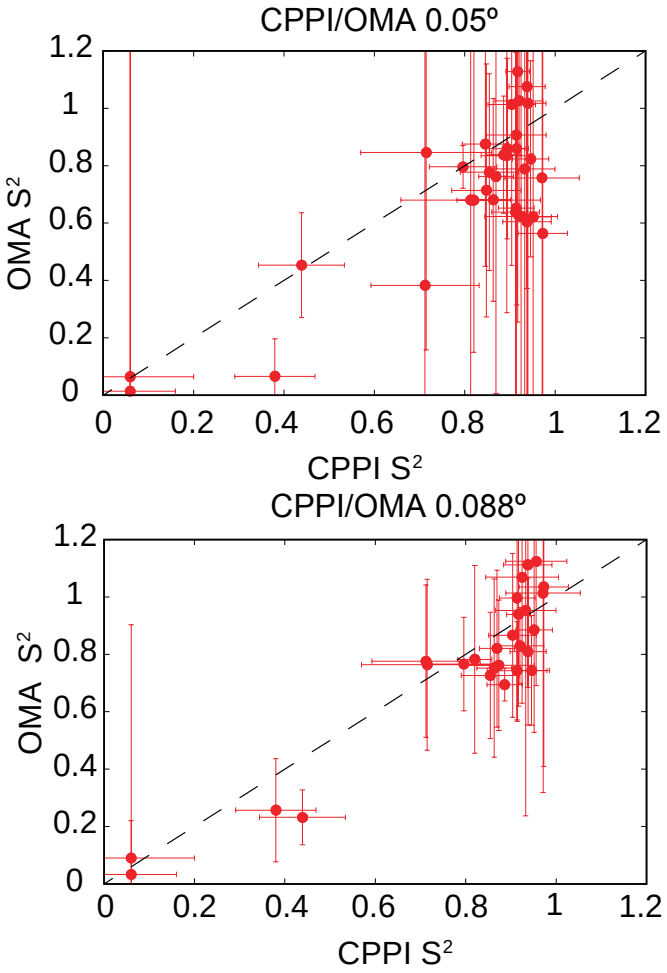

Figure 7.8 *Correlation diagram representing parameters obtained from OMA and CPPI experiment data for two $\Delta\theta_{RL}$ data are shown. (53).*

As described in the introductions of this chapter, dipolar couplings together with J-couplings under off-magic angle conditions yield a modulation of the spin echo curve. Consequently, the accuracy of dipolar coupling determination also depends on setting of off-magic angle. In **Figure 7.8**, dipolar couplings are more accurately determined when the off-magic angle is set to 0.088°. Still for, dynamic residues with order parameter less than 0.5 (DD < 7kHz), the error range is large. There are several reasons that give rise to the error bar here. One is the influence from other nearby protons in the sample. This effect is discussed in ***Figure 7.6***. One possible

solution to this is a faster MAS frequency. Another source of error could be the finite refocusing π pulses on both channels.

In **Table 7.1,** fitting parameters for **Figure 7.8 right** spin echo curves are given.

Table 7.1 *For off magic angle 0.088°, Fitting parameters are as follow*

Residue	T20(S)	T2J(S)	D(Hz)	J(Hz)	P
8	4.50E-02	2.16E-02	1.21E+04	9.96E+01	3.41E-02
9	3.48E-02	1.63E-02	1.25E+04	1.02E+02	4.00E-02
13	1.12E-01	5.16E-02	1.03E+04	9.34E+01	1.28E-02
16	5.34E+00	4.31E-02	1.02E+04	9.76E+01	7.99E-03
18	6.01E-03	2.91E-02	1.03E+04	9.20E+01	1.25E-01
21	3.84E-02	2.60E-02	5.05E+03	9.07E+01	9.57E-03
24	2.05E-02	2.44E-02	1.14E+04	9.40E+01	5.83E-02
25	1.02E-01	4.16E-02	1.05E+04	9.61E+01	2.22E-02
26	4.88E-03	4.40E-02	1.03E+04	9.60E+01	2.73E-01
27	3.26E-03	6.65E-02	1.07E+04	9.53E+01	2.84E-01
28	6.45E-03	5.61E-02	1.13E+04	9.52E+01	1.62E-01
29	4.92E-03	3.82E-02	1.05E+04	9.47E+01	2.51E-01
31	2.20E-02	1.70E-02	1.12E+04	1.00E+02	8.37E-02
32	4.48E-02	1.84E-02	1.13E+04	9.86E+01	3.14E-02
33	4.84E-02	3.13E-02	1.09E+04	9.65E+01	4.89E-02
34	7.64E+00	1.74E-02	1.06E+04	9.26E+01	4.62E-03
35	1.89E-02	5.15E-02	1.04E+04	9.49E+01	6.71E-02
39	5.03E-03	4.72E-02	9.62E+03	9.38E+01	1.85E-01
40	8.78E-03	4.53E-02	1.08E+04	9.23E+01	1.07E-01
42	5.18E-03	2.83E-02	1.09E+04	9.36E+01	2.84E-01
44	6.04E-03	2.41E-02	1.18E+04	9.70E+01	2.48E-01
45	6.54E-03	1.71E-02	9.92E+03	9.65E+01	1.49E-01
49	4.01E-03	3.37E-02	8.29E+03	9.47E+01	1.09E-01
51	9.69E-03	2.33E-02	9.92E+03	1.00E+02	8.15E-02
52	4.74E-02	2.90E-02	1.14E+04	9.63E+01	5.09E-02
53	6.61E-03	2.44E-02	1.10E+04	9.61E+01	1.72E-01
55	4.70E-03	6.48E-02	1.05E+04	9.21E+01	3.38E-01
56	2.13E-02	8.38E-02	1.03E+04	9.52E+01	7.42E-02
57	9.83E-03	5.85E-02	1.13E+04	9.75E+01	1.35E-01
58	6.02E-03	5.66E-02	1.02E+04	9.45E+01	8.77E-02
60	4.64E-02	3.37E-02	1.04E+04	9.60E+01	4.35E-02
61	5.96E-01	2.17E-02	9.87E+03	9.70E+01	4.31E-05
62	1.47E-02	2.40E-02	4.06E+03	9.50E+01	3.64E-02

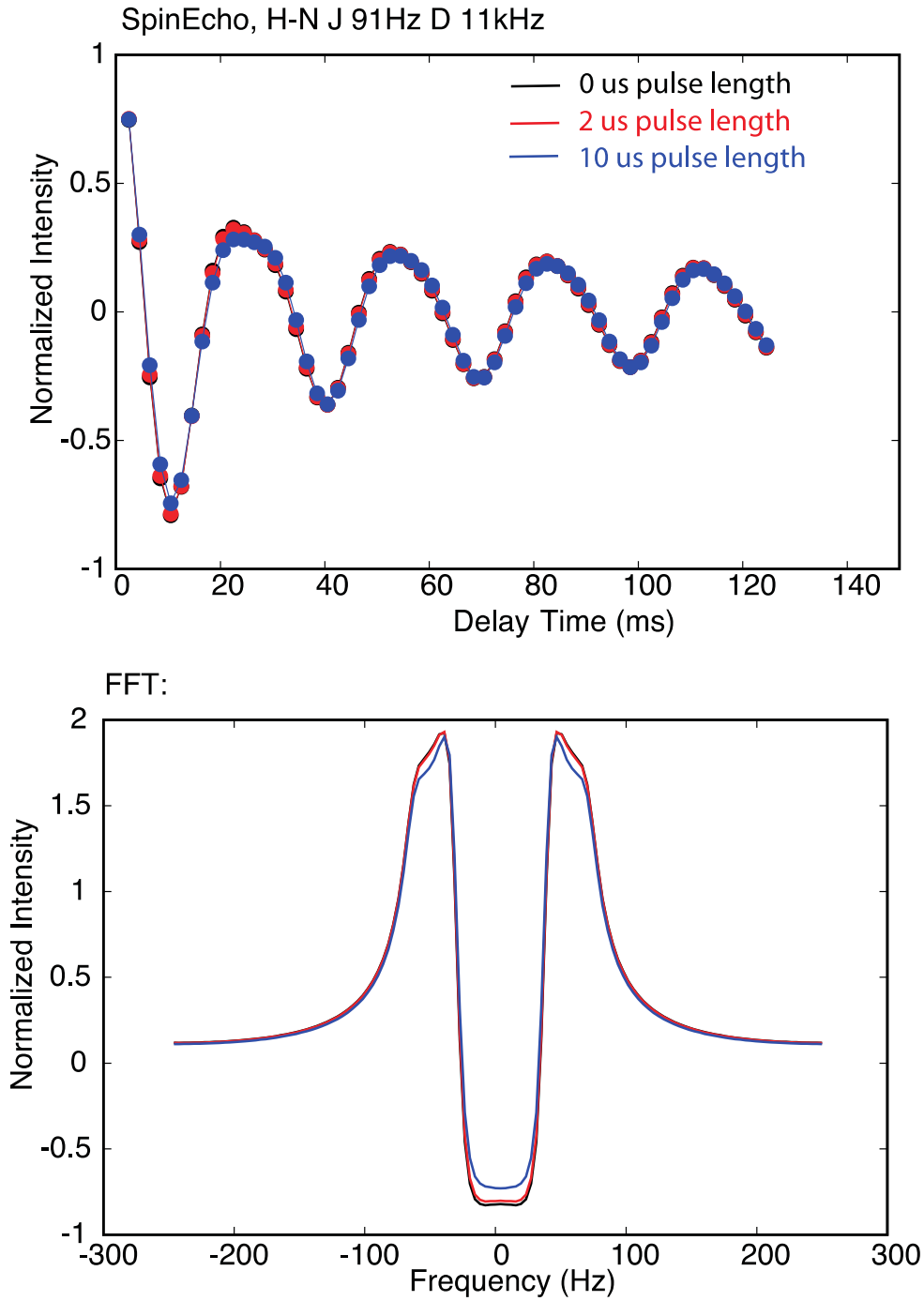

Figure 7.9 *Simulation is performed with 0.08° off-magic angle. A simple N-H directly bonded two spin system is assumed. MAS frequency is 20kHz and 400MHz B_0 field. Effects of finite pulse lengths in spin-echo refocusing are compared. In 2us and 10us finite pulse echo curves and the curves after a Fast Fourier Transform (FFT), from 2us to 10 us, increasing offsets were introduced.*

For **Figure 7.8** data were fit using FIT function in MATLAB. In **Figure 7.9**, SIMPSON simulate for the finite pulse effect on spin-echo curve. 0us, 2us and 10us pulse

lengths were applied. Offsets in ***Figure 7.9*** can be another source of error in the fitting. Offsets is introduced because residual heteronuclear dipolar coupling evolves during the finite pulse length. It can be expected that at a faster MAS spinning, this source of error will also be mitigated.

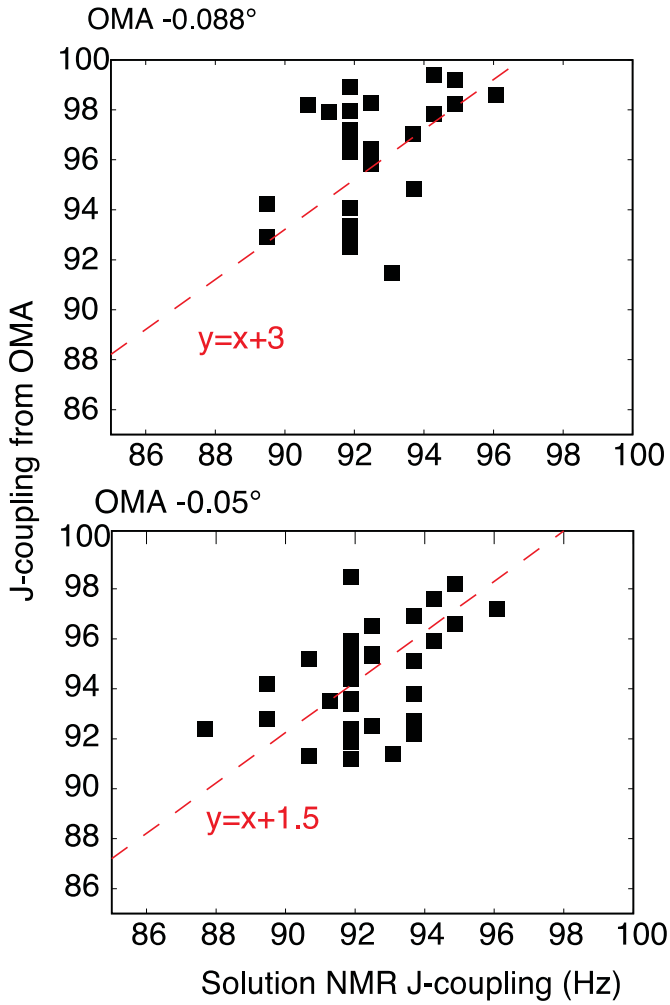

Figure 7.10 *Correlation diagram containing J coupling extracted with the OMA fit and as determined by solution state NMR*.

In the previous section, it is shown that the accuracy of the extracted dipolar coupling increases when $\Delta\theta_{RL}$ becomes larger. For quantification of J coupling, on the contrary, accuracy increases when $\Delta\theta_{RL}$ is small, as the J coupling effect then dominates in the spin-echo oscillation. In **Figure 7.10,** the two fittings converge when $\Delta\theta_{RL}$ becomes small.

7.3 INEPT OMA Experiments for Dynamic Residues

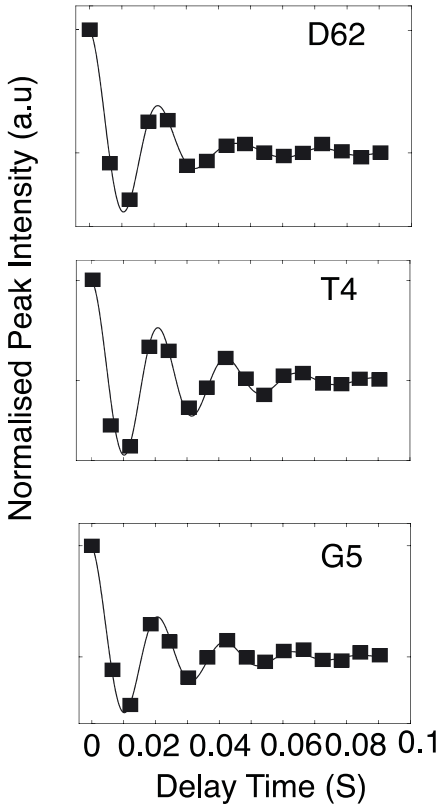

Figure 7.11 *A INEPT sequence spin-echo fit. Dynamic residues are fitted for order parameter determination. An off-Magic angle of 0.088° is used.*

As it is discussed in previous section, INEPT efficiency is influenced by the reintroduction of dipolar couplings in off magic angle measurement. The influence is less significant when it is dynamic residues. Here an INEPT transfer step is applied instead of CP transfer for polarization transfer. T4 and G5 cross peaks are visualized in INEPT experiment and fitted for off magic angle, spin-echo curve. In INEPT spin-echo experiment, T4 has a single to noise ratio of 30.5 in the first point and 1.5 in the last point.

The above most residue is D62 with effective dipolar coupling of approximately 6 kHz, second residue is T4 and the third is G5. These residues have a dipolar coupling of less than 5kHz. Difference modulation to J coupling in these three residues could be obviously seen starting from the fourth and fifth point.

Table 7.2 *Order parameter fit results of D62, T4 and G5. These results are measured at 0.088° from magic angle in INEPT based OMA experiments. MAS frequency is adjusted to 20kHz, B0 field is 400 MHz*

Residues	Dipolar Couplings	Order Parameter (S^2)
D62	5614+/- 827 Hz	0.26+/-0.07
T4	3302+/- 1910Hz	0.09+/-0.13
G5	2131+/- 4154Hz	0.04+/-0.33

7.4 Experimental results for methyl groups

Samples

In this section, selectively Pro-S methyl protonated micro-crystalline sample of the chicken α-spectrin SH3 domain is used. The protein was produced by adding α-ketoisovalerate to the perdeuterated M9 minimal medium yielding CHD_2 isotopomers.

Results:

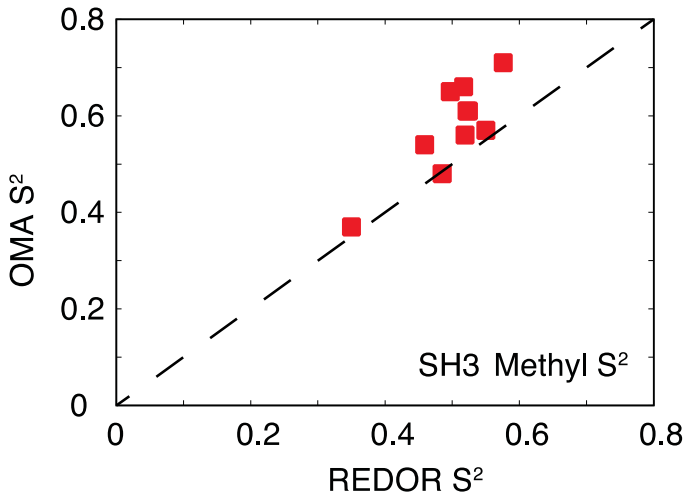

Figure 7.12 Correlation diagram for methyl groups order parameters by employing data from OMA and REDOR experiments. Data is obtained with 1.3 mm rotor, 50kHz of MAS frequency and 500MHz B_0 field.

In this section, the results of methyl side chain order parameter experiments are discussed. The employed SH3 sample is perdeuterated. Only methyl groups of valine

and leucine side chains are labelled with CHD_2. With incorporation, exclusively into the pro-R or pro-S position. The order parameter displayed on the x-axis is taken from the REDOR experiment (54). We observe a correlation. The experiment is performed with a $\Delta\theta_{RL}$ value of 0.088°.

The same experiment was also performed with a perdeuterated SH3 domain sample. valine and leucine methyl groups are labelled as CH_3. For the denser proton pool, the off-magic angle spin-echo curves become more difficult to fit. It shows that a simple 2-spin system is needed for the off-magic angle method.

7.5 Conclusion

A new method is introduced for the determination of dipolar couplings. This method makes use of the residual dipolar coupling that is introduced by the sample rotation off the magic angle. Since order parameters and J coupling are accurate information about protein structure and dynamics, a dilute protonated system and fast MAS frequency would be advised.

Summary

In the last decade, proton detection in MAS solid state NMR became a popular strategy for biomolecular structure determination. In particular, probe technology has experienced tremendous progress with smaller and smaller diameter rotors achieving even higher MAS frequencies. MAS rotation frequencies beyond 100 kHz allow to observe and assign protons in fully protonated samples. In these experiments, resolution is however compromised as homogeneous proton-proton dipolar coupling interactions are not completely averaged out.

Using a combination of experiments and simulation, we analyze the MAS frequency dependent intensities of the $^{1}H,^{13}C$ methyl correlation peaks of a selectively methyl protonated microcrystalline sample of the chicken α-spectrin SH3 domain (α-SH3). Extensive simulations involving 9 spins employing the program SIMPSON allow to predict the MAS frequency dependence of the proton intensities. Our results show that this frequency is site-specific and strongly depends on the local methyl density. We find that the characteristic MAS frequency ranges from as low as 20 kHz up to 324 kHz with the average value of (135 ± 88) kHz for this particular sample at a magnetic field strength of 11.7 T.

A novel method for order parameter determination in biosolids is introduced. This method makes use of the residual dipolar coupling from off-magic angle spinning and analyse the corresponding J coupling/Dipolar coupling modulation of spin-echo curve. Experiments are conducted for rigid and dynamic residues on both back-boned amide sites and methyl side chains. It opens a new perspective for J coupling and dipolar coupling determination in solids.

Appendix 1 List of Publications

K Xue, R Sarkar, B Reif. *Obtaining Order Parameters from a New Perspective in Solid-State NMR* (manuscript in preparation)

K Xue, R Sarkar, C Motz, V Decker, S Wegner, Z Tosner, B Reif. *Magic Angle Spinning Frequencies Beyond 300 kHz are Necessary to Yield Maximum Sensitivity in Selectively Methyl Protonated Protein Samples in Solid State NMR, J. Phys. Chem. C* **2018**. 122 (28)

K Xue, R Sarkar, C Motz, S Asami, D C R Camargo, V Decker, S Wegner, Z Tosner, B Reif, *Limits of Resolution and Sensitivity of Proton Detected MAS Solid- State NMR Experiments at 111 kHz in Deuterated and Protonated Proteins*, Sci. Rep 7:7444

M Hora, R Sarkar, V Morris, **K Xue**, E Prade, E Harding, J Buchner, B Reif, *MAS33 Antibody Light Chain Amyloid Fibrils are Similar to Oligomeric Precursors*, Plos One, 12(7)

DCR Camargo, K J Korshavn, A Jussupow, K Raltchev, D Goricanec, M Fleisch, R Sarkar, **K Xue**, M Aichler, G Mettenleiter, A K Walch, C Camilloni, F Hagn, B Reif, A Ramamoorthy, *Stabilization and Structural Analysis of a Membrane-associated hIAPP Aggregation Intermediate*, eLife 2017;6;e31226

Appendix 2 Scripts

Pymol script to extract structural information from a PDB file:

```
#! /opt/local/bin/python2.7

import __main__
__main__.pymol_argv = [ 'pymol', '-qc'] # Quiet and no GUI
import sys, time, os
import pymol
from pymol import stored

pymol.finish_launching()

# Load Structures

pymol.cmd.load('2nuz.pdb', '2nuz')
pymol.cmd.disable("all")
pymol.cmd.enable('2nuz')

#pymol.cmd.h_add ('(resn LEU and (name CD1 or name CD2)) or (resn VAL and (name CG1 or name
CG2))')
# select all the methyl protons of a leucine residue
#select bb, (neighbor 2nuz and resn LEU and resi 12 and (name CD1 or name CD2)) and (not elem c)
#pymol.cmd.png("my_image.png")
pymol.cmd.h_add("all")
#select1= '((neighbor 2nuz and resn LEU and (name CD1 or name CD2)) or (neighbor 2nuz and resn
Val and (name CG1 or name CG2)))  and (not elem c)'
#no_of_Leu_1H= pymol.cmd.select('aa', select1)
#atoms = pymol.cmd.get_model(select1)
#select2= '((neighbor 2nuz and resn LEU and (name CD1 or name CD2)) or (neighbor 2nuz and resn
Val and (name CG1 or name CG2)))  and (not elem c) and name '

stored.a, stored.b = [], []
pymol.cmd.iterate_state(1, "((neighbor 2nuz and resn LEU and (name CD1 or name CD2)) or
(neighbor 2nuz and resn VAL and (name CG1 or name CG2)))  and (not elem c)",
"stored.a.append(ID)")
pymol.cmd.iterate_state(1, "((neighbor 2nuz and resn LEU and (name CD1 or name CD2)) or
(neighbor 2nuz and resn VAL and (name CG1 or name CG2)))  and (not elem c)",
"stored.b.append(ID)")

for a in stored.a:
    for b in stored.b:
        if a==b or pymol.cmd.distance( "id %s" % a, "id %s" % b,'5')==0.0:
            pass
        else:
            atoms1= pymol.cmd.get_model("id %s" % a)
            for at in atoms1.atom:
                atoms2= pymol.cmd.get_model("id %s" % b)
                for at1 in atoms2.atom:
                    if str(at.resn)==str(at1.resn) and str(at.resi_number)==str(at1.resi_number):
                        pass
```

```
            #print
str(at.resn)+str(at.resi_number)+str(at.name),str(at1.resn)+str(at1.resi_number)+str(at1.name),"%s" % (pymol.cmd.distance( "id %s" % a, "id %s" % b,'5'))
          else:
            #pass
            print
str(at.resn)+str(at.resi_number)+str(at.name),str(at1.resn)+str(at1.resi_number)+str(at1.name),"%s" % (pymol.cmd.distance( "id %s" % a, "id %s" % b,'5'))
#outFile.close()
pymol.cmd.quit()
```

Matlab scripts for the OMA analysis:

1. Run script

```
clear;
happy = transpose( dir( '*.txt' ) );

fid1=fopen('list','wt');
for file = happy;
    disp( file.name );
    FileName = (file.name);
  %   [num text raw] = xlsread(FileName)
     Fit
end
fclose(fid1);
```

2. Fit script

```
y1=dlmread(FileName,' ','A1..A16');
y=y1/max(y1);
x1=dlmread('vclist',' ','A1..A16');
x=x1*0.0004;
noise=dlmread('noise',' ','A1..A16');
noise=noise/max(y1);

%%%%%%%%%%%%%%%%%%zerofilling%%%%%%%%%%%%%%%%%
%nfft1=length(x);
%zfill=zeros(1,nfft1*2);
%totzfdat=[transpose(y),zfill];
%y=transpose(totzfdat);5
%for i=1:nfft1*3;
%    x(i)=0.0004*i;
%end;
%%%%%%%%%%%%%%%%%%%%%%%%%%%%%%%%%%%%%%%%%%%%%%%%%%%%%

%%%%%%%%%%%%%%%%%%apodization%%%%%%%%%%%%%%%%%
%for i=1:nfft1*3;
%    y(i)=y(i)*(100-90/0.384*x(i));
%     y(i)=y(i)*(0.1/x(i));
%end;

%Eqn = '(0.1/x)*((p*exp(-1*x/b)+(1-p)*exp(-1*x/c)*(fresnelc(sqrt(6*d*2*pi*a*x/pi/sqrt(2)))*cos((pi*e+d*2*pi*a/sqrt(2))*x)+fresnels(sqrt(6*d*2*pi*a*x/pi/sqrt(2)))*sin((pi*e+d*2*pi*a/sqrt(2))*x))/(sqrt(6*d*2*pi*a*x/pi/sqrt(2)))))';
%Eqn = '(100-90/0.384*x)*((p*exp(-1*x/b)+(1-p)*exp(-1*x/c)*(fresnelc(sqrt(6*d*2*pi*a*x/pi/sqrt(2)))*cos((pi*e+d*2*pi*a/sqrt(2))*x)+fresnels(sqrt(6*d*2*pi*a*x/pi/sqrt(2)))*sin((pi*e+d*2*pi*a/sqrt(2))*x))/(sqrt(6*d*2*pi*a*x/pi/sqrt(2)))))';
%%%%%%%%%%%%%%%%%%%%%%%%%%%%%%%%%%%%%%%%%%%%%%%%%%%%
```

```
Eqn = '(p*exp(-1*x/b)+(1-p)*exp(-1*x/c)*(fresnelc(sqrt(6*d*2*pi*a*x/pi/sqrt(2)))*cos((pi*e+d*2*pi*a/sqrt(2))*x)+fresnels(sqrt(6*d*2*pi*a*x/pi/sqrt(2)))*sin((pi*e+d*2*pi*a/sqrt(2))*x))/(sqrt(6*d*2*pi*a*x/pi/sqrt(2))))';
options=fitoptions(Eqn);
  options.start=[-0.00154,0.001,0.05,10000,93,0.1];
  options.lower=[-0.00154,0.001,0.001,2000,80,0];
  options.upper=[-0.00154,inf,inf,20000,110,1];
  options.Weights=abs(noise)
  f1=fit(x,y,Eqn,options);
  disp(f1);%disp(f2)
  n=figure();
  plot(f1,x,y);
  hold on;
  errorbar(x,y,noise,'linestyle','none');
  hold on;
  %title(f1);
  %saveas(n,strcat(FileName,'.fig'));
  f2 = coeffvalues(f1);
  f3 = confint(f1);
  k =f2(4)-f3(1,4);
  l =f2(5)-f3(1,5);
  fprintf('%e\n',f2(4));
fprintf(fid1,FileName);
%fprintf(fid1,'  -0.0018 %e  %e  %e  %e %e\n',f2(2),f2(3),f2(4),f2(5),f2(6));
fprintf(fid1,'  %e\t%e\t%e\t%e\n',f2(4),k,f2(5),l);
```

Matlab FFT for the analysis of a spin echo curve:

```
figure;hold on
x1=dlmread('23.txt',' ','A1..A16');
T1=6*10^(-3);
Fs1=1/T1;
%%%%%%%%%%%%%%%%%%%%apodization%%%%%%%%%%%%%%%%%%%
for i=1:16;
x1(i)=x1(i)*(100-90/16*i);
%     x1(i)=x1(i)*(0.1/i/T1);
end;
%%%%%%%%%%%%%%%%%%%%%%%%%%%%%%%%%%%%%%%%%%%%%%%%%%%%%%%%%%%%%%%%%%%%%%%%%%%%%%%

nfft1=length(x1);
zfill= zeros(1,nfft1*8);

totzfdat= [transpose(x1), zfill];
x1= transpose(totzfdat);
nfft1= length(x1);
X1=fftshift(fft(x1));

%X1=X1(nfft1/2+1:nfft1);
mx1=abs(X1);
mx2=mx1/max(mx1)
f1=(0:nfft1-1)*Fs1/nfft1-Fs1/2;
a1=plot(f1,mx2);
%xlim([-200 200]);
%m1="L8"
%xlabel('Frequency (Hz)');
%ylabel('Power');
%legend([a1],[m1]);
%hold off;

Q=mx2;
W=transpose(f1);
```

```
N=zeros(2,length(Q));
N(1,1:length(Q))=W;
N(2,1:length(Q))=Q;
L=zeros(2,length(Q));
j=1;
for i=1:length(Q)
if N(2,i)>0.7
L(1,j)=N(1,i)
L(2,j)=N(2,i)
j=j+1
end
end

X=transpose(L(1,1:length(Q)));
Y=transpose(L(2,1:length(Q)));
eqn='((1/(1+((x-a)/b)^2)+1/(1+((x+a)/b)^2)))*e+((1/(1+((x-c)/d)^2)+1/(1+((x+c)/d)^2)))*f';
options=fitoptions(eqn);
options.start=[50,20,50,20,1,0];
options.lower=[0,0,0,0,0,0];
options.upper=[110,200,110,200,1,0];
f2=fit(X,Y,eqn,options);
b1=plot(f2,X,Y);
xlim([-200 200]);
xlabel('Frequency (Hz)');
ylabel('Power');
m1="13"
legend([a1],[m1]);
disp(f2);
hold off
% f3 = coeffvalues(f2);
%  fprintf('%e\n',f3(1));
%fprintf(fid1,FileName);
%fprintf(fid1,'     %e\n',f3(1));
```

SIMMOL script to extract the spin system from a PDB file:

```
# obtained from ubi_1d3z.pdb, frame 0, using VMD and simmolvmd
# load  ubi_1d3z.pdb to VMD first and then use
# commands:
#> package require simmol
#> cd my/directory
#> mnewspinsys
#> set s1 [atomselect top "index 686 695 696 697"]
#> mdipole $s1 $s1 0AA 0Hz
#> msavespinsys ch3.spinsys -simpson

spinsys {
  # 1: 0 C CD2 43 A {} 686
  # 2: 0 H 1HD2 43 A {} 695
  # 3: 0 H 2HD2 43 A {} 696
  # 4: 0 H 3HD2 43 A {} 697
  channels 1H 13C
  nuclei 13C 1H 1H 1H
  dipole 2 4 -21949.204393756958 0 135.22575990119816 -102.23325760089932
  dipole 1 4 -23937.605394164664 0 161.86539969269555 -152.36868493085922
  dipole 3 4 -21999.260808447398 0 162.56357114531434 43.61768014046981
  dipole 1 2 -23913.64340713163 0 78.04124164970187 91.89670528961673
  dipole 2 3 -22147.380121094793 0 75.86728355761379 -112.24471798299754
  dipole 1 3 -24206.435810614115 0 52.66294526760982 -142.59482885284478
}
```

Python script for a peak intensity analysis:

```
import numpy as np
import nmrglue as ng
import matplotlib.pyplot as plt
import matplotlib.cm

# plot parameters
xpad = 5                    # padding around peak box on x-axis
ypad = 5                    # padding around peak box on y-axis
cmap = matplotlib.cm.Blues_r    # contour map (colors to use for contours)

# contour levels
cl = 3000000 * 1.30 ** np.arange(10)
peak_list = np.recfromtxt("boxes_sigch3.in", names=True)

# read in the spectral data
dic, data = ng.bruker.read_pdata('/Network/Servers/server.reif/Volumes/DATA_RAID/NetUsers/kaixue/Desktop/Ultrafastspinning_042017/BReif_SH3_2H13C15N_March2017/20/pdata/991')
fig = plt.figure()
ax = fig.add_subplot(111)
ax.contour(data, cl, cmap=cmap)
#ax.set_ylim(81,390)
#ax.set_xlim(4790,5511)
add=1000
for peak, x0, y0, x1, y1 in peak_list:

    if x0 > x1:
        x0, x1 = x1, x0
    if y0 > y1:
        y0, y1 = y1, y0

        # create the figure

        # plot the contours
        #print "Plotting:", peak, spec_number

        #extent = (x0 - xpad + 1, x1 + xpad - 1, y0 - ypad + 1, y1 + ypad - 1)
        #extent=(ppm_15n_0, ppm_15n_1,ppm_1h_0,ppm_1h_1)
        #ax.contour(slice, cl, cmap=cmap, extent=extent)          # when you want to create box
        ax.plot([x0+add, x1+add, x1+add, x0+add, x0+add], [y0, y0, y1, y1, y0], 'k-', linewidth=2.0)
        ax.text(x1+add+ 1, y0, peak, size=14, color='b')
plt.show()
#fig.savefig("spec_with_peak_picking.png")
# draw a box around the peak
#ax.plot([x0, x1, x1, x0, x0], [y0, y0, y1, y1, y0], 'k--')
```

Python script to extract 2D spectra peak intensities using a fix-sized boxes integration:

```
#! /usr/bin/env python
# Scipt to extract trajectories from a series a 2D spectrum.

import nmrglue as ng
import numpy as np

# read in the integration limits and list of spectra
peak_list = np.recfromtxt("boxes_sigchd2.in")
spectra_list = np.recfromtxt("spectra_chd2.in")
add= 1000     # peaks are translated by this amount in the x axis
```

```
# prepare the trajs records array
#num_spec = spectra_list.size
#num_peaks = peak_list.size
#elist = [np.empty(num_spec, dtype="float") for i in xrange(num_peaks)]
#trajs = np.rec.array(elist, names=list(peak_list.f0))
f= open("chd2_volumes.txt", 'w')
f.write("# Name \t Volume \n" )

# loop over the spectra
for sn, spectra in enumerate(spectra_list):

    # read in the data from a NMRPipe file
    print "Extracting from:", spectra
    dic, data = ng.bruker.read_pdata(spectra)
    data= (data*(2**(dic["procs"]["NC_proc"])))

    # loop over the integration limits
    for name, x0, y0, x1, y1 in peak_list:

        # integrate the region and save in trajs record array
        if x0 > x1:
            x0, x1 = x1, x0
        if y0 > y1:
            y0, y1 = y1, y0
        #trajs[name][sn] = data[y0:y1 + 1, x0:x1 + 1].sum()
        vol = data[y0:y1+1, x0+add:x1+1+add].sum()
        f.write("%s\t%.3f\n"%(name, vol))
# normalize each trajectory
#for peak in trajs.dtype.names:
#    trajs[peak] = trajs[peak]

# save the trajectories records array to disk
#np.save("traj.npy", trajs)
f.close()
```

GNUPLOT scripts:

1. Bar plot

```
#!/usr/bin/gnuplot
set style data histogram
set style histogram cluster gap 1 errorbars
set style fill solid border rgb "black"
plot "T2.list" u 5:8:xtic(1) title col linecolor rgb "black","T2.list" u 7:9:xtic(1) title col linecolor rgb "red"
set yrange [0:0.055]
set xtics rotate
set xlabel "Residues" font "Helvetica,20"
set ylabel "T2 (s)" font "Helvetica,20"
set tics font "Helvetica,20"
#unset key
set terminal postscript eps color solid linewidth 2
set output "T2.eps"
replot
set output
```

2. Correlation plot

```
#!/usr/bin/gnuplot
plot "Instaneous_fitting_OMA.list"u 5:11:6 with xerrorbars pt 7 ps 2 linecolor "red","Instaneous_fitting_OMA.list"u 5:11:12 with yerrorbars pt 7 ps 2 linecolor "red"
set xrange [0:1.2]
set yrange [0:1.2]
set xlabel "CPPI S^2" font "Helvetica,20"
```

```
set ylabel "OMA simu S^2" font "Helvetica,20"
unset key
set title "CPPI OMAsimu" font "Helvetica,20"
set tics font "Helvetica,20"
set terminal postscript eps color solid linewidth 2
set output "CPPI_OMAsimu.eps"
replot
set output
```

3. Normal curve/dotted plot

```
#!/usr/bin/gnuplot
plot "Simulation.list"u 1:2 w lp pt 6 ps 3 linecolor "black", "Experiment.list" u 1:2 w lp pt 6 ps 3 linecolor
"red"
set logscale x
set xrange [8:12000]
set yrange [0:110]
set xlabel "MAS (kHz)" font "Helvetica,20"
set ylabel "Intensity (a.u)" font "Helvetica,20"
unset key
set title "8D1" font "Helvetica,20"
set tics font "Helvetica,20"
set terminal postscript eps color solid linewidth 2
set output "8D1.eps"
replot
set output
```

SIMPSON scripts:

1. OMA simulation

```
spinsys {
  channels 15N 1H
  nuclei 15N 1H
  shift 1 0 0 0 0 0 0
  shift 2 0 0 0 0 0 0
  jcoupling 1 2 91 0 0 0 0 0
  dipole    1 2 11000.0 0 0 0
}

par {
  proton_frequency 400e6
  start_operator   I1x
  detect_operator  -I1p
  spin_rate        20000
  crystal_file     zcw986
  gamma_angles     1
  sw               spin_rate*gamma_angles
  np               30
  variable t       1.0e6/spin_rate*5
#  rotor_angle      54.72
#  variable pl      0.5e6/sw
#  verbose          1101
  method           direct
}

proc pulseq {} {
global par
maxdt 1.0

reset
delay $par(t)
```

```
pulseid 1 500000 y 500000 x
delay $par(t)
store 1

reset
delay $par(t)
store 2

for {set i 2} {$i <$par(np)} {incr i} {
reset
prop 2
prop 2
prop 2
prop 2
prop 2
prop 2
prop 2
prop 1
prop 2
prop 2
prop 2
prop 2
prop 2
prop 2
prop 2
store 1
acq
}
}

proc main {} {
global par

set f [fsimpson]
#fsave $f $par(rotor_angle).fid
fsave $f OMA.fid
funload $f
}
```

2. CH3 MAS dependent peak amplitude:

```
spinsys {
channels 1H
  nuclei 1H 1H 1H
  dipole 1 3 -15281.39716833282 0 138.66968836935894 -37.32794458648066
  dipole 2 3 -5500 0 148.3264955777185 -150.35187007753458
  dipole 1 2 -15281.39716833282 0 155.86518663311486 -127.94753648945152
}


par {
gamma_angles                                    32
crystal_file                                    zcw986
num_cores      48
np                                              32768
start_operator                                  Inx
detect_operator                                 Inp
method                                          gcompute freq block_diag
#variable rf                                    0
#variable flip      180
#variable tp        1.0e6*flip/(rf*360.0)
```

```
#variable ph   25
#spin_rate          300000
sw              250000
#variable dw                                                    (1e06/sw)
#verbose 1101
}



proc pulseq {} {
global par
maxdt [expr 1.0e6/$par(spin_rate)/36]
#maxdt 1
acq_block {
delay $par(dw)
}
}

proc main {} {
global par

set fp [ open "intensities_3H.dat" "w"]

for {set dd 10500} { $dd <=10500 } { incr dd 1000 } {
# 4000 6000 8000 10000 12000 15000 20000 25000 35000 45000 55000 65000 75000 85000 95000
foreach par(spin_rate) {4000 6000} {
set par(dw) [expr 1.0e6/$par(spin_rate)/$par(gamma_angles)]
puts "MAS = $par(spin_rate) Hz"
puts "dipole coupling with 2nd spin = $dd"
set f [fsimpson [ list [list dipole_1_3_aniso [expr -1* $dd]] [list dipole_1_2_aniso [expr -1*$dd]] ] ]
#set f [fsimpson [ list [list  dipole_1_2_aniso [expr -1*$dd]] ] ]
#set f [fsimpson]
fft $f -inv
faddlb $f 50 0
set z [findex $f 1]
fsetindex $f 1 [expr [lindex $z 0]*0.5] [expr [lindex $z 1]*0.5]
fft $f
fsave $f [lindex [format "3Hspec_at%.2f_%.2f.spe" $par(spin_rate) $dd]]

set z [fint $f {{-2000 2000}}]
set x [fint $f {{-125000 125000}}]

puts "[expr 1.000*$z/$x] [expr $par(spin_rate)] [expr $dd]"
puts $fp "[expr 1.000*$z/$x] [expr $par(spin_rate)] [expr $dd]"


funload $f
}
}
}
```

Appendix 3 Bruker Pulse Sequences

1. Residue specific T2 prime measurement:

```
;hCH2D.dcp

;version: 1.0/ TS3.2 /2014/07/11

;written: Veda 2014/07/11
;checked: Veda 2015/03/17

;1D & 2D 13C-1H CP experiment
;HC CP, CH CP, and H-detection

;13C hard pulse optimization possible via 'ZGOPTNS'
;triple channel mode possible via 'ZGOPTNS'

;Avance III version
;Parameters:
;f1 : H
;f2 : N (using '-DTC')
;f3 : C
;o1 : H offset, on resonance with water peak (~5 ppm, water suppression!)
;o2 : N offset, center of 15N signal (~119 ppm, using '-DTC')
;o3 : C offset, center of 13C signal (~100 ppm)
;p1 : C 90 hard pulse at pl1
;p2 : C 180 hard pulse at pl1
;p3 : H 90 hard pulse at pl2
;p21 : N 90 hard pulse at pl21 (using '-DTC')
;p22 : N 180 hard pulse at pl21 (using '-DTC')
;p15 : HC CP at sp40 (H) & sp41 (C), (~1 to 3 ms)
;p48 : CH CP at sp44 (H) & sp45 (C), (~400 to 800 us)
;pl1 : C hard pulse power (can be optimized with '-DC90')
;pl2 : H hard pulse power
;pl3 : not used
;pl12 : H dec power ('sltppm_12nofq' at RF=1/4*MAS rate --> ~15 kHz)
;pl13 : H dec power during H2O suppression (~15 kHz, 'cwX_13nofq', 'cwY_13nofq')
;pl16 : N dec power ('waltz16_16nofq' at 10 kHz, using '-DTC')
;pl18 : C dec power ('waltz16_18nofq' at 10 kHz)
;pl21 : N hard pulse power (using '-DTC')
;sp40 : H HC CP power (50 kHz RF recommended at 60 kHz MAS)
;sp41 : C HC CP power (10 kHz RF recommended at 60 kHz MAS)
;sp44 : H CH CP power (50 kHz RF recommended at 60 kHz MAS)
;sp45 : C CH CP power (10 kHz RF recommended at 60 kHz MAS)
;d0 : incremented delay (t1)
;d1 : recycle delay; 1 to 5 times T1 (~0.8 to 1 s)
;d19 : delay for water suppression (~100 to 300 ms)
;d30 : extra time for constant duty cycle (t1)
;cpdprg1 : H dec ('sltppm_12nofq' at pl12 (15 kHz))
;cpdprg2 : N dec ('waltz16_16nofq' at pl16 (10 kHz), using '-DTC')
```

```
;cpdprg3 : C dec ('waltz16_18nofq' at pl18 (10 kHz))
;cpdprg4 : H Water suppression along X ('cwX_13nofq' at pl13 (15 kHz))
;cpdprg5 : H Water suppression along Y ('cwY_13nofq' at pl13 (15 kHz))
;pcpd1 : H dec pulse: 33.33 us ('sltppm_12nofq' at 15kHz)
;pcpd2 : N dec pulse: 25 us ('waltz16_16nofq' 10 kHz, using '-DTC')
;pcpd3 : C dec pulse: 25 us ('waltz16_18nofq' 10 kHz)
;spnam40 : H shape (ramp up for CH CP, e.g. 'ramp70100.1000')
;spnam41 : C shape (e.g. 'square.1000' for HC CP (=no shape))
;spnam44 : H shape (ramp down for CH CP, e.g. 'ramp10070.1000')
;spnam45 : C shape (e.g. 'square.1000' for CH CP (=no shape))
;cnst30 : expected td1 for use in constant duty cycle (-DCDC)
;inf1 :  1/SW(C) = 2 * DW(C)
;in0 : = inf1
;in30 : = inf1
;l0 : loopcounter for F1
;ZGOPTNS : -DCDC  : for constant duty cycle (same heating effects/scan)
;         -DTC   : for HNC triple channel mode
;                  (default: HC double channel mode)
;         -DC90  : optimize 13C 90 pulse (ZERO crossing)
;         -Dlacq : acquisition times > 50ms
;         or blank
;FnMODE : States-TPPI
;ns : MIN. 4 (full: 8)
;ds : 2 or 4


;#############################################################
;#                                                           #
;# hCH2D.cp based on hNH2D.dcp                               #
;# Knight et al, Angew. Chem. Int. Ed. Engl.                 #
;# 2011, 50, 11697-11701.                                    #
;#                                                           #
;#############################################################


;$COMMENT=hCH CP-based HSQC
;$CLASS=BioSolids
;$DIM=1D, 2D
;$TYPE=H detection
;$SUBTYPE=CP, Heteronuclear

prosol relations=<biosolHCN>

#include <HNC_defs.incl>
       ; defines H:f1, N:f2, C:f3

#include <trigg.incl>
       ; definition of external trigger output

"acqt0=-(p1*2/3.1416)-0.5u"     ; baseopt correction

"spoff40=0.0"              ;############################
"spoff41=0.0"              ;#     ensure correct     #
"spoff44=0.0"              ;#     shape offsets      #
"spoff45=0.0"              ;############################

"p2=p1*2"
"p22=p21*2"

"in0=inf1"                ;############################
```

```
"d0=1u"                  ;#    t1_init => 0, 0     #
"in30=inf1"              ;#                        #
"l0=0"                   ;############################

define delay ONTIME      ;############################
define loopcounter T1evo    ;#                       #
#ifdef CDC               ;#   Constant Duty Cycle  #
"T1evo=larger(td1,cnst30)"  ;#                       #
"d30=T1evo*(in30+1u)/2"     ;#                       #
#else                    ;#                       #
"d30=1u"                 ;#                       #
#endif                   ;############################

                         ;############################
;$EXTERN                 ;# python insertion point #
                         ;############################

"ONTIME=aq+d0+d30+p15+p48+d19"

Prepare, ze

;#############################################################
;#              Protections: Pre-Check               #
;#############################################################

#ifdef lacq
#else
#include <acq_prot.incl>
       ;Max. 50 ms acquisition time
#include <ONTIME_H_prot.incl>
       ;total RF deposition restriction to < 1 s
#endif               /* end of lacq */

#include <p15bio_prot.incl>
       ;p15 max. 10 ms
#include <p48bio_prot.incl>
       ;p48 max. 10 ms
#include <noH2Obio_prot.incl>
       ;water suppression d19 max. 500 ms

;#############################################################
;#          Start of Active Pulse Program           #
;#############################################################

 Start, 30m  do:C

#ifdef TC
  0.5u do:N
#endif         /* end of TC */

  d1
  trigg

if "l0>0"
{
  "d51=d0-1u"
}

;#############################################################
;#            Initial excitation & HC CP            #
```

```
;#########################################################

  (p3 pl2 ph1):H
0.5u pl19:C
0.5u cpds6:C
vd
(p3*2 pl2 ph19):H
vd
0.5u do:C
  (p15:sp40 ph0):H  (p15:sp41 ph2):C

;#########################################################
;#                 t1 evolution                  #
;#           Polarization is on 13C              #
;#########################################################

  0.5u pl12:H

#ifdef TC
if "l0>0"
{
  0.5u cpds1:H
  (center (d51) (p22 pl21 ph20):N)
  0.5u do:H  pl13:H
}
#else
if "l0>0"
{
  0.5u cpds1:H
  d51
  0.5u do:H  pl13:H
}
#endif         /* end of TC */

;#########################################################
;#           Water suppression                   #
;#########################################################

  (p1 pl1 ph3):C          ; brings magn. to z

  0.5u cpds4:H
  d19*0.25
  0.5u do:H

  0.5u cpds5:H
  d19*0.25
  0.5u do:H

  0.5u cpds4:H
  d19*0.25
  0.5u do:H

  0.5u cpds5:H
  d19*0.25
  0.5u do:H

  (p1 pl1 ph4):C          ; brings magn. to y

;#########################################################
;#          13C hard pulse optimization          #
```

```
;#########################################################

#ifdef C90              ; brings magn. to z
  (p1 pl1 ph22):C
#endif          /* end of C90 */

;#########################################################
;#                  C-H CP                       #
;#########################################################

  (p48:sp45 ph5):C  (p48:sp44 ph6):H

;#########################################################
;#                  Acquisition                  #
;#########################################################

;#ifdef TC
 ; 0.5u pl16:N  pl18:C
 ; 0.5u cpds2:N  cpds3:C
;#else
  0.5u pl18:C
  0.5u cpds3:C
;#endif         /* end of TC */

 ; gosc ph31     ;start ADC with ph31 signal routing

;#ifdef CDC
 ; d30
;#endif         /* end of CDC */

;#ifdef TC
 ; 1m do:C  do:N
;#else
 ; 1m do:C
;#endif         /* end of TC */

;lo to Start times ns
;30m mc #0 to Start F0(zd)
go= Start ph31
1m do:C
30m wr #0 if #0 ivd
lo to Start times td1
;30m mc #0 to Start
;F1PH(calph(ph2, +90), caldel(d0, +in0) & caldel(d30, -in30) & calclc(l0, 1))


HaltAcqu, 1m
exit

;#######################################
;#           Phase Cycle          #
;#######################################

ph1 = 1 3               ; H 90 hard pulse
ph0 = 0                 ; H HC CP Spin lock
ph2 = 1                 ; C HC CP Spin lock
ph3 = 0                 ; C 1st 90 hard pulse (flip to z)
ph4 = 0 0 2 2             ; C 2nd 90 hard pulse (flip back)
ph5 = 1                 ; C CH CP Spin lock
ph6 = 1 1 1 1  3 3 3 3     ; H CH CP Spin lock
```

```
ph19= 1
ph31= 1 3 3 1  3 1 1 3     ; receiver

#ifdef TC
ph20= 0                    ; N 180 hard pulse
#endif                     /* end of TC */

#ifdef C90
ph22= 0 0 2 2              ; C hard pulse
#endif                     /* end of C90 */

;############################################################



;$Id: hCH2D.dcp,v 1.1.2.1 2015/08/14 14:58:57 ber Exp $

      2.    OMA CP based experiment:
;1h detected cp hsqc
;avance-version (07/04/04)
;HSQC
;with decoupling during acquisition
;
;R sarkar
;
;$CLASS=HighRes
;$DIM=2D
;$TYPE=
;$SUBTYPE=
;$COMMENT=

prosol relations=<solids_cp>
#include <Avance.incl>
#include <Delay.incl>
#include <trigg.incl>

"d11=30m"
;"d0=3u"
"in10=inf2"


define list <loopcounter> t2list = <$VCLIST>

;define loopcounter COUNTER

aqseq 312




1 ze
  d11

2 1m do:f2 st0
3 1m
4 d1

;;;;2u "COUNTER = t2list"
2u
```

```
5u

5u reset:f1 reset:f2


(p1  pl1 ph1):f1
(p15 pl2 ph2):f2 (p15:spf0 pl10 ph10):f1


;;;;;; evolution of 15N;;;;;;;;;;;;;;;;;;;

5 20u
lo to 5 times t2list        ;t2list

(center (p3*2 pl1 ph19):f1 (p7*2 pl7 ph19):f2)


6 20u
lo to 6 times t2list                ;t2list
0.5u do:f2

;;;;;;;;;;;;;;;;;;;;;;;;;



;;;;

1u pl12:f1
1u cpds1:f1
d10
1u do:f1

(p7 pl7 ph5):f2
1u pl13:f1

(p30*0.25 ph21):f1
(p30*0.25 ph22):f1
(p30*0.25 ph23):f1
(p30*0.25 ph24):f1

(p6 pl7 ph6):f2

(p17 pl20 ph7):f2 (p17:sp10 ph11):f1

  ;0.5u pl14:f2
 ; 0.5u  cpds2:f2
  ;go=2 ph31
  ;1m do:f2
 ; 10m mc #0 to 2
  ;F1PH(ip2, id0)
;HaltAcqu, 1m
;exit



;###########################################################
;#                    Acquisition                    #
;###########################################################
0.5u pl14:f2
```

```
0.5u cpds2:f2
goscnp ph31
3m do:f2
  3m st t2list.inc
  lo to 3 times nbl

  3m t2list.res
  3m ipp1 ipp11 ipp6 ipp31

  lo to 4 times ns

  d31 mc #0 to 4
     F1QF()
     F2PH(calph(ph2) & exec(rppall), caldel(d10, +in10))
     d31
exit
```

```
ph0=0
ph1  = 1 3
ph10 = 0
ph2 =  1
ph5 =  0
ph6 =  0 0 2 2
ph12 = 1 1 1 1
ph7 =  1
ph11 = 1 1 1 1 3 3 3 3
ph19= 0 0 0 0 0 0 0 0 1 1 1 1 1 1 1 1 2 2 2 2 2 2 2 2 3 3 3 3 3 3 3 3
ph17= 1
ph21 = 2
ph22 = 3
ph23 = 0
ph24 = 1
ph31 = 1 3 3 1 3 1 1 3 3 1 1 3 1 3 3 1
```

References

1. Williamson MP, Havel TF, Wuethrich K. Solution Conformation of Proteinae Inhibitor IIA from Bull Seminal Plasma by 1H NMR and Distance Geometry. JMolBiol. 1985;182:295-315.
2. Andrew ER, Bradbury A, Eades RG. Nuclear Magnetic Resonance Spectra from a Crystal Rotated at High Speed. Nature. 1958;182(4650):1659.
3. Wasmer C, Lange A, Van Melckebeke H, Siemer AB, Riek R, Meier BH. Amyloid fibrils of the HET-s(218-289) prion form a beta solenoid with a triangular hydrophobic core. Science. 2008;319(5869):1523-6.
4. Waugh JS. Sixty years of nuclear moments. Annu Rev Phys Chem. 2009;60:1-19.
5. Bak M, Rasmussen JT, Nielsen NC. SIMPSON: A General Simulation Program for Solid-State NMR Spectroscopy. Journal of Magnetic Resonance. 2000;147(2):296-330.
6. Bockmann A, Ernst M, Meier BH. Spinning proteins, the faster, the better? J Magn Reson. 2015;253:71-9.
7. Straus SK, Bremi T, Ernst RR. Experiments and strategies for the assignment of fully 13C/15N-labelled polypeptides by solid state NMR. J Biomol NMR. 1998;12(1):39-50.
8. McDermott A, Polenova T, Bockmann A, Zilm KW, Paulson EK, Martin RW, et al. Partial NMR assignments for uniformly (13C, 15N)-enriched BPTI in the solid state. J Biomol NMR. 2000;16(3):209-19.
9. Rienstra CM T-KL, Jaoniec CP, Hohwy M, Reif B, McMahon MT, Tidor B, Perez, TL, Griffin RG. De novo determination of peptide structure with solid-state magic-angle spinning NMR spectroscopy. Proc Natl Acad Sci U S A. 2002;99:12060-0265.
10. Castellani F, van Rossum B, Diehl A, Schubert M, Rehbein K, Oschkinat H. Structure of a protein determined by solid-state magic-angle-spinning NMR spectroscopy. Nature. 2002;420(6911):98-102.
11. Jaroniec CP, MacPhee CE, Bajaj VS, McMahon MT, Dobson CM, Griffin RG. High-resolution molecular structure of a peptide in an amyloid fibril determined by magic angle spinning NMR spectroscopy. P Natl Acad Sci USA. 2004;101(3):711-6.
12. Siemer AB, Ritter C, Ernst M, Riek R, Meier BH. High-resolution solid-state NMR spectroscopy of the prion protein HET-s in its amyloid conformation. Angew Chem Int Ed Engl. 2005;44(16):2441-4.
13. Tuttle MD, Comellas G, Nieuwkoop AJ, Covell DJ, Berthold DA, Kloepper KD, et al. Solid-state NMR structure of a pathogenic fibril of full-length human alpha-synuclein. Nat Struct Mol Biol. 2016;23(5):409-15.
14. Bertini I, Bhaumik A, De Paepe G, Griffin RG, Lelli M, Lewandowski JR, et al. High-resolution solid-state NMR structure of a 17.6 kDa protein. J Am Chem Soc. 2010;132(3):1032-40.

15. Hong M, Jakes K. Selective and extensive 13C labeling of a membrane protein for solid-state NMR investigations. J Biomol NMR. 1999;14(1):71-4.
16. Lange A, Becker S, Seidel K, Giller K, Pongs O, Baldus M. A concept for rapid protein-structure determination by solid-state NMR spectroscopy. Angew Chem Int Ed Engl. 2005;44(14):2089-92.
17. Agarwal V, Diehl A, Skrynnikov N, Reif B. High Resolution ^{1}H Detected ^{1}H,^{13}C Correlation Spectra in MAS Solid-State NMR using Deuterated Proteins with Selective ^{1}H,^{2}H Isotopic Labeling of Methyl Groups. J Am Chem Soc. 2006;128(39):12620-1.
18. Barbet-Massin E, Huang C-T, Daebel V, Hsu S-TD, Reif B. Site-Specific Solid-State NMR Studies of "Trigger Factor" in Complex with the Large Ribosomal Subunit 50S. Angewandte Chemie Int Edt Engl. 2015;54(14):4367–9.
19. Chevelkov V, Rehbein K, Diehl A, Reif B. Ultra-high resolution in proton solid-state NMR at high levels of deuteration. Angew Chem Int Ed. 2006;45(23):3878-81.
20. Huber M, Hiller S, Schanda P, Ernst M, Bockmann A, Verel R, et al. A proton-detected 4D solid-state NMR experiment for protein structure determination. Chemphyschem. 2011;12(5):915-8.
21. Andreas LB, Jaudzems K, Stanek J, Lalli D, Bertarello A, Le Marchand T, et al. Structure of fully protonated proteins by proton-detected magic-angle spinning NMR. Proc Natl Acad Sci U S A. 2016;113(33):9187-92.
22. Comellas G, Rienstra CM. Protein Structure Determination by Magic-Angle Spinning Solid-State NMR, and Insights into the Formation, Structure, and Stability of Amyloid Fibrils. Annu Rev Biophys. 2013;42:515-36.
23. Baldus M, Petkova AT, Herzfeld J, Griffin RG. Cross polarization in the tilted frame: assignment and spectral simplification in heteronuclear spin systems. Mol Phys. 1998;95(6):1197-207.
24. Suter D, Ernst RR. Spectral Spin Diffusion in the Presence of an Extraneous Dipolar Reservoir. Phys Rev B. 1982;25(9):6038-41.
25. Takegoshi K, Nakamura S, Terao T. 13C–1H dipolar-assisted rotational resonance in magic-angle spinning NMR. Chemical Physics Letters. 2001;344(5-6):631-7.
26. Lange A, Luca S, Baldus M. Structural constraints from proton-mediated rare-spin correlation spectroscopy in rotating solids. J Am Chem Soc. 2002;124(33):9704-5.
27. Lewandowski JR, De Paëpe G, Griffin RG. Proton Assisted Insensitive Nuclei Cross Polarization. Journal of the American Chemical Society. 2007;129(4):728-9.
28. De Paepe G, Lewandowski JR, Loquet A, Bockmann A, Griffin RG. Proton assisted recoupling and protein structure determination. J Chem Phys. 2008;129(24):245101.
29. Bennett AE, Ok JH, Griffin RG, Vega S. Chemical-Shift Correlation Spectroscopy in Rotating Solids - Radio Frequency-Driven Dipolar Recoupling and Longitudinal Exchange. Journal of Chemical Physics. 1992;96(11):8624-7.
30. Tycko R, Dabbagh G. Measurement of Nuclear Magnetic Dipole-Dipole Couplings in Magic Angle Spinning Nmr. Chemical Physics Letters. 1990;173(5-6):461-5.
31. Nielsen NC, Bildsoe H, Jakobsen HJ, Levitt MH. Double-Quantum Homonuclear Rotary Resonance - Efficient Dipolar Recovery in Magic-Angle-Spinning Nuclear-Magnetic-Resonance. Journal of Chemical Physics. 1994;101(3):1805-12.
32. Lee YK, Kurur ND, Helmle M, Johannessen OG, Nielsen NC, Levitt MH. Efficient dipolar recoupling in the NMR of rotating solids. A sevenfold symmetric radiofrequency pulse sequence. Chemical Physics Letters. 1995;242(3):304-9.

33. Verel R, Ernst M, Meier BH. Adiabatic dipolar recoupling in solid-state NMR: the DREAM scheme. J Magn Reson. 2001;150(1):81-99.
34. Kiihne S, Mehta MA, Stringer JA, Gregory DM, Shiels JC, Drobny GP. Distance measurements by dipolar recoupling two-dimensional solid-state NMR. J Phys Chem A. 1998;102(13):2274-82.
35. Weingarth M, Demco DE, Bodenhausen G, Tekely P. Improved magnetization transfer in solid-state NMR with fast magic angle spinning. Chemical Physics Letters. 2009;469(4-6):342-8.
36. Hu B, Lafon O, Trébosc J, Chen Q, Amoureux J-P. Broad-band homo-nuclear correlations assisted by 1H irradiation for bio-molecules in very high magnetic field at fast and ultra-fast MAS frequencies. Journal of Magnetic Resonance. 2011;212(2):320-9.
37. Gullion TS, J. Detection of Weak Heteronuclear Dipolar Coupling by Rotational-Echo Double-Resonance Nuclear Magnetic Resonance. Advances in Magnetic and Optical Resonance. 1989;13:57-83.
38. Hing AW, Vega S, Schaefer J. Transferred-echo double-resonance NMR. Journal of Magnetic Resonance (1969). 1992;96(1):205-9.
39. Graesser DT, Wylie BJ, Nieuwkoop AJ, Franks WT, Rienstra CM. Long-range19F · 15N distance measurements in highly-13C,15N-enriched solid proteins with19F-dephased REDOR shift (FRESH) spectroscopy. Magnetic Resonance in Chemistry. 2007;45(S1):S129-S34.
40. Hohwy M, Jaroniec CP, Reif B, Rienstra CM, Griffin RG. Local Structure and Relaxation in Solid-State NMR: Accurate Measurement of Amide N−H Bond Lengths and H−N−H Bond Angles. Journal of the American Chemical Society. 2000;122(13):3218-9.
41. Zhao X, Eden M, Levitt MH. Recoupling of heteronuclear dipolar interactions in solid-state NMR using symmetry-based pulse sequences. Chemical Physics Letters. 2001;342(3-4):353-61.
42. Chan JCC, Tycko R. Solid-State NMR Spectroscopy Method for Determination of the Backbone Torsion Angle ψ in Peptides with Isolated Uniformly Labeled Residues. Journal of the American Chemical Society. 2003;125(39):11828-9.
43. Carver TR, Slichter CP. Polarization of Nuclear Spins in Metals. Physical Review. 1953;92(1):212-3.
44. Overhauser AW. Polarization of Nuclei in Metals. Physical Review. 1953;92(2):411-5.
45. Mentink-Vigier F, Paul S, Lee D, Feintuch A, Hediger S, Vega S, et al. Nuclear depolarization and absolute sensitivity in magic-angle spinning cross effect dynamic nuclear polarization. Phys Chem Chem Phys. 2015;17(34):21824-36.
46. Lilly Thankamony AS, Wittmann JJ, Kaushik M, Corzilius B. Dynamic nuclear polarization for sensitivity enhancement in modern solid-state NMR. Progress in Nuclear Magnetic Resonance Spectroscopy. 2017;102-103:120-95.
47. Corzilius B, Smith AA, Griffin RG. Solid effect in magic angle spinning dynamic nuclear polarization. J Chem Phys. 2012;137(5):054201.
48. Thurber KR, Tycko R. Theory for cross effect dynamic nuclear polarization under magic-angle spinning in solid state nuclear magnetic resonance: the importance of level crossings. J Chem Phys. 2012;137(8):084508.
49. Jaudzems K, Bertarello A, Chaudhari SR, Pica A, Cala-De Paepe D, Barbet-Massin E, et al. Dynamic Nuclear Polarization-Enhanced Biomolecular NMR Spectroscopy at High Magnetic Field with Fast Magic-Angle Spinning. Angewandte Chemie International Edition. 2018.

50. Chevelkov V, Rehbein K, Diehl A, Reif B. Ultrahigh resolution in proton solid-state NMR spectroscopy at high levels of deuteration. Angew Chem Int Ed Engl. 2006;45(23):3878-81.
51. Agarwal V, Penzel S, Szekely K, Cadalbert R, Testori E, Oss A, et al. De novo 3D structure determination from sub-milligram protein samples by solid-state 100 kHz MAS NMR spectroscopy. Angew Chem Int Ed Engl. 2014;53(45):12253-6.
52. Schanda P, Meier BH, Ernst M. Quantitativ Analysis of Protein Backbone Dynamics in Microcrystalline Ubiquitin by Solid-State NMR Specroscopy. J AM CHEM SOC. 2010(132):15957-67.
53. Chevelkov VF, V.; Reif, B. Accurate Determination of Order Parameters from 1H, 15N dipolar couplings in MAS Solid-State NMR Experiments. J AM CHEM SOC. 2009(131):14018-22.
54. Asami S, Reif B. Comparative Study of REDOR and CPPI Derived Order Parameters by (1)H-Detected MAS NMR and MD Simulations. J Phys Chem B. 2017;121(37):8719-30.
55. Bodenhausen GR, David J. Natural abundance nitrogen-15 NMR by enhanced heteronuclear spectroscopy. Chemical Physics Letters. 1980;69:185-9.
56. L. Lorieau JME. Conformational Flexibility of Microcrystalline Globular Protein: Order Parameters by Solid-State NMR Spectroscopy. J AM CHEM SOC. 2006(128):11505-12.
57. Penzel S, Smith AA, Agarwal V, Hunkeler A, Org M-L, Samoson A, et al. Protein resonance assignment at MAS frequencies approaching 100 kHz: a quantitative comparison of J-coupling and dipolar-coupling-based transfer methods. Journal of Biomolecular NMR. 2015;63(2):165-86.
58. Loquet A, Sgourakis NG, Gupta R, Giller K, Riedel D, Goosmann C, et al. Atomic model of the type III secretion system needle. Nature. 2012;486(7402):276-9.
59. Wang S, Munro RA, Shi L, Kawamura I, Okitsu T, Wada A, et al. Solid-state NMR spectroscopy structure determination of a lipid-embedded heptahelical membrane protein. Nature methods. 2013;10(10):1007-12.
60. Samoson A, Tuherm T, Past J, Reinhold A, Anupold T, Heinmaa I. New horizons for magic-angle spinning NMR. Topics in current chemistry. 2005;246:15-31.
61. Chevelkov V, Rehbein K, Diehl A, Reif B. Ultrahigh resolution in proton solid-state NMR spectroscopy at high levels of deuteration. Angew Chem Int Edit. 2006;45(23):3878-81.
62. Reif B. Ultra-high resolution in MAS solid-state NMR of perdeuterated proteins: Implications for structure and dynamics. J Magn Reson. 2012;216:1-12.
63. Penzel S, Smith AA, Agarwal V, Hunkeler A, Org ML, Samoson A, et al. Protein resonance assignment at MAS frequencies approaching 100 kHz: a quantitative comparison of J-coupling and dipolar-coupling-based transfer methods. Journal of biomolecular NMR. 2015;63(2):165-86.
64. Asami S, Reif B. Assignment strategies for aliphatic protons in the solid-state in randomly protonated proteins. Journal of biomolecular NMR. 2012;52(1):31-9.
65. Asami S, Reif B. Proton-detected solid-state NMR spectroscopy at aliphatic sites: application to crystalline systems. Accounts of chemical research. 2013;46(9):2089-97.
66. Asami S, Schmieder P, Reif B. High resolution 1H-detected solid-state NMR spectroscopy of protein aliphatic resonances: access to tertiary structure information. Journal of the American Chemical Society. 2010;132(43):15133-5.
67. Asami S, Szekely K, Schanda P, Meier BH, Reif B. Optimal degree of protonation for (1)H detection of aliphatic sites in randomly deuterated proteins as a function of the MAS frequency. Journal of biomolecular NMR. 2012;54(2):155-68.

68. Maricq MM, Waugh JS. Nmr in Rotating Solids. J Chem Phys. 1979;70(7):3300-16.
69. Barbet-Massin E, Pell AJ, Retel JS, Andreas LB, Jaudzems K, Franks WT, et al. Rapid proton-detected NMR assignment for proteins with fast magic angle spinning. Journal of the American Chemical Society. 2014;136(35):12489-97.
70. Sprangers R, Kay LE. Probing supramolecular structure from measurement of methyl (1)H-(13)C residual dipolar couplings. Journal of the American Chemical Society. 2007;129(42):12668-9.
71. Sprangers R, Velyvis A, Kay LE. Solution NMR of supramolecular complexes: providing new insights into function. Nature methods. 2007;4(9):697-703.
72. Pines A, Gibby MG, Waugh JS. Proton-Enhanced Nmr of Dilute Spins in Solids. J Chem Phys. 1973;59(2):569-90.
73. Bodenhausen G, Ruben DJ. Natural Abundance N-15 Nmr by Enhanced Heteronuclear Spectroscopy. Chem Phys Lett. 1980;69(1):185-9.
74. Lewandowski JR, Sass HJ, Grzesiek S, Blackledge M, Emsley L. Site-specific measurement of slow motions in proteins. Journal of the American Chemical Society. 2011;133(42):16762-5.
75. Lewandowski JR, Dumez JN, Akbey U, Lange S, Emsley L, Oschkinat H. Enhanced Resolution and Coherence Lifetimes in the Solid-State NMR Spectroscopy of Perdeuterated Proteins under Ultrafast Magic-Angle Spinning. J Phys Chem Lett. 2011;2(17):2205-11.
76. Zorin VE, Brown SP, Hodgkinson P. Origins of linewidth in 1H magic-angle spinning NMR. J Chem Phys. 2006;125(14):144508.
77. Bak M, Rasmussen JT, Nielsen NC. SIMPSON: a general simulation program for solid-state NMR spectroscopy. J Magn Reson. 2000;147(2):296-330.
78. Kurauskas V, Crublet E, Macek P, Kerfah R, Gauto DF, Boisbouvier J, et al. Sensitive proton-detected solid-state NMR spectroscopy of large proteins with selective CH3 labelling: application to the 50S ribosome subunit. Chemical communications. 2016;52(61):9558-61.
79. Asami S, Schmieder P, Reif B. High resolution 1H-detected solid-state NMR spectroscopy of protein aliphatic resonances: Access to tertiary structure information. J Am Chem Soc. 2010;132:15133–5.
80. Goto NK, Gardner KH, Mueller GA, Willis RC, Kay LE. A robust and cost-effective method for the production of Val, Leu, Ile (d1) methyl-protonated ^{15}N-, ^{13}C-, ^{2}H-labeled proteins. J Biomol NMR. 1999;13:369-74.
81. Agarwal V, Xue Y, Reif B, Skrynnikov NR. Protein side-chain dynamics as observed by solution- and solid-state NMR: a similarity revealed. J Am Chem Soc. 2008;130:16611–21.
82. Gans P, Hamelin O, Sounier R, Ayala I, Dura MA, Amero CD, et al. Stereospecific Isotopic Labeling of Methyl Groups for NMR Spectroscopic Studies of High-Molecular-Weight Proteins. Angewandte Chemie Int Ed. 2010;49(11):1958-62.
83. Lewandowski JR, Dumez JN, Akbey U, Lange S, Emsley L, Oschkinat H. Enhanced Resolution and Coherence Lifetimes in the Solid-State NMR Spectroscopy of Perdeuterated Proteins under Ultrafast Magic-Angle Spinning. J Phys Chem Lett. 2011;2:2205-11.
84. Bockmann A, Ernst M, Meier BH. Spinning proteins, the faster, the better? J Magn Reson. 2015;253:71-9.
85. Kurauskas V, Crublet E, Macek P, Kerfah R, Gauto DF, Boisbouvier J, et al. Sensitive proton-detected solid-state NMR spectroscopy of large proteins with selective CH3 labelling: application to the 50S ribosome subunit. Chem Comm. 2016;52(61):9558-61.

86. Lewandowski JR, Sein J, Sass HJ, Grzesiek S, Blackledge M, Emsley L. Measurement of site-specific 13C spin-lattice relaxation in a crystalline protein. Journal of the American Chemical Society. 2010;132(24):8252-4.
87. Paulson EK, Morcombe CR, Gaponenko V, Dancheck B, Byrd RA, Zilm KW. Sensitive High Resolution Inverse Detection NMR Spectroscopy of Proteins in the Solid State. J Am Chem Soc. 2003;125(51):15831-6.
88. Zhou DH, Shah G, Cormos M, Mullen C, Sandoz D, Rienstra CM. Proton-detected solid-state NMR Spectroscopy of fully protonated proteins at 40 kHz magic-angle spinning. J Am Chem Soc. 2007;129(38):11791-801.
89. Agarwal V, Reif B. Residual Methyl Protonation in Perdeuterated Proteins for Multidimensional Correlation Experiments in MAS solid-state NMR Spectroscopy. J Magn Reson. 2008;194(1):16-24.
90. Asami S, Reif B. Proton-detected solid-state NMR at aliphatic sites: Applications to Crystalline Systems. Acc Chem Res. 2013;46(9):2089-97.
91. Paulson EK, Martin RW, Zilm KW. Cross polarization, radio frequency field homogeneity, and circuit balancing in high field solid state NMR probes. J Magn Reson. 2004;171(2):314-23.
92. Reif B. Ultra-high resolution in MAS solid-state NMR of perdeuterated proteins: Implications for Structure and Dynamics. J Magn Reson. 2012;216:1-12.
93. Sinnige T, Daniels M, Baldus M, Weingarth M. Proton Clouds to Measure Long-Range Contacts between Nonexchangeable Side Chain Protons in Solid-State NMR. Journal of the American Chemical Society. 2014;136(12):4452-5.
94. Paulson EK, Morcombe CR, Gaponenko V, Dancheck B, Byrd RA, Zilm KW. Sensitive high resolution inverse detection NMR spectroscopy of proteins in the solid state. Journal of the American Chemical Society. 2003;125(51):15831-6.
95. Zhou DH, Shah G, Cormos M, Mullen C, Sandoz D, Rienstra CM. Proton-detected solid-state NMR spectroscopy of fully protonated proteins at 40 kHz magic-angle spinning. Journal of the American Chemical Society. 2007;129(38):11791-801.
96. Hoult DI, Richards RE. The signal-to-noise ratio of the nuclear magnetic resonance experiment. 1976. J Magn Reson. 2011;213(2):329-43.
97. Xue K, Sarkar R, Motz C, Asami S, Camargo DCR, Decker V, et al. Limits of Resolution and Sensitivity of Proton Detected MAS Solid-State NMR Experiments at 111 kHz in Deuterated and Protonated Proteins. Sci Rep. 2017;7(1):7444.
98. Zorin VE, Brown SP, Hodgkinson P. Origins of linewidth in 1H magic-angle spinning NMR. J Chem Phys. 2006;125(14):144508.
99. Agarwal V, Penzel S, Szekely K, Cadalbert R, Testori E, Oss A, et al. De Novo 3D Structure Determination from Sub-milligram Protein Samples by Solid-State 100 kHz MAS NMR Spectroscopy. Angewandt Chem Int Edt. 2014;53(45):12253-6.
100. Penzel S, Smith AA, Agarwal V, Hunkeler A, Org ML, Samoson A, et al. Protein resonance assignment at MAS frequencies approaching 100 kHz: a quantitative comparison of J-coupling and dipolar-coupling-based transfer methods. J Biomol NMR. 2015;63(2):165-86.
101. Campbell G, Galya L, Beeler A, English A. Effect of RF inhomogeneity upon quantitative solid-state NMR measurements. Journal of Magnetic Resonance, Series A. 1995;112(2):225-8.
102. Idziak S, Haeberlen U. Design and construction of a high homogeneity rf coil for solid-state multiple-pulse NMR. Journal of Magnetic Resonance (1969). 1982;50(2):281-8.

103. Bak M, Rasmussen JT, Nielsen NC. SIMPSON: A General Simulation Program for Solid-State NMR Spectroscopy. J Magn Reson. 2000;147(2):296-330.
104. Tosner Z, Andersen R, Stevenss B, Eden M, Nielsen NC, Vosegaard T. Computer-intensive simulation of solid-state NMR experiments using SIMPSON. J Magn Reson. 2014;246:79-93.
105. Chevelkov V, Faelber K, Schrey A, Rehbein K, Diehl A, Reif B. Differential Line Broadening in MAS solid-state NMR due to Dynamic Interference. J Am Chem Soc. 2007;129(51):10195-200.
106. Hologne M, Faelber K, Diehl A, Reif B. Characterization of Dynamics of Perdeuterated Proteins by MAS Solid-State NMR. J Am Chem Soc. 2005;127(33):11208-9.
107. Schanda P, Meier BH, Ernst M. Accurate measurement of one-bond H-X heteronuclear dipolar couplings in MAS solid-state NMR. J Magn Reson. 2011;210(2):246-59.
108. Linser R, Fink U, Reif B. Probing Surface Accessibility of Proteins Using Paramagnetic Relaxation in Solid-State NMR Spectroscopy. J Am Chem Soc. 2009;131:13703–8.
109. Linser R, Chevelkov V, Diehl A, Reif B. Sensitivity Enhancement Using Paramagnetic Relaxation in MAS Solid State NMR of Perdeuterated Proteins. J Magn Reson. 2007;189(2):209-16.
110. Helmus JJ, Jaroniec CP. Nmrglue: an open source Python package for the analysis of multidimensional NMR data. J Biomol NMR. 2013;55(4):355-67.
111. Maricq MM, Waugh JS. NMR in rotating solids. J Chem Phys. 1979;70(7):3300-16.
112. E.Maciel JSFG. Setting the Magic Angle Using a Quadrupolar Nuclide. Journal of Magnetic Resonance. 1982(48):125-31.
113. Sarkar R, Rodriguez Camargo DC, Pintacuda G, Reif B. Restoring Resolution in Biological Solid-State NMR under Conditions of Off-Magic-Angle Spinning. J Phys Chem Lett. 2015;6(24):5040-4.
114. Pileio G, Guo Y, Pham TN, Griffin JM, Levitt MH, Brown SP. Residual Dipolar Couplings by Off-Magic-Angle Spinning in Solid-State Nuclear Magnetic Resonance Spectroscopy. J AM CHEM SOC. 2007(129):10972-3.